Hydrogenated Amorphous Silicon Germanium Alloys for High Efficiency and Stable Solar Cells

Akira TERAKAWA

April 1999

Hydrogenated Amorphous Silicon Germanium Alloys for High Efficiency and Stable Solar Cells

Akira TERAKAWA

April 1999

Abstract

This work investigates the properties of hydrogenated amorphous silicon germanium (a-SiGe:H) alloys as photovoltaic materials, which are good candidates for use as the bottom photo-absorber of tandem solar cells. a-SiGe:H films were deposited by a plasma-CVD method using SiH_4, GeH_4, and H_2 gas mixtures. The difficulties of a-SiGe:H as ternary alloys due to the intermixing of respective parameters, such as the deposition conditions, compositions, hydrogen bonding structures, optical gap (E_{opt}), electronic properties, solar cell performance and photo-instability, were systematically unraveled. This work provided new insights into a wide variety of aspects, from particular issues related to a-SiGe:H alloys, to the universal issues of a-Si related materials, and from fundamental material properties to device characteristics.

In Chapter 2, the correlations among deposition conditions, compositions and material properties were systematically investigated. E_{opt} of a-SiGe:H, which is an essential factor in designing photovoltaic material, was quantitatively represented as a function of the hydrogen content (C_H) and germanium content (C_{Ge}). Furthermore, it was shown that the optimum composition for a certain E_{opt} (= 1.32 eV) exists, and shifts to the lower C_H region after light soaking. C_H and hydrogen bonding configurations were suggested as being important in determining both the initial properties and the photo-instability.

In Chapter 3, the composition dependence of the inhomogeneous hydrogen bonding structures in a-SiGe:H was investigated by means of an infrared (IR) absorption spectroscopy method. It was shown that the structural differences of a-SiGe:H with C_H are mainly caused in the regions around Si atoms. H-Si bonding configurations of the samples deposited from highly-H_2-diluted source gas are almost random, while those from low-diluted source gas selectively contain polyhydride bonds. Besides, the coefficient of the preferential hydrogen attachment to Si over to Ge (P), which causes inhomogeneity of hydrogen bonding structures, has positive correlations to both C_H and C_{Ge}. The P value is considered to be determined not simply by the statistical difference of the bonding probabilities of H to Si and to Ge, but by the kinetics of H elimination during film growth.

In Chapter 4, in order to reveal the effects of i-layer E_{opt} and the composition of a-SiGe solar cells on stability against light soaking, the light-induced degradation and thermally-induced

recovery behaviors of a-SiGe cells with a constant E_{opt} and different compositions, and those with various E_{opt}, were systematically investigated. It was suggested that compositional factors such as C_H mainly affect the saturated defect density after intense light soaking (N_{sat}), while E_{opt} affects the degradation time constant. It was clearly shown that a-SiGe cells with lower C_H and/or Si-H_2 content were more stable in a constant E_{opt} system. This result confirms the contribution of incorporated hydrogen atoms on metastable defect creation. a-SiGe solar cells with a narrower E_{opt} degrade more slowly than, but recover as fast as, cells with a wider E_{opt}. This is because light-induced processes are suppressed in materials with a narrower E_{opt}, while thermally-induced processes do not depend on E_{opt}. Furthermore, it was proved that N_{sat} depends on the temperature more strongly for narrower E_{opt} alloys. Therefore, operating conditions should be considered in the design of highly-efficient solar cell submodules.

In Chapter 5, the knowledge gained in the present study was applied to a-SiGe:H material design for high-efficiency solar cells and modules. The world's highest stabilized efficiency of 3.3% for an a-SiGe single junction solar cell (1 cm^2) was achieved under R65 filtered light. Using this a-SiGe cell at the bottom, the world's highest stabilized efficiencies of 10.6% for an a-Si/a-SiGe tandem cell (1 cm^2) was also achieved. Furthermore, the world's highest stabilized efficiencies of 9.5% for an a-Si/a-SiGe superstrate submodule (30×40 cm^2) was achieved by combining the cell design technique with some other technologies.

Finally in Chapter 6, the conclusions of the present work were summarized together with suggestions for future work.

Acknowledgments

The author wishes to express his sincere gratitude to Professor Hiroyuki Matsunami of Kyoto University for his continuous guidance and for helpful suggestions throughout Ph.D course and for this thesis.

The author is also grateful to Professor Shigeo Fujita and Professor Kunihide Tachibana of Kyoto University for their guidance and suggestions during the preparation of this thesis.

Sincere appreciation is extended to Professor Hajime Yamashina of Kyoto University for his recommendation and support upon the author's applying for admission to the Graduate School of Kyoto University.

This work was done at the New Materials Research Center of Sanyo Electric Co., Ltd., and was in part supported by the New Energy and Industrial Technology Development Organization (NEDO) as a part of the New Sunshine Program under the Ministry of International Trade and Industry.

The author would like to express a special thank to Dr. Yukinori Kuwano, the president of Sanyo Semiconductor Company (the ex-executive director of the R&D Headquarters of Sanyo) and Dr. Fusao Terada, the present executive director of the R&D Headquarters, for their immeasurable and valuable support. He also wishes to express his great appreciation to Dr. Shoichi Nakano, the general manager of the General Management Planning Office of the R&D Headquarters (the ex-general manager of the New Materials Research Center), Dr. Osamu Ota, the present general manager of the New Materials Research Center, and Dr. Masato Osumi, the general manager of Sanyo Home Appliance Company (the ex-general manager of the Mechatronics Research Center), for their continuous support and encouragement.

The author is also indebted to Dr. Shinya Tsuda, the deputy general manager of the New Battery Division of Sanyo and concurrently the president of Solec Co. Ltd, (the ex-senior manager of the New Electronic Materials Department of the New Materials Research Center) for his guidance, critical reading of technical papers and helpful discussions. He is also grateful to Dr. Seiichi Kiyama, the senior manager of the PV Group of the New Electronic Materials Department of the New Materials Research Center, Dr. Hisaki Tarui, Dr. Makoto Tanaka and Dr. Kenichiro Wakisaka, the managers of the PV Group, for their helpful guidance and continuous encouragement.

The author would also like to thank to the following people at Sanyo:

Tsuyoshi Takahama and Dr. Masato Nishikuni for their kind tutorial guidance when the author

started his research activities in the field of amorphous silicon solar cells in Sanyo.

Katsunobu Sayama and Masaki Shima for their helpful cooperation in the experiments of thin film deposition processes, their analysis sequences of materials and devices, and for fruitful technical discussions.

Akiko Tabata, Mio Saito, Akira Mikami, Shigeki Matsuda and Hiroshi Nonoue, the members of the Materials Characterization Laboratory, for their experimental assistance and advice in the composition analysis of alloy materials by SIMS, XPS and FT-IR measurements.

Dr. Yoshihiro Hishikawa for his fruitful discussions and valuable comments particularly on the construction of kinetic model for hydrogen bonding configurations.

Dr. Masao Isomura and Dr. Shingo Okamoto for their critical reading of some of the technical articles, discussions and useful comments.

Ritsuyo Ikemoto for her assistance in prepareing some figures and editing the manuscript, and for her friendship.

Norihiro Terada and Shigeo Yata for following him in Sanyo during his Ph.D course.

Dr. Hisao Haku, Kunimoto Ninomiya, Dr. Eiji Maruyama, Yukihiro Yoshimine and Toshihiro Kinoshita for their helpful assistance and discussions, and all other research members working on amorphous silicon solar cells for their support in so many ways.

And the author finally thanks to his family: his sister and brother-in-law Nobuko and Dr. Mark Buonanno, his parents Katsuko and Makoto Terakawa, and his grandmother Masago Terakawa for their material and moral support and continuous encouragement.

Table of Contents

Chapter 1
Introduction

1.1 Historical background of solar cells

It was 1954 when the first solar cell was invented by Pearson *et al.* in the Bell Laboratory of AT&T in the USA.[1] Solar cells are energy conversion devices that apply the photovoltaic effect of the p-n junction of semiconductors, and which can cleanly produce electric power from inexhaustible sunlight without any waste. Due to these features, solar cells are expected to be used as a renewable energy source in the next generation, taking the place of fossil fuels such as coal and oil. Since the oil shock in 1973, the research and development of solar cell technologies for practical large-scale photovoltaic use has been accelerated in national projects in many countries and regions including Japan, the USA and Europe. In recent years, solar cells have attracted considerable attention as a solution to increasing serious environmental problems such as the greenhouse effect which causes global warming, the destruction of forests by acid rain and the ultraviolet rays that penetrate the ozone hole. The production volume of solar cells is drastically increasing year by year around the world.[2,3] The Japanese government started a financial support program in 1994 to accelerate the spread of solar power generation systems for private houses and buildings, and is planning to install 5000 MW systems by 2010.

At present, solar cells are expensive compared to commercial electricity generated by thermal or nuclear power plants. Further reduction of the production cost is necessary in order to achieve the spontaneous spread without financial support. The most widely used semiconductor materials for solar cells are single- and poly-crystalline silicon (c-Si and poly-Si), which shared more than 80% of the world's shipment of cells and modules in 1997.[3] The cost limiting factor of c-Si and poly-Si solar cells is 200-400 μm thick Si substrate wafers, which are fabricated through complex and high-temperature processes. Hydrogenated amorphous silicon (a-Si:H) is a good candidate for large-scale and low-cost devices in place of Si wafers. The use of a-Si:H for solar cells made it possible to reduce the thickness of semiconductor layers to less than 0.5 μm. This is because a-Si:H is a direct transition semiconductor and has a remarkably larger absorption coefficient against visible

light than crystalline Si, which is an indirect transition semiconductor. This is a great advantage from the point of view of the material cost.

1.2 Progress in a-Si solar cell technology

a-Si:H was first made in 1969 by Chittick *et al.* in the UK, using a glow discharge with SiH_4 gas.[4] However, in those days, it was believed that amorphous materials were insensitive against doping due to the lack of periodicity of atomic arrangement[5,6] and were not feasible for junction devices. A breakthrough was reported in 1975 by Spear and LeComber of Dundee University in the UK. They succeeded in substitutional p-type and n-type doping by adding B_2H_6 and PH_3 to source SiH_4 gas.[7] The significance of their observations was widely acknowledged, and a-Si:H has received considerable attention as a new electronic material.

The research of a-Si solar cells was started by Carlson and Wronski of RCA in 1976. They initially reported a conversion efficiency of 2.4 % by adopting a p-i-n junction structure.[8] They also reported a conversion efficiency of 5.5 % with a Schottky junction structure.[9] In 1978, an improved efficiency of 4.5 % for a p-i-n junction cell was reported by Hamakawa *et al.* of Osaka University.[10] In 1979, Kuwano *et al.* of Sanyo developed two key technologies in this field; one is an "integrated type structure,[11]" and the other is a "consecutive, separated chamber reaction method.[12]" The concept of the integrated type structure is to connect multiple cells in series on a single substrate in order to generate high output voltage. While, the consecutive, separated chamber reaction method achieved a drastic reduction of impurities in the a-Si:H i-layer contaminated by the source gas intermixing during film deposition. Based on these technologies, Sanyo marketed the first devices — hand-held calculators — powered by a-Si solar cells in 1980. Since then, subsequent research resulted in numerous technologies, such as the minimized optical loss by a-SiC:H window layers,[13] a reduction of the intermixing of impurities by the ultra-high-vacuum (UHV) deposition system,[14] and fabrication of integrated-type structures by the laser patterning method.[15] By the use of these techniques, the conversion efficiency of a-Si solar cells has been improved year by year. The world's highest initial efficiencies of 12.7 % for a p-i-n single-junction cell (1 cm^2) and of 12.0 % for a submodule (100 cm^2) were achieved by Sanyo in

1993.[16]

1.3 Importance of a-SiGe:H alloys for solar cells

For large-scale power generation utilizing a-Si solar cells outside, however, there still are some problems. One of them is the lower sensitivity for near-infrared lights due to their wider optical gap (E_{opt}) than c-Si. Another is a degradation of efficiency due to an increase in the number of metastable defects of the photovoltaic layer during strong-light irradiation, or the so-called Staebler-Wronski effects (SWE).[17] Multi-junction solar cells — also sometimes called "multi-band-gap cells" — are expected to alleviate these problems.[18-20] These cells consist of two or three p-i-n junctions stacked in series in the order of the i-layer E_{opt} as illustrated in Fig. 1.1. Figure 1.2 shows a schematic comparison of the wavelength sensitivity of a triple-junction solar cell and a solar spectrum. Multi-junction structures allow the utilization of higher energy photons as a current at a higher voltage in the top cell with a wider E_{opt} i-layer, while also absorbing lower energy photons in the bottom cell with a narrower E_{opt} i-layer, as shown in Fig. 1.2. Therefore, long-wavelength sensitivity can be improved by narrowing the E_{opt} of the bottom cells. Furthermore, a strong internal electric field, which is due to the thinner photovoltaic layers, prevents carrier recombination and maintains a higher fill factor after illumination than single-junction cells.

Hydrogenated amorphous silicon germanium (a-SiGe:H) alloys are considered to be good candidates as the bottom optical-absorber for double- or triple-junction solar cells,[20,21] since their E_{opt} can easily be narrowed by adding Ge to match the solar spectra outside. The main problem of a-SiGe:H is its deteriorating electronic properties with alloying. It is thus important to reveal the criteria in improving the material quality of a-SiGe:H, which is, however, more complicated than that of a-Si:H due to the complicated microstructure of a-SiGe:H as a ternary alloy.

1.4 Purpose of the present study

Most difficulties when dealing with a-SiGe:H alloys are caused by the intricate intertwining of

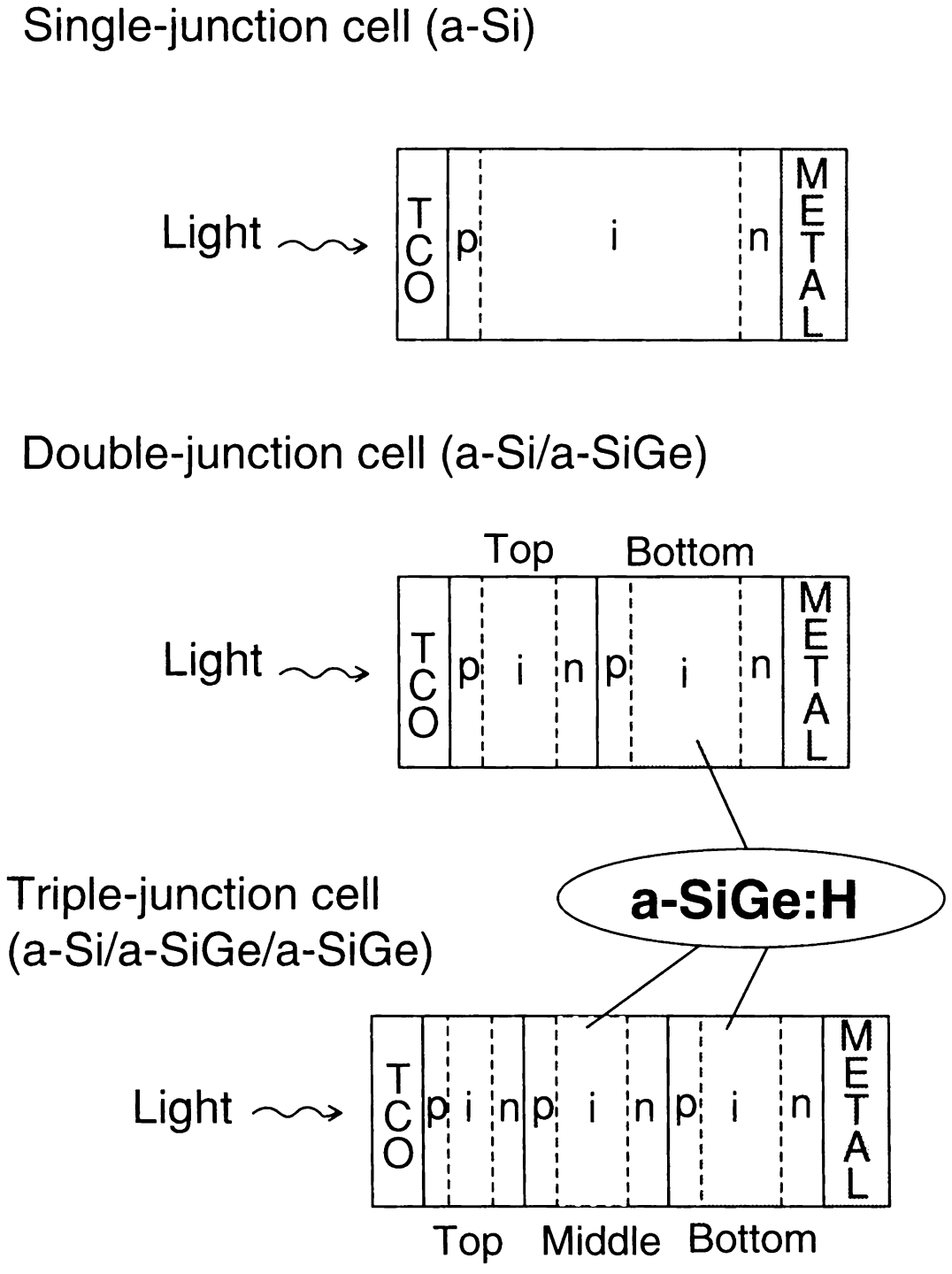

Fig. 1.1 Cross section structures of single- and multi-junction solar cells.

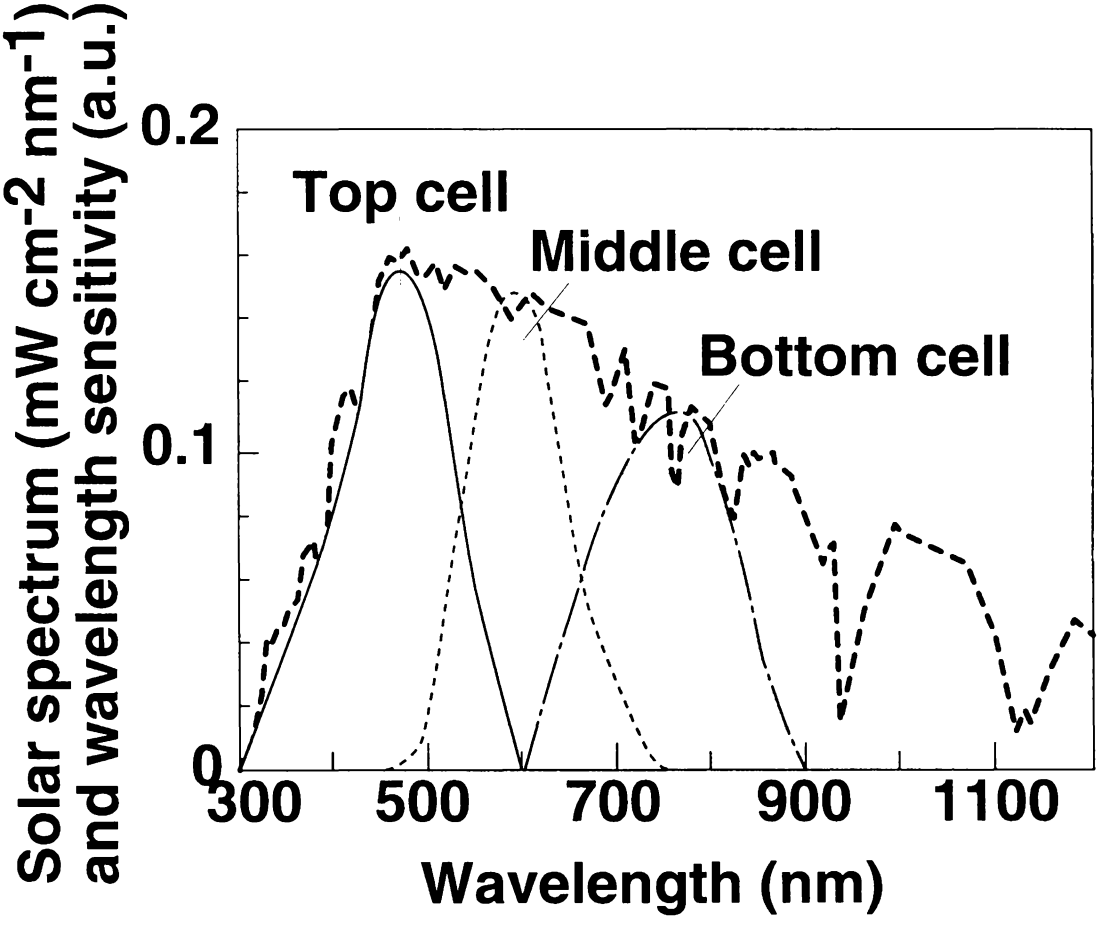

Fig. 1.2 Comparison of the solar spectrum and the wavelength sensitivitiy of a multi (triple)-junction solar cell.

the composition, E_{opt} and material properties, which are particularly important in the alloys for determining solar cell performance. The purpose of the present study is to unravel the difficulty. The detailed features, as photovoltaic materials, of a-SiGe:H alloys deposited by plasma-CVD were systematically investigated with regards to both the compositions and E_{opt}.

Figure 1.3 illustrates a block diagram of the organization of this thesis. In Chapter 2, the film properties of a-SiGe:H including E_{opt}, conductivity, defect density, hydrogen bonding configurations and photostability are studied as functions of the compositions, and criteria for optimizing compositions are discussed. In Chapter 3, the hydrogen bonding configurations in a-SiGe:H, which is a factor determining both the initial properties and stability, are studied for various compositions, and the kinetic formation of microstructures and preferential hydrogen attachment are discussed. In Chapter 4, the effects of the compositions and E_{opt} on the photo-induced instability of a-SiGe solar cells are investigated, and the origins of experimental observations are discussed. In Chapter 5, the progress in the performance of a-SiGe solar cells fabricated by the author's research group, to which the knowledge gained in the present study about material design was applied, is reviewed. Finally, the conclusions of the present study are summarized in Chapter 6.

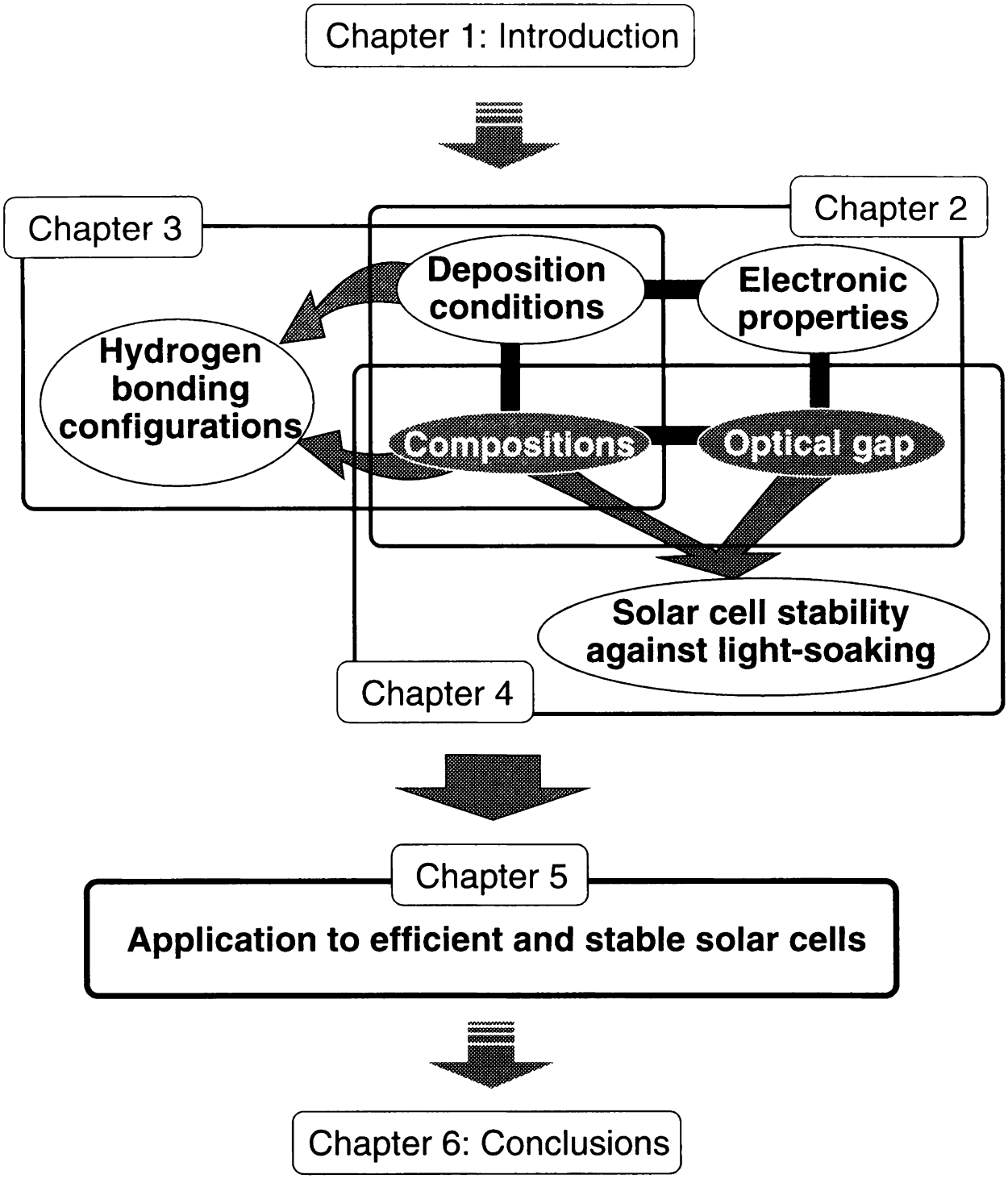

Fig. 1.3 A block diagram of the organization of this thesis.

References

1. D.M. Chapin, C.S. Fuller and G.L. Pearson, J. Appl. Phys. **25**, 676 (1954).
2. Photovoltaic Insider's Report edited by R. Curry, February (1998).
3. PV NEWS Vol.**17**, No.2 (1998).
4. R.C. Chittick, J.H. Alexander and H.F. Sterling, J. Electrochemical Soc. **116**, 77 (1969).
5. A.I. Gubanov, Sov. Phys. Solid State **3**, 1694 (1962).
6. N.F. Mott, Philos. Mag. **19**, 835 (1969).
7. W.E. Spear and P.G. LeComber, Solid State Comm. **17**, 1193 (1975).
8. D.E. Carlson and C.R. Wronski, Appl. Phys. Lett. **28**, 671 (1976).
9. D.E. Carlson, IEEE Trans. on Electron Devices **ED-24**, 449 (1977).
10. H. Okamoto, Y. Nitta, T. Adachi and Y. Hamakawa, Proc. Int. Conf. Solid Films and Surfaces, 486 (Tokyo, 1978).
11. Y. Kuwano, T, Imai, M. Ohnishi and S. Nakano, Proc. IEEE Photovoltaic Specialists Conf., 1408 (San Diego, 1980).
12. Y. Kuwano, M. Ohnishi, S. Tsuda, Y. Nakashima and N. Nakamura, Jpn. J. Appl. Phys. **21**, 413 (1982).
13. Y. Tawada, K. Tsuge, H. Okamoto and H. Hamakawa, J. Appl. Phys. **53**, 5273 (1982).
14. S. Tsuda, T. Takahama, M. Isomura, H. Tarui, Y. Nakashima, Y. Hishikawa, N. Nakamura, T. Matsuoka, H. Nishiwaki, S. Nakano, M. Ohnishi and Y. Kuwano, Jpn. J. Appl. Phys. **26**, 33 (1987).
15. S. Nakano, T. Matsuoka, S. Kiyama, H. Kawata, N. Nakamura, Y. Nakashima, S. Tsuda, H. Nishiwaki, M. Ohnishi, I. Nagaoka and Y. Kuwano, Jpn. J. Appl. Phys. **25**, 1936 (1986).
16. Y. Hishikawa, M. Sasaki, S. Tsuge, S. Okamoto and S. Tsuda, Mater. Res. Soc. Symp. Proc. **297**, 792 (1993).
17. D. L. Staebler and C. R. Wronski, Appl. Phys. Lett. **31**, 292 (1977).
18. E.D. Jackson, Transactions of the Conference on the use of Solar Energy, Tucson, Arizona 122 (1955).
19. Y. Marfaing, the 2nd Photovoltaic Solar Energy Conf. Rec. 287 (1979).
20. S. Tsuda, N. Nakamura, Y. Nakashima, H. Tarui, H. Nishiwaki, M. Ohnishi and Y. Kuwano, Jpn. J. Appl. Phys. **21**, 251 (1982).
21. Thin film poly-crystalline silicon (poly-Si) and microcrystalline silicon (μ c-Si) deposited by plasma-CVD are other alternatives for the narrow-gap photovoltaic layer. At the present stage, however, they are not feasible yet for industrialization because the i-layer of c-Si which is an indirect transition semiconductor should be several μ m thick (1-2 order thicker than a-SiGe:H i-layer) and the deposition process for poly- and μ c-Si costs too long time.

Chapter 2
Composition Dependence of Optical Gap and Other Properties of a-SiGe:H alloys

2.1 Background

Plasma chemical vapor deposition (plasma-CVD) has been the most common technique for preparing a-Si related materials, and a-SiGe:H has been deposited from a plasma mixture of SiH_4, GeH_4 and H_2 (Fig. 2.1). The main problem of this alloy has been its poor photoelectric performance, which deteriorates rapidly with increase in the germanium atomic ratio. The deterioration, which was explained by the hydrogen preferential attachment to Si atoms[1] or by Ge–Ge clustering bonds,[2] was found to strongly depend on the fabrication conditions. Matsuda *et al.* succeeded in obtaining higher quality in a wide optical gap range, from hydrogen-diluted gas mixtures of SiH_4 and GeH_4.[3] A reduction in impurities by an ultra high-vacuum (UHV) system was also reported to be effective.[4] The deposition mechanism and the relations between the film properties and the structure of a-SiGe:H alloys are, however, less understood than those of a-Si:H, because the additional parameter, germanium, complicates the situation.

Numerous studies which relate film properties to germanium content (C_{Ge}) have been performed. For example, the optical gap (E_{opt}) of a-SiGe:H was previously reported to have a negative linear dependence on C_{Ge} by Chevalier *et al.*[5] and many other authors.[6-11] Smith *et al.*, however, pointed out that this relationship did not agree with the experimental results in films deposited at different substrate temperatures.[12] This was probably due to the difference in the hydrogen content (C_H).

In the case of a-Si:H, C_H is known to be important for determining the photoelectric properties. Papaconstantopoulos and Economou indicated a widening of the gap energy with bonded hydrogen in a quantitative simulation.[13] A positive linear relationship between E_{opt} and C_H has been experimentally observed by several groups including ourselves.[14-17] Furthermore, the current study carried out by the author's group verified that most properties, namely the photo and dark-conductivities, Si–H_2/Si–H, and defect density of "device quality" film deposited from pure SiH_4

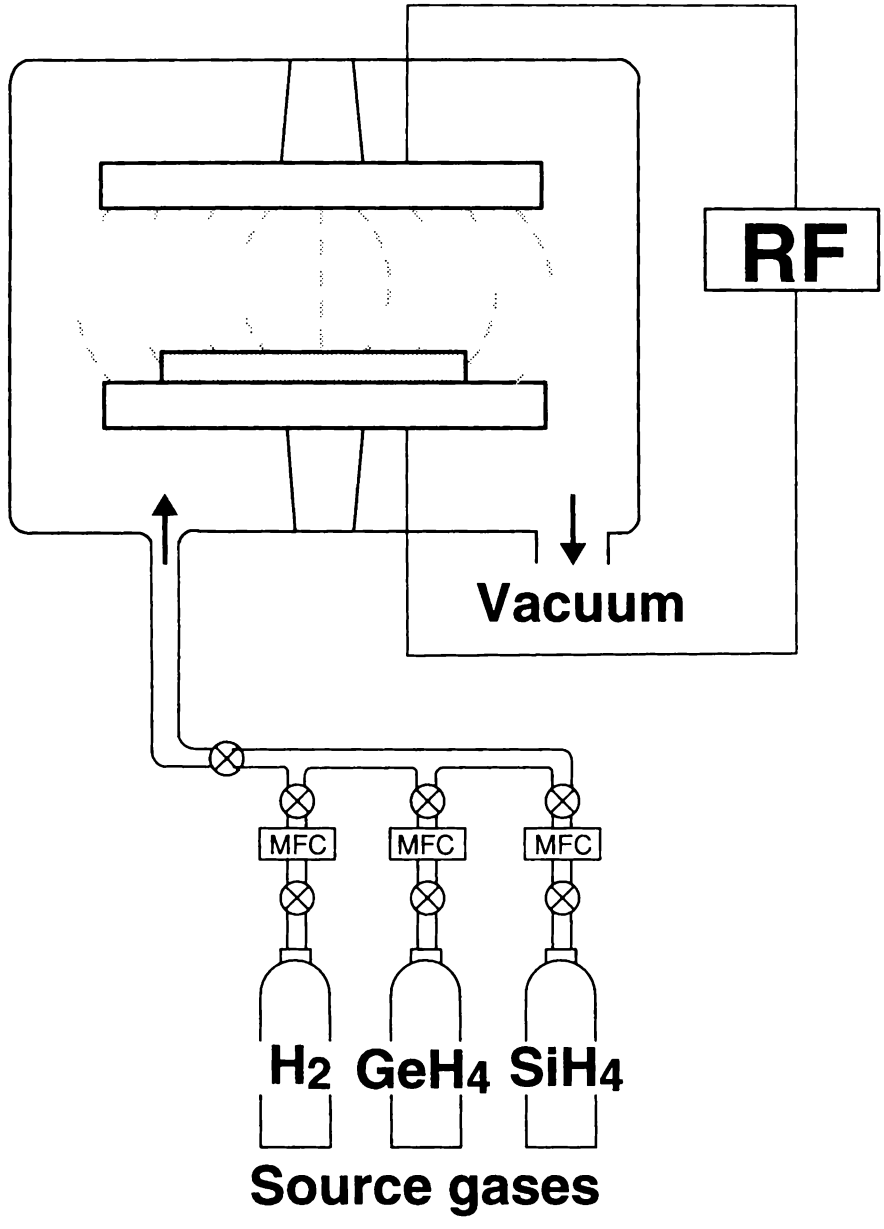

Fig. 2.1 A schematic illustration of plasma-CVD system for a-SiGe:H deposition.

plasma, were almost entirely characterized by C_H.[17,18]

These results in a-Si:H suggest that a-SiGe:H should be regarded as a ternary alloy of silicon, germanium and hydrogen. Nevertheless, there have been few reports in which a-SiGe:H film properties were treated as functions of both C_{Ge} and C_H. In this chapter, the photoelectric properties of a-SiGe:H films, deposited by the plasma-CVD method using SiH_4, GeH_4, and H_2 gas mixtures, are indicated by considering C_H addition to C_{Ge}. A clear relationship is observed between E_{opt} and the compositions. Furthermore, the guiding principle for the optimization of the alloy composition is demonstrated.

2.2 Experimental

The a-SiGe:H samples used in this study were prepared with a capacitively coupled RF plasma chemical vapor deposition (plasma-CVD) reactor from a gas mixture of SiH_4, GeH_4 and H_2. An ultrahigh vacuum (UHV) system called the "superchamber" was used to reduce the amount of impurities.[19] The concentrations of oxygen, nitrogen and carbon were estimated to be ~10^{18}, ~10^{17} and ~$10^{17}cm^{-3}$, respectively. The typical fabrication conditions are shown in Table 2.1. The samples for measuring optical and electronic properties were deposited on Corning #7059 glass and silver-coated glass substrates.

Table 2.1 Deposition conditions of a-SiGe:H.

Substrate temperature		120-350	℃
Reaction pressure		~20	Pa
Background pressure		10^{-5}-10^{-6}	Pa
RF power density		10-100	mW/cm^2
Gas flow rate	SiH_4	30	sccm
	GeH_4	2-5.2	sccm
	H_2	75	sccm

The optical gap (E_{opt}) was determined from $h\nu$ versus $(\alpha h\nu)^{-1/3}$ plots,[20-22] where α and $h\nu$ denote the optical absorption coefficient and photon energy, respectively. The optical absorption coefficient (α) spectra were calculated from transmittance (T) and reflectance (R) spectra, and the optical interference effect was suppressed by the $T/(1-R)$ calculation in the analysis.[21] The midgap defect density (N_D) and characteristic energy of the Urbach tail (E_{ch}) were evaluated from the subgap absorption coefficient spectra measured by the constant photocurrent method (CPM).[23,24] The CPM is an effective method to determine a very small optical absorption due to optical transitions between gap- and band-states by detecting the photocurrent under long-wavelength light soaking.[23] The optical interference effect in the CPM spectra was also canceled by a calculation similar to that mentioned above.[24] N_D is assumed to be proportional to the integral of the excess absorption fitted by a Gaussian curve. The dark conductivities and photoconductivities under AM-1, 100 mW/cm^2 irradiation were also measured. The samples, on which aluminum coplanar electrodes were deposited, were used for the CPM and conductivity measurements. The germanium content, C_{Ge} (= [Ge]/([Si]+[Ge]) atomic ratio), was determined by an X-ray photoelectron spectroscopy (XPS) method. The XPS detects the integrated intensities of energy distribution of the X-ray excited electrons from the core states (Si 2*p* and Ge 3*d*), and C_{Ge} was calibrated by using the previously reported photoionic cross sections of Si and Ge as the atomic sensitivity factors.[25] The hydrogen content, C_H (= [H]/([Si]+[Ge]) atomic ratio), was evaluated by combining the XPS and secondary ion mass spectroscopy (SIMS) methods, based on

$$C_H = [H]/([Si]+[Ge]) = \alpha_{CH} \times [Si]/([Si]+[Ge]) \times I(H^+)/I(^{28}Si^+), \quad (2.1)$$

where [Si]/([Si]+[Ge]) is the silicon content determined by the XPS method, and $I(H^+)$ and $I(^{28}Si^+)$ are the peak intensities of secondary ions for masses 1 and 28, respectively. The proportionality constant, α_{CH}, in Eq. (2.1) was estimated by comparison with an infrared (IR) absorption method. The hydrogen bonding configurations were observed using the reflectance IR absorption spectra measured for the samples on the silver-coated glass substrates and subtracted from the silver reflectance spectra. The IR absorption spectra were decomposed to the three Gaussian curves centered at the frequencies of ~1860, ~2000, and ~2100 cm^{-1}, which were assigned to the stretched

vibrational modes of Ge–H, Si–H, and Si–H_2, respectively. The bonded hydrogen content in each configuration ($C_{H(Ge-H)}$, $C_{H(Si-H)}$, and $C_{H(Si-H2)}$) was evaluated by distributing C_H proportional to the product of the calibration factor (A_{Si} or A_{Ge}) and the area under the Gaussian curve of each mode. A_{Ge} (= $6x10^{19}$ cm^{-2}) and A_{Si} (= $1.4x10^{20}$ cm^{-2}) are the previously reported A factors for the Ge–H and Si–H bonds.[26] The IR absorption peaks of the Si–H mode (~2000 cm^{-1}) and Ge–H_2 mode (~1980 cm^{-1}) are close to each other, thus, $C_{H(Si-H)}$ in this study may include the content of Ge-H_2. However, some research groups fitted the IR spectrum of a-SiGe:H films precisely to four Gaussian curves assigned to the Ge–H, Ge–H_2, Si–H, and Si–H_2 modes and suggested that the amount of Ge–H_2 was very small.[27,28] In addition, we observed that the IR absorption peak of Ge–H_2 was much smaller than that of Ge–H (factor < 0.2) in a-Ge:H deposited under conditions similar to those shown in Table 2.1. For these reasons, we assumed that the amount of Ge–H_2 is negligible in the a-SiGe:H samples.

2.3 Deposition parameters, compositions and film properties under a constant mixture gas flow

2.3.1 GeH_4 flow dependence

Figures 2.2(a)-2.2(c) show the C_{Ge}, C_H, and E_{opt} of the a-SiGe:H films as functions of [GeH_4]/[SiH_4] flow ratio. The hydrogen dilution ratio of source gas mixture, [H_2]/([SiH_4]+[GeH_4]), was kept ~2.5 and T_s was kept at 230°C. As [GeH_4]/[SiH_4] increases, C_{Ge} monotonously increases and C_H slightly decreases (Figs. 2.2(a) and 2.2(b)). E_{opt} decreases with increases in [GeH_4]/[SiH_4] mainly due to the increase in C_{Ge}. C_{Ge} does not have a linear relation to [GeH_4]/[SiH_4] flow ratio (Fig. 2.2(a)). This is due to the difference in the incorporation ratio of Si and Ge from the source gas into the film.[11] The solid line in Fig. 2.2(a) is a fitting curve by the following function,

$$C_{Ge} = p(Ge)\,[GeH_4]/(p(Si)\,[SiH_4]+p(Ge)\,[GeH_4])$$

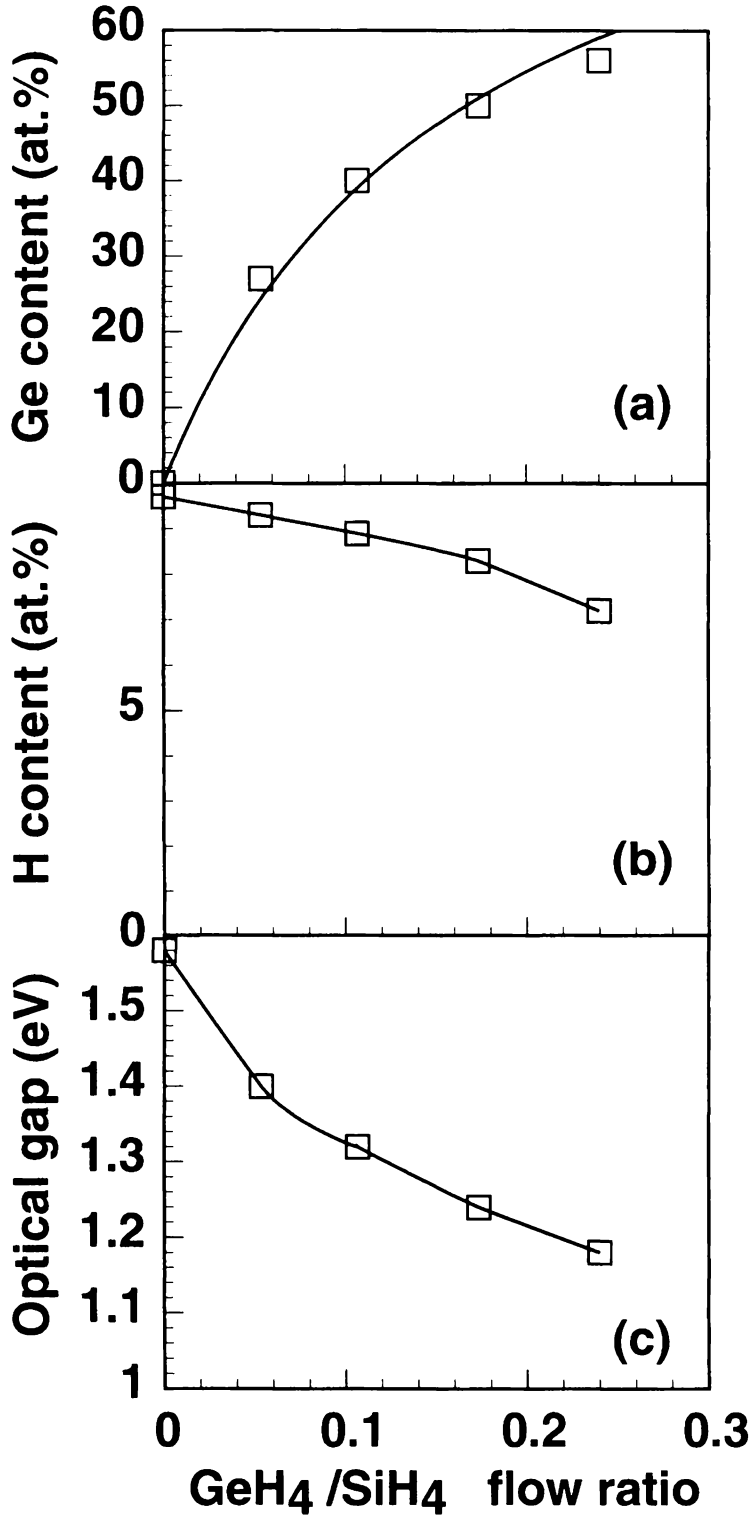

Fig. 2.2 (a) Germanium content (C_{Ge}), (b) hydrogen content (C_H) and (c) optical gap (E_{opt}) of a-SiGe:H films as a function of the $[GeH_4]/[SiH_4]$ flow ratio. The substrate temperature (T_s) is constant at 230℃.

$$= (p(\mathrm{Ge})/p(\mathrm{Si}))\,([\mathrm{GeH_4}]/[\mathrm{SiH_4}]) / \{1 + (p(\mathrm{Ge})/p(\mathrm{Si}))\,([\mathrm{GeH_4}]/[\mathrm{SiH_4}])\}. \quad (2.2)$$

In Eq. (2.2), p(Si) and p(Ge) are the incorporation probabilities of silicon and germanium, and are defined as $p(\mathrm{Si}) = C_{\mathrm{Si}} / C_{gas\mathrm{Si}}$ and $p(\mathrm{Ge}) = C_{\mathrm{Ge}}/C_{gas\mathrm{Ge}}$, where $C_{gas\mathrm{Si}}$ and $C_{gas\mathrm{Ge}}$ are the atomic fractions of Si and Ge in the gas phase, respectively. $p(\mathrm{Ge})/p(\mathrm{Si}) = 5.9$ was obtained by the fitting. This means that Ge atoms are 5.9 times more preferentially incorporated into the growing film from gas mixture plasma than Si atoms.

Figure 2.3 shows the photoconductivity, σ_{ph}, and dark conductivity, σ_d, of a-SiGe:H samples deposited at T_s = 230°C plotted against E_{opt}. σ_{ph} drastically decreases in the region $E_{opt} < 1.3$ eV ($C_{\mathrm{Ge}} > \sim 40$ at.%), probably due to the increase in N_D by alloying. These tendencies are qualitatively consistent to previous reports.[5-7,11,28]

2.3.2 T_s and R_D dependence

Although it is known that the E_{opt} of a-SiGe:H is strongly dependent on the [Ge]/[Si] atomic ratio, C_H is also important in defining the E_{opt} of a-SiGe:H. The deposition parameters, such as the substrate temperature (T_s) and the deposition rate (R_D) were found to be essential in determining C_H and film properties of a-Si:H when the effects of gas-phase polymerization or ion bombardment are not significant.[18] Therefore, in this section, T_s and R_D during a-SiGe:H deposition were related to the film properties under a constant mixture gas flow condition. The source gas mixture ratio was fixed as SiH_4:GeH_4:H_2 = 30:3.2:75 (sccm). This ratio was chosen because it resulted in 30-40 (at.%) of C_{Ge}, which was useful for stacked solar cells. A relatively low hydrogen-dilution ratio was used. R_D was mainly controlled by the rf power.

Figures 2.4(a)-2.4(c) show the C_{Ge}, C_H, and E_{opt} of the a-SiGe:H films as functions of T_s. C_{Ge} shows little change with T_s (Fig. 2.4(a)). This indicates that the relative incorporation probability for Si and Ge atoms does not depend on T_s very much, as has already been reported.[11,28] On the other hand, C_H decreases with the increase in T_s (Fig. 2.4(b)). This means that the growing surface reaction which determines C_H is thermally activated.[29] The incline of C_H versus T_s is about $6\text{-}7 \times 10^{-2}$ (at.%/K). E_{opt} also goes down as T_s becomes larger (Fig. 2.4(c)). The change in E_{opt}, thus, is mainly due to the change in C_H.

Figures 2.5(a)-2.5(d) show that the C_{Ge}, C_H, E_{opt}, and σ_{ph}/σ_d of the a-SiGe:H films deposited

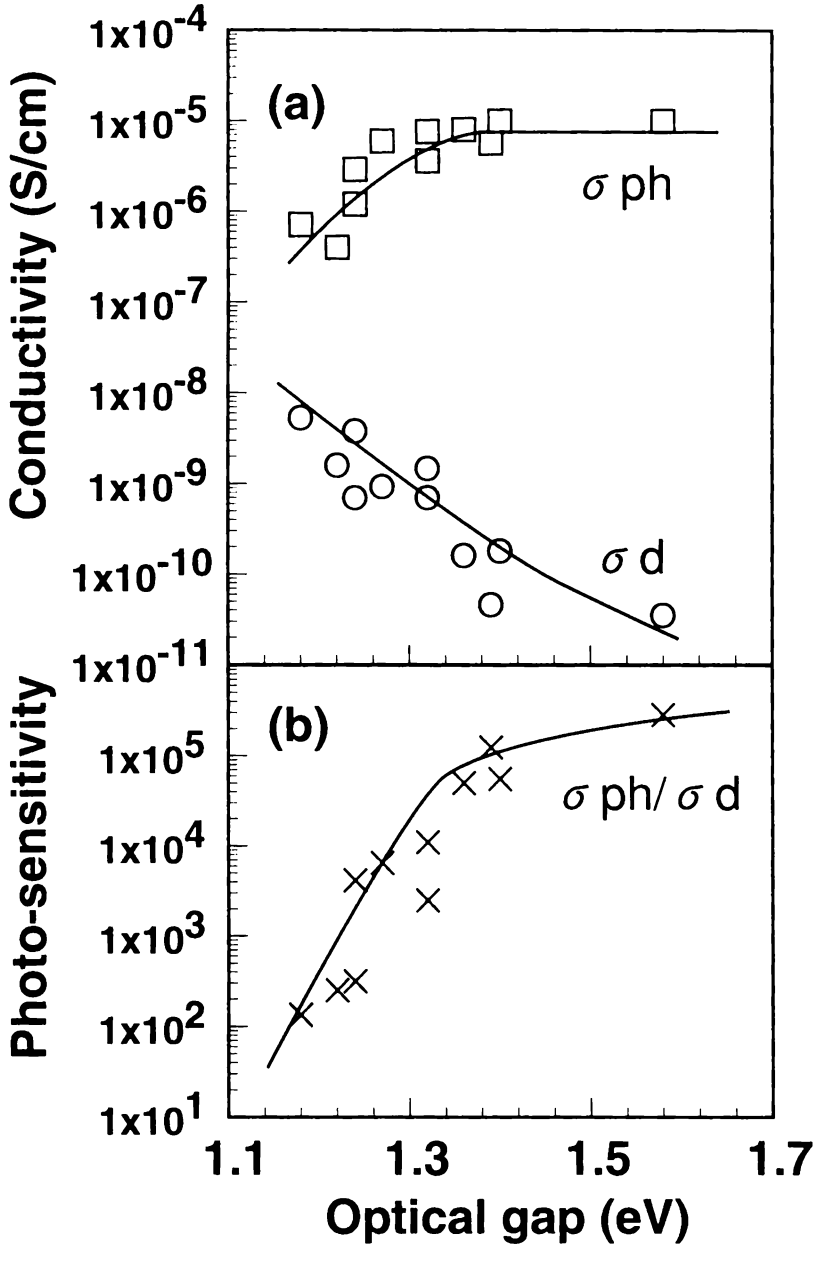

Fig. 2.3 Photoconductivity (σ_{ph}) and dark conductivity (σ_{d}) of a-SiGe:H deposited at 230℃ as a function of the optical gap (E_{opt}).

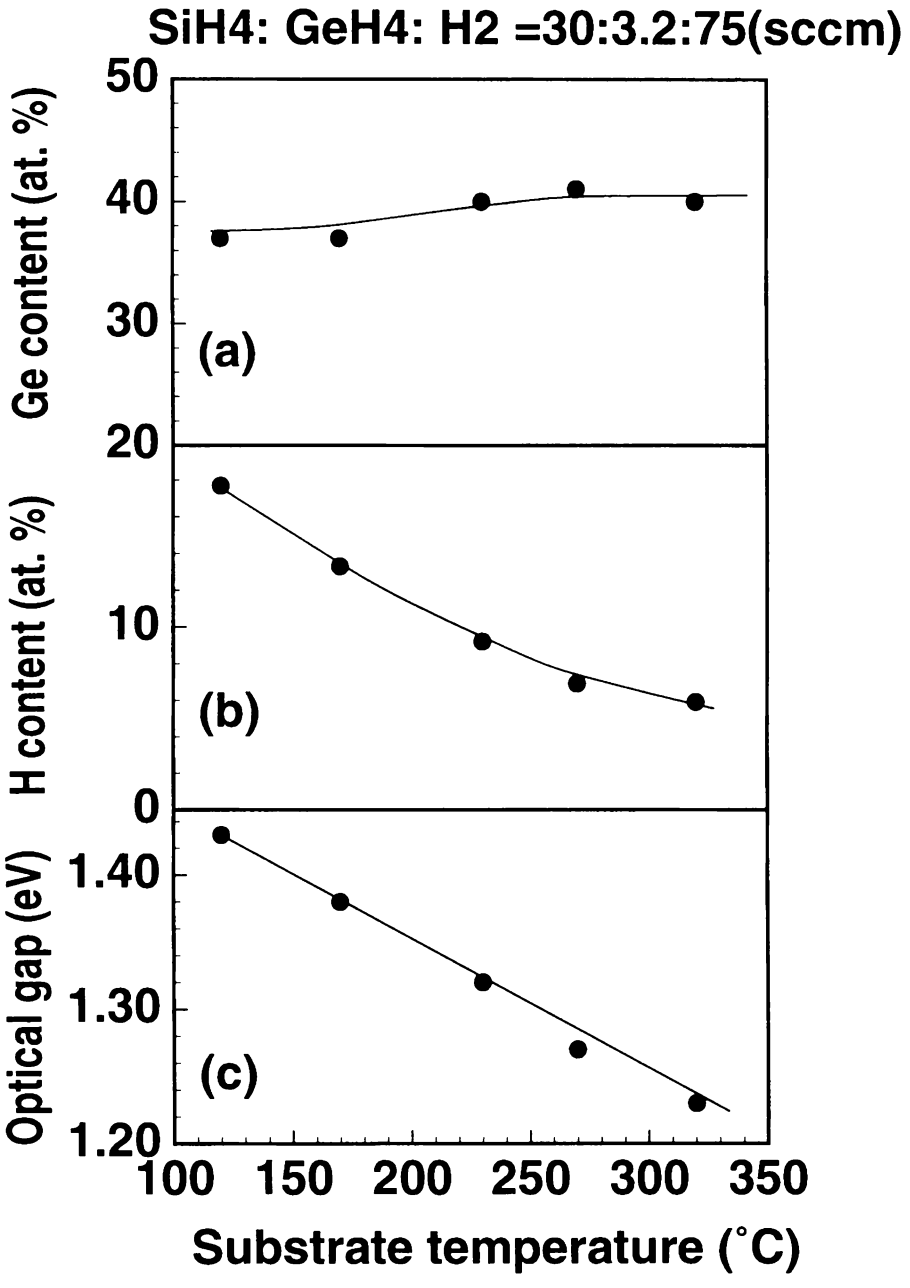

Fig. 2.4 (a) Germanium content (C_{Ge}), (b) hydrogen content (C_H) and (c) optical gap (E_{opt}) of a-SiGe:H films as function of the substrate temperature (T_s). The flow ratio is constant; SiH_4:GeH_4:H_2 = 30:3.2:75 (sccm).

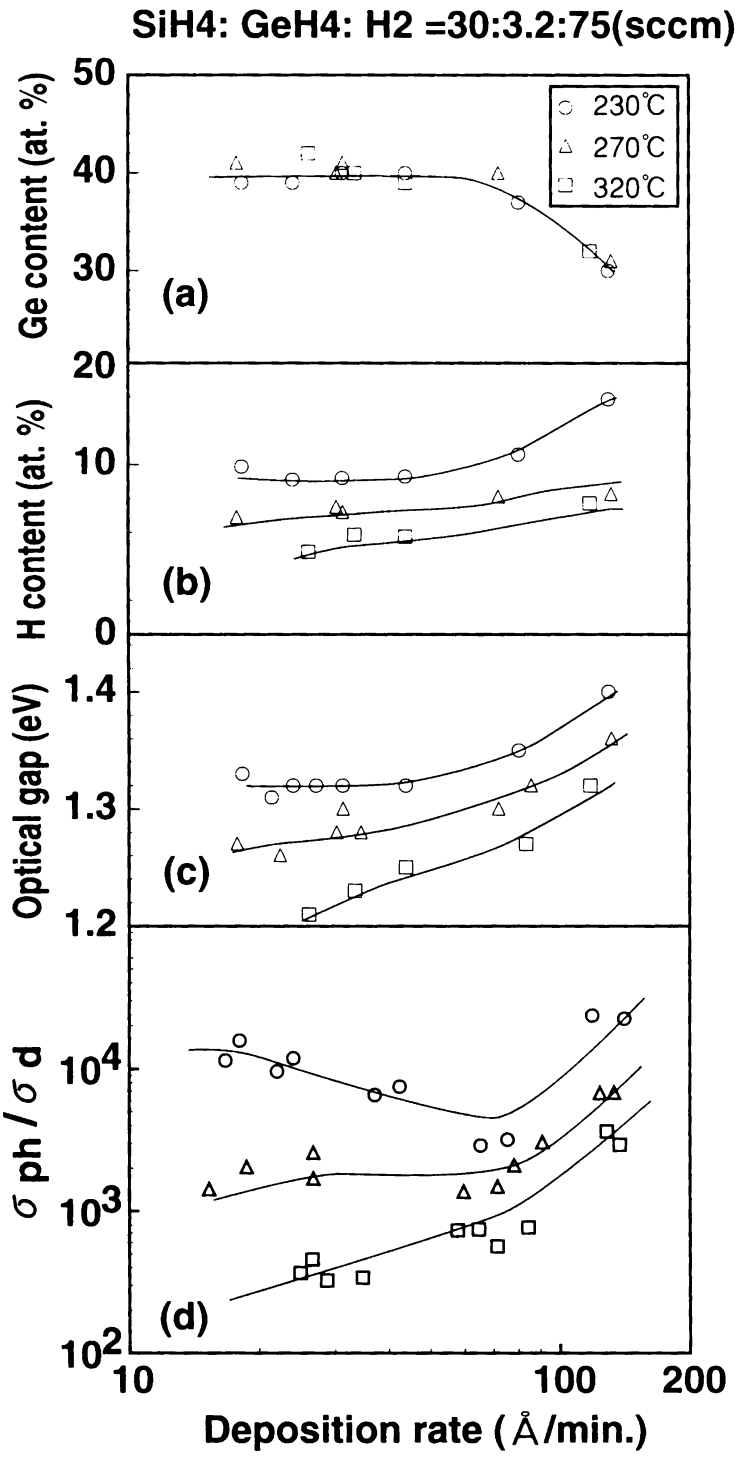

Fig. 2.5 (a) Germanium content (C_{Ge}), (b) hydrogen content (C_H), (c) optical gap (E_{opt}) and (d) photo-sensitivity (σ_{ph}/σ_d) of a-SiGe:H films as a function of the deposition rate (R_D). The flow ratio is constant; SiH_4:GeH_4:H_2 = 30:3.2:75 (sccm).

at various T_s are plotted versus R_D. At each T_s, C_{Ge} becomes smaller with increase in R_D (Fig. 2.5(a)), and both C_H and E_{opt} increase (Figs. 2.5(b) and 2.5(c)). Thus, the dependency of E_{opt} on R_D is attributed to the change in both C_{Ge} and C_H. As reasons for the C_{Ge} alternation, the following two possibilities exist: (1) the radical flux density ratio [Ge radicals]:[Si radicals]:[H radicals] changes with rf power, because the decomposition efficiency of GeH_4, SiH_4, and H_2 is different from each other, (2) the incorporation probability ratio p(Ge)/p(Si) depends on R_D. At present, it is not clear which of these two phenomena is a dominant factor. Stutzmann *et al.* reported the opposite trend (C_{Ge} rises with rf power) in non-diluted SiH_4 and GeH_4 deposition system.[11] This different tendency may be due to variations in the gas (SiH_4 and GeH_4) dissolving rate or radical sticking coefficient with H_2 dilution,[30] or it may be due to the limited radical feeding by the source gas flow rate in one of the cases. When R_D goes up, the time permitted for surface reactions, such as the hydrogen-eliminating reaction on the growing surface, becomes shorter, and this causes higher C_H in the film (Fig. 2.5(b)). At low R_D (< 40 Å/min) and low T_s (= 230℃), C_H seems to be saturated (Fig. 2.5(b)).

At high R_D (> 100 Å/min), σ_{ph}/σ_d was improved at all T_s (230, 270, and 320℃), due to the large decrease in C_{Ge} (Fig. 2.5(a)). Noticing the low R_D (< 80 Å/min) range, in which the varieties of C_{Ge} should be small (see Fig. 2.5(a)), a decrease in R_D causes the σ_{ph}/σ_d of a-SiGe:H films to advance at T_s = 230℃, to change slightly at T_s = 270℃, and to decline at T_s = 320℃. The lower R_D is generally considered to correspond to higher film qualities, since the time available for network relaxation in the growing surface becomes longer. However, the results in Fig. 2.5(d) indicate that it depends on T_s. It is supposed that an excess of the hydrogen-eliminating reaction on the growing surface led to the film quality degrading at high T_s (= 320℃).

In the case of a-Si:H deposition from pure SiH_4 plasma, Hishikawa *et al.* reported that an optimum R_D which corresponds to the minimum defect density exists for every T_s, and that the optimum R_D becomes higher for higher T_s.[18] This is because the film properties are determined by the balance between the surface reaction velocity (which has a positive relation with T_s) and the time available for the surface reaction (which has a negative relation with R_D). This effect seems to be similar to that in Fig. 2.5(d).

2.4 Optical gap as a function of C_H and C_{Ge}

Figure 2.6 shows E_{opt} versus C_{Ge} for samples in which T_s and the rf power were constant (T_s = 230℃ and rf power density = 20 mW/cm^2), and only the gas mixture ratio [GeH_4]/[SiH_4] varied (SiH_4:GeH_4:H_2 = 30:0-3.2:75 (sccm)). The E_{opt} of a-SiGe:H in Fig. 2.6 follows the relation,

$$E_{opt} = a\, C_{Ge} + b \ \text{(eV)}, \tag{2.3}$$

which has been reported by several authors,[5-11] and is partly enumerated in Table 2.2 where E_{Tauc} in the table is the optical gap determined by the Tauc's plot.[31] The coefficient a for C_{Ge} in Eq. (2.3), which is estimated to be about –0.78 (eV) from Fig. 2.6, is consistent with the other authors' results (see Table 2.2). But, it has been pointed out that this linear relation could not represent the E_{opt} of films deposited at different T_s from each other,[12] and we also mentioned this above (see Figs. 2.4(c) and 2.5(c)). This disagreement is most likely due to the difference in C_H.

Figure 2.7 indicates the E_{opt} contour map of a-SiGe:H films deposited at various T_s (120-320℃), rf power (10-100 mW/cm^2), and gas mixture ratios (SiH_4:GeH_4:H_2 = 30:2-5.2:75 (sccm)), as a function of C_H and C_{Ge}. Each symbol represents a composition with a close E_{opt} value. It can be seen that E_{opt} is determined by the combination of C_H and C_{Ge}. The variations in the E_{opt} of a-Si:H, a-Ge:H, and a-SiGe:H (C_{Ge}=0.35-0.40) with the C_H are plotted in Fig. 2.8. C_H of the a-Si:H and a-Ge:H samples was determined from IR absorption spectra. The E_{opt} seems to have an almost linear relationship with both C_H and C_{Ge}, as shown by the solid lines in Fig. 2.7 and the meshed lines in Fig. 2.8, and can be represented by the following equation,

Table 2.2 Previously reported dependence of E_{Tauc} on C_{Ge}.

Mackenzie *et al.*[7]	$E_{Tauc} = -0.78C_{Ge} + 1.76$ (eV)
Chen *et al.*[8]	$E_{Tauc} = -0.74C_{Ge} + 1.74$ (eV)
Wagner *et al.*[9]	$E_{Tauc} = -0.7C_{Ge} + 1.7$ (eV)

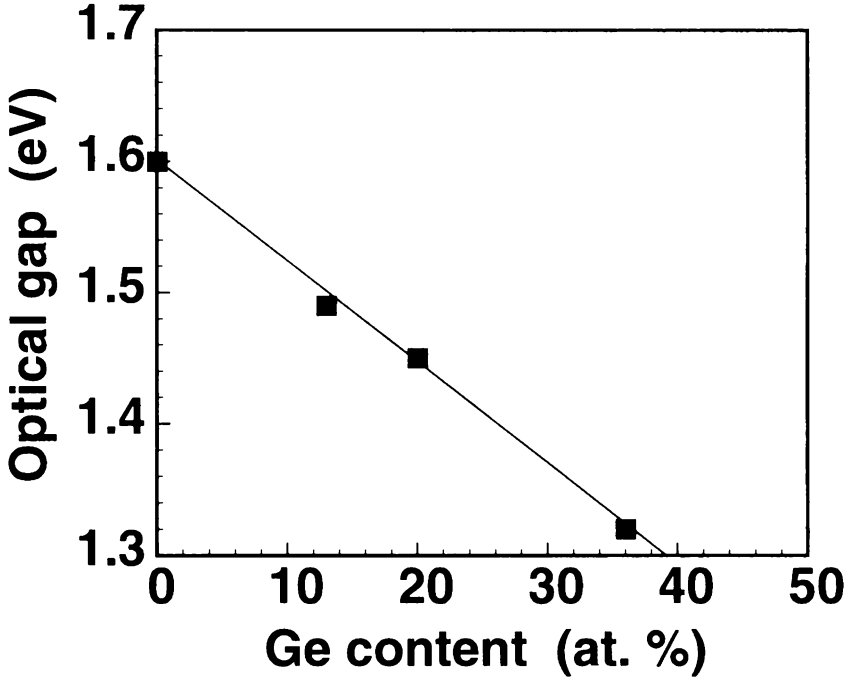

Fig. 2.6 Optical gap (E_{opt}) of a-SiGe:H deposited at 230℃ as a function of the germanium content (C_{Ge}).

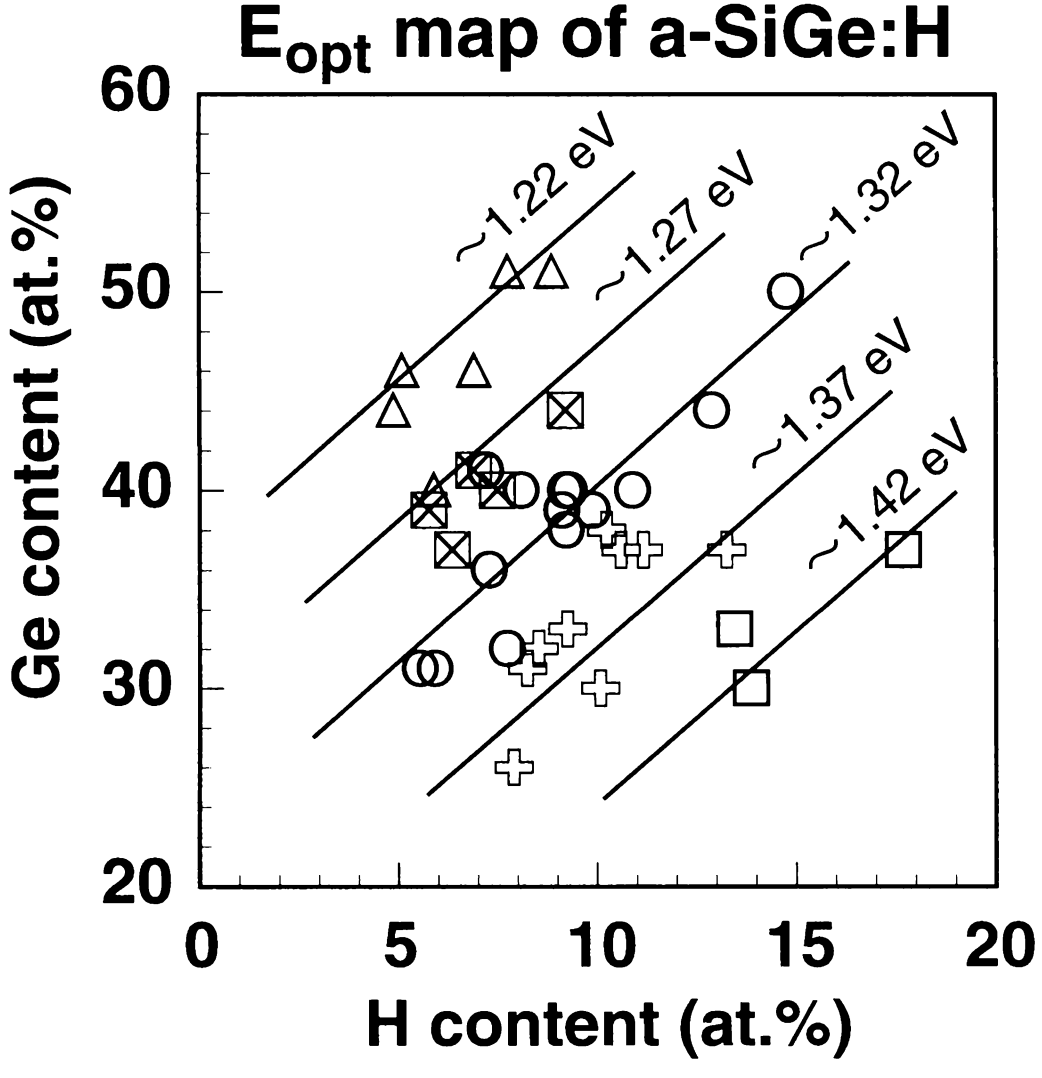

Fig. 2.7 Optical gap (E_{opt}) contour map of a-SiGe:H deposited at various temperatures and gas flow ratios as a function of the germanium content (C_{Ge}) and hydrogen content (C_H).

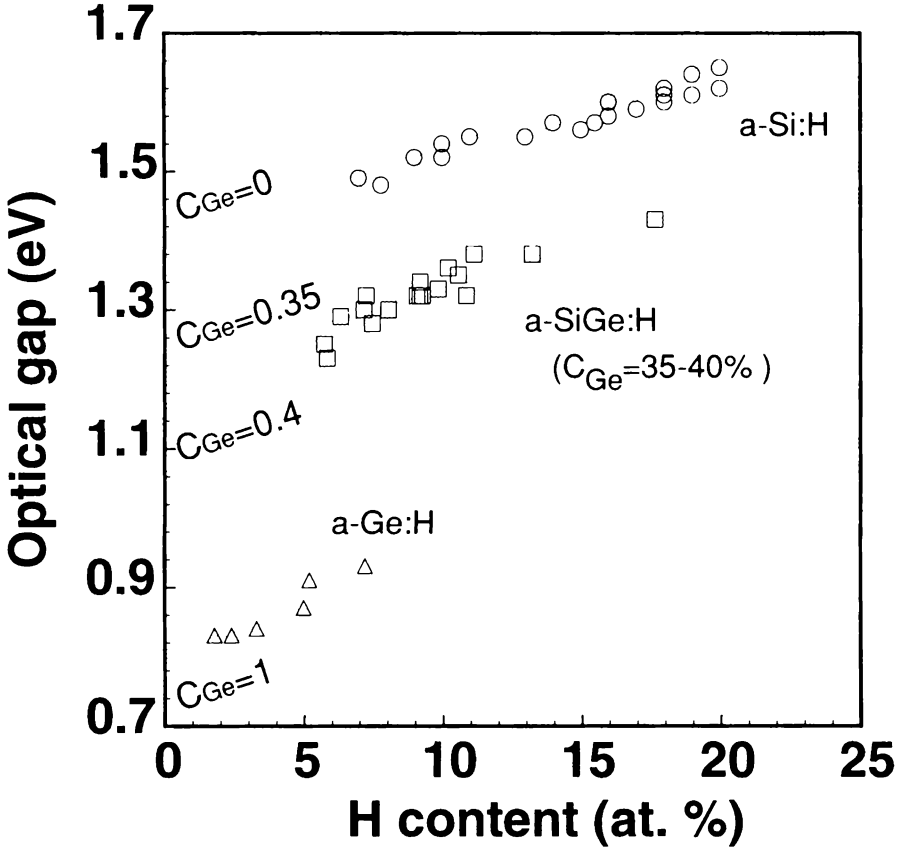

Fig. 2.8 Optical gap (E_{opt}) of a-Si:H (open circle), a-Ge:H (open triangle) and a-SiGe:H (open square) as a function of the hydrogen content (C_H).

$$E_{opt} = 1.3C_H - 0.6C_{Ge} + 1.4 \text{ (eV)}. \quad (2.4)$$

The absolute coefficient of C_{Ge}, –0.6, in Eq. (2.4) is smaller than –0.78 from Fig. 2.6. A part of the change in E_{opt} with C_{Ge} in Fig. 2.6 should be ascribed to the variation in C_H, which is known to decrease with the increase in C_{Ge} at a fixed T_s and rf power [32,33] as shown in Figs. 2.2(a) and 2.2(b). C_{Ge} does not make much difference on the gradient of E_{opt} versus C_H in Fig. 2.8. Disregarding the existence of atomic vacancies or voids, and the transition of the film rigidness caused by the difference in C_H, the widening of E_{opt} with C_H is due to the valence band energy being pushed down because the Si–H (3.35eV) or Ge–H (2.99eV) bonds are stronger than Si–Si (1.83eV) or Ge–Ge (1.63eV) bonds.[13,34-36] An increase in the bond energy per hydrogen atom, caused by switching Si–Si bonds to Si–H bonds, or Ge–Ge bonds to Ge–H bonds, can be respectively represented as follows,

$$E(\text{Si–H}) - E(\text{Si–Si})/2 \fallingdotseq 2.4 \text{ (eV)}, \quad (2.5)$$

$$E(\text{Ge–H}) - E(\text{Ge–Ge})/2 \fallingdotseq 2.2 \text{ (eV)}, \quad (2.6)$$

where E(X–Y) indicates X–Y bond energy. The nearness of these two values is probably the reason why the incline of E_{opt} to C_H is only slightly dependent on the [Ge]/[Si] atomic ratio. Although the physical grounds are insufficient, Eq. (2.4) shows good agreement with the experimental results in a wide range of C_{Ge} as a first order approximation (see Fig. 2.8). Generally, the tendency has been to indicate a-SiGe:H film properties as functions of C_{Ge} or E_{opt}. However, a clearer demonstration can be expected by using the functions of C_H and C_{Ge} as shown in Fig. 2.7, with regarding a-SiGe:H as a ternary alloy of silicon, germanium and hydrogen.

2.5 Optimized composition for a certain optical gap (E_{opt} = 1.32 eV)

In designing solar cells, E_{opt} of the photovoltaic layer is an essential factor which should be

optimized beforehand, because it limits the output current and voltage of the devices. However, E_{opt} of a-SiGe:H depends strongly on not only C_{Ge} but also C_H and follows a linear function of C_H and C_{Ge}, as pointed out in the previous section. For this reason, a-SiGe:H samples with various combinations of C_H and C_{Ge} can have the same E_{opt}. However, their electronic properties can differ from each other due to variations in their composition. In this section the optimum composition was investigated for a-SiGe:H with a certain E_{opt} for stable solar cells. The properties of both films and p-i-n devices were compared among samples with constant E_{opt} and various compositions. The film properties and performance of solar cells before and after light soaking were investigated. The results were related to the C_H and hydrogen bonding configurations.

2.5.1 Composition dependence of film properties

a-SiGe:H films with the same E_{opt} and various compositions were prepared. The substrate temperature and $[SiH_4]/[GeH_4]$ flow ratio were carefully controlled by the combinations of C_{Ge} and C_H to keep E_{opt} constant. A relatively low hydrogen dilution was used: the dilution ratio, $[H_2]/([SiH_4]+[GeH_4])$ was kept at ~2.5. The samples were 300-500 nm thick. E_{opt} of 1.32eV (which corresponds to 1.4-1.45eV by Tauc's method) was chosen in this study because it is empirically known to be suitable as the bottom i layer of double- or triple-junction stacked solar cells. Figure 2.9 shows the relationship between C_H and C_{Ge} for the samples in which E_{opt} is constant at 1.32 ± 0.005 eV. E_{opt} of these samples approximately follows Eq. (2.4). The sample with more C_H contains more C_{Ge} because of the constant E_{opt}. Figures 2.10(a)-2.10(c) show σ_{ph}, σ_d, E_{ch}, and N_D as functions of C_H. More than 10 at.% of C_H results in deterioration of σ_{ph} and σ_d (Fig. 2.10(a)). The C_H values for both the minimum E_{ch} and the minimum N_D exist at ~10 at.%, and they are close to each other (Figs. 2.10(b) and 2.10(c)). A similar correspondence between the N_D and E_{ch} for a-Si:H has also been reported.[37,38] To explain this tendency, Stutzmann has ascribed the initial N_D in a-Si:H to the equilibrium of the weak-bond state and the dangling-bond state which arises from the breaking of weak Si-Si bonds.[37] The correlation between E_{ch} and N_D in Figs. 2.10(b) and 2.10(c) is quantitatively consistent with Stutzmann's bond-breaking model.

Figure 2.11 illustrates the bonded hydrogen content in the different configurations, such as

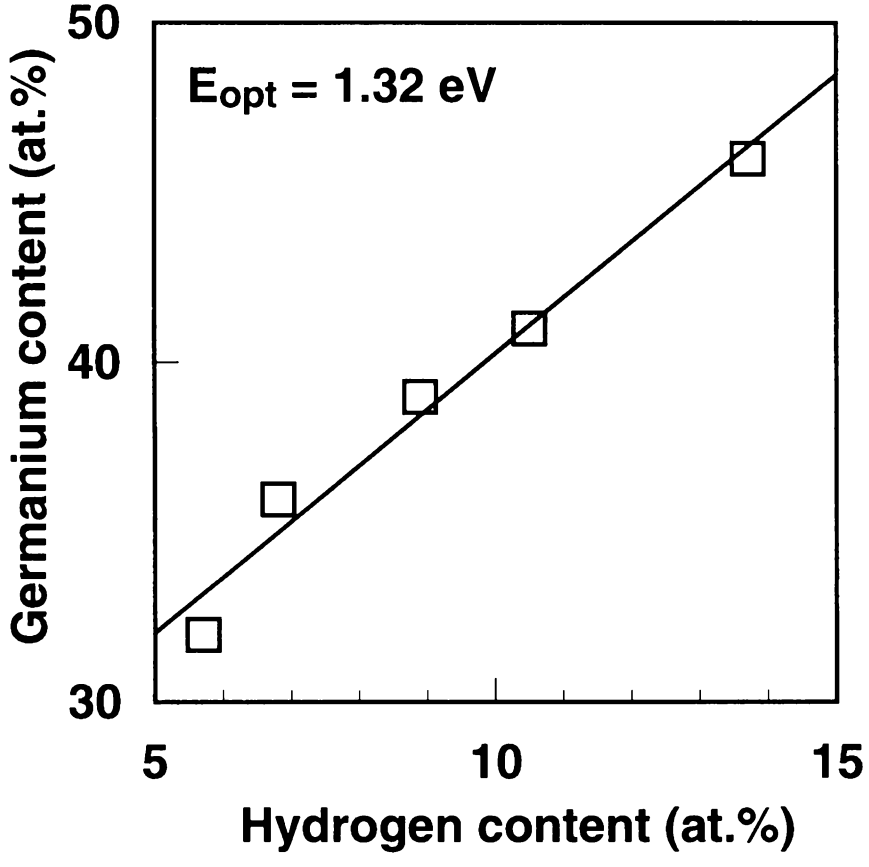

Fig. 2.9 The relationship of the germanium content (C_{Ge}) and hydrogen content (C_H) for a-SiGe:H with a constant optical gap (E_{opt}) of 1.32 eV.

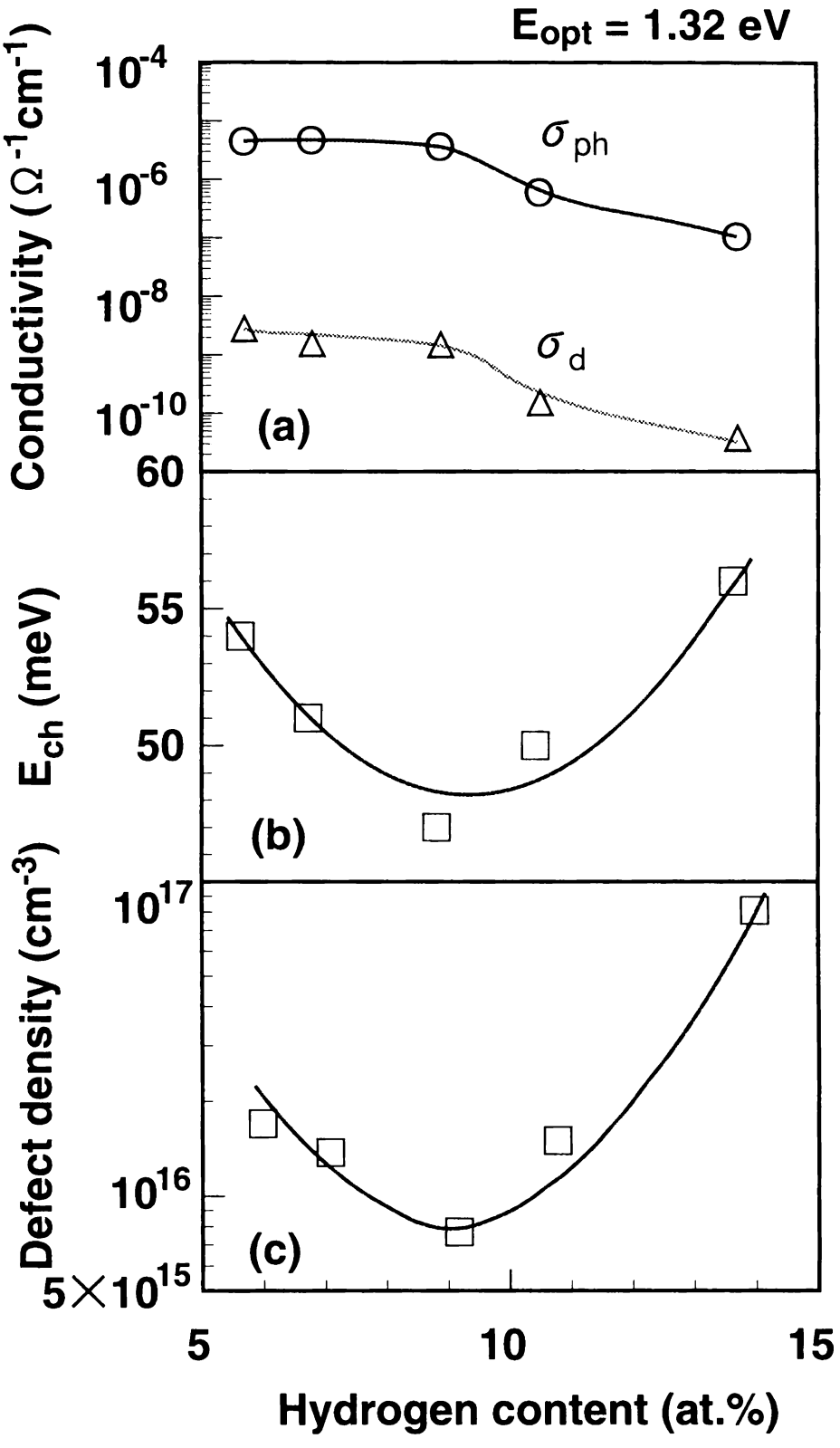

Fig. 2.10 (a) The photoconductivity (σ_{ph}) and dark conductivity (σ_{d}), (b) the characteristic energy of the Urbach tail (E_{ch}), and (c) the defect density (N_D) of the a-SiGe:H samples with a constant E_{opt} (~1.32 eV) as functions of the hydrogen content (C_H).

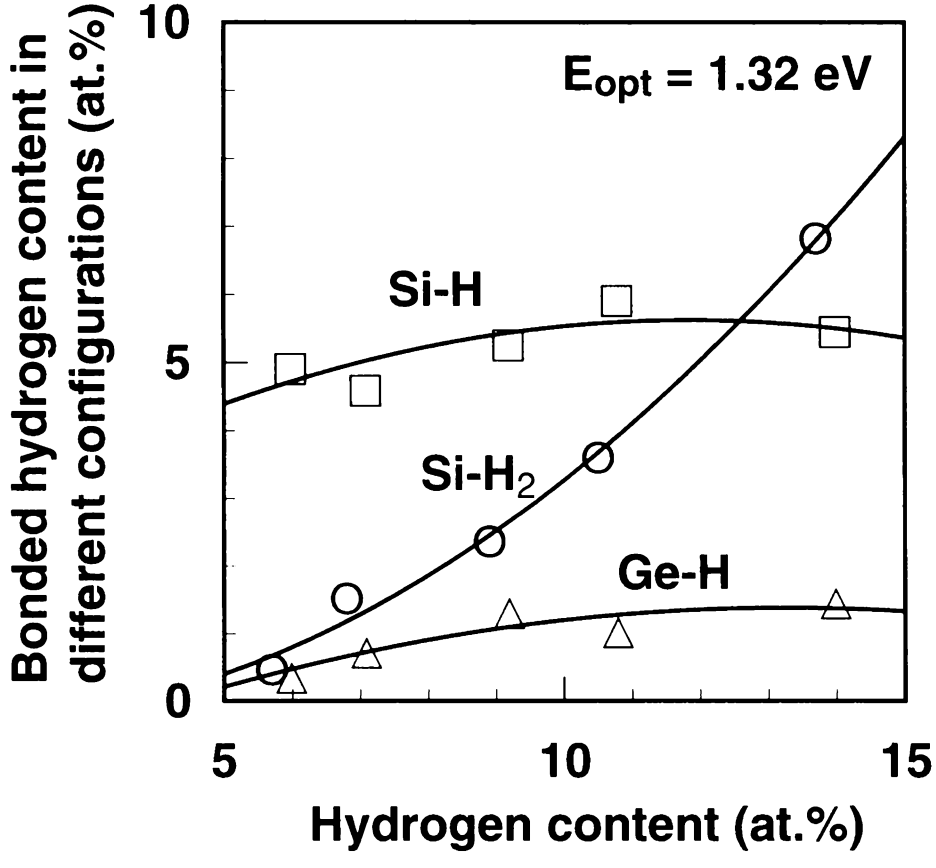

Fig. 2.11 The bonded hydrogen content of a-SiGe:H samples with a constant E_{opt} (~1.32eV) in different configurations, such as Si-H, Si-H_2, and Ge-H, as functions of the total hydrogen content (C_H).

$C_{H(Ge-H)}$, $C_{H(Si-H)}$, and $C_{H(Si-H2)}$, determined from IR absorption spectra, as a function of the total hydrogen content, C_H. The amount of hydrogen bonded to germanium, $C_{H(Ge-H)}$, is much less (factor 5) than that to silicon, ($C_{H(Si-H)}$+ $C_{H(Si-H2)}$), although C_{Ge} of these samples is 30-45 at.% (Fig. 2.9). This is due to the preferential attachment of hydrogen to silicon rather than to germanium as previously reported.[1,27] The dependence of $C_{H(Ge-H)}$ on C_H is weaker than that of ($C_{H(Si-H)}$ + $C_{H(Si-H2)}$) on C_H, and thus, it is suggested that the difference in film properties shown in Figs. 2.10(a)-2.10(c) is caused by the hydrogen bonded to silicon. The most important role of the hydrogen in a-Si alloys is (a) to terminate dangling bonds and (b) to relax the bonding network. In the region where C_H is lower than 8 at.%, the lack of hydrogen debases these functions, and E_{ch} and N_D increase (Figs. 2.10(b)-2.10(c)). On the other hand, the dihydride hydrogen content, $C_{H(Si-H2)}$, monotonically increases with the increase in C_H, while the monohydride hydrogen contents, $C_{H(Ge-H)}$ and $C_{H(Si-H)}$ are almost constant (Fig. 2.11). Too much Si-H_2 degrades the electronic and structural properties in the region where C_H is higher than 12 at.% (Figs. 2.10(b) and 2.10(c)). The balance between the defect termination and structural relaxation due to added hydrogen atoms, and the deterioration caused by the increasing density of Si-H_2 determine the optimum C_H at around 10 at.% in the system of E_{opt}=1.32eV. Generally, for a-Si:H deposited by the ordinary plasma-CVD method, C_H of ~15 at.% is considered to be appropriate. The optimum C_H of ~10 at.% for the a-SiGe:H samples is smaller than the value for a-Si:H. This may be due to the preferential attachment of hydrogen to silicon over germanium. a-SiGe:H contains more $C_{H(Si-H2)}$ than a-Si:H, when their C_H is the same, because the larger number of hydrogen atoms provided per silicon atom in a-SiGe:H raises the probability of existence of Si-H_2. Therefore, in a-SiGe:H, the deterioration in the high C_H region occurs more swiftly and the suitable C_H is lower than in a-Si:H. More details of the inhomogeneous hydrogen bonding configurations in a-SiGe:H are discussed in Chapter 3.

2.5.2 Composition dependence of cell performance

These a-SiGe:H films with constant E_{opt} were applied to the i layers of a-SiGe single-junction and a-Si/a-SiGe double-junction solar cells, which consisted of TCO/ p(a-SiC:H)/ i(a-SiGe:H)/ n(a-Si:H)/ metal, and TCO/ p(a-SiC:H)/ i(a-Si:H)/ n(a-Si:H)/ p(a-SiC:H)/ i(a-SiGe:H)/ n(a-Si:H)/ metal,

respectively. The thin and flat-gap a-SiGe:H was used for the i layer.[39] Figure 2.12 indicates the initial conversion efficiency of a-SiGe single-junction solar cells under red light (1sun AM-1.5 with an optical filter "R65", which sharply cuts out the light wavelengths shorter than 650nm) as a function of C_H of the i layer. The i-layer thickness of these cells was constant at ~150 nm. The variation in the conversion efficiency is mainly due to that of the fill factor (*FF*). An optimum C_H ~10 at.% also exists for the maximum conversion efficiency. The tendencies of the conversion efficiency in Fig. 2.12 reflect those of N_D (see Fig. 2.10(c)), which control the recombination loss of generated carriers in the i-layer and affect the conversion efficiency via *FF*.

In addition to N_D, E_{opt}, which limits the built-in potential and the number of absorbed photons, also affects the conversion efficiency via the product of the open circuit voltage (V_{oc}) and the short-circuit current (I_{sc}), — and probably via *FF* as well. Using an experimental system in which only the substrate temperature or $[SiH_4]/[GeH_4]$ flow ratio is changed, a composition for the lowest N_D will also be observed, but this will not always offer the highest conversion efficiency because of the variation of E_{opt}. The influence of N_D upon the conversion efficiency becomes even smaller when the i layer becomes thinner, because the stronger internal electric field tends to keep *FF* higher. In this study, in spite of the thin i-layer, a very clear correspondence was observed between the film properties and the cell performance, because the constant E_{opt} kept V_{oc}, I_{sc}, and the internal electric field constant.

The optimum composition of a-SiGe:H for the initial properties of both films and solar cells was observed for the constant E_{opt} (Figs. 2.10 and 2.12). For photovoltaic materials, however, the stability against light irradiation is also an important factor. Figure 2.13 shows the normalized conversion efficiency, which is the value divided by the initial conversion efficiency, of a-SiGe single-junction solar cells after red light soaking for 0.25, 6 and 140 hours (5 sun, AM-1.5 with R65 filter at 48°C under open circuit condition) as a function of C_H of the i layer. The normalized conversion efficiency against almost has a negative linear relation to C_H, and the incline against C_H becomes larger with greater light soaking time. This means that the degradation ratio of the solar cell becomes lager with the increase in C_H (or C_{Ge}) of the i-layer. These results suggest that the incorporated hydrogen or Si-H_2 (which increases with C_H, as shown in Fig. 2.11) enhances or

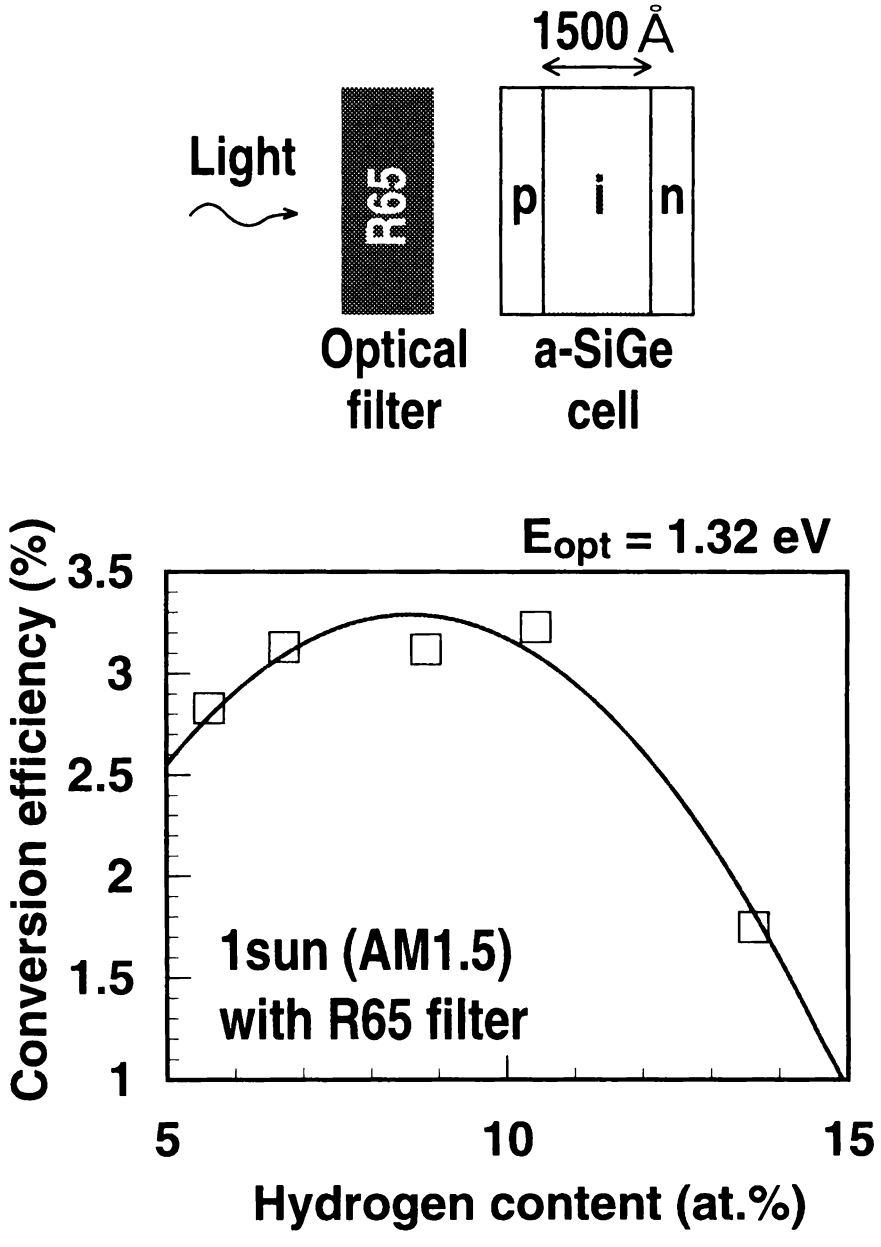

Fig. 2.12 The initial conversion efficiency of a-SiGe single-junction solar cells with a constant E_{opt} (~1.32 eV) under red light illumination (1sun, AM-1.5 through R65 optical filter) as a function of the hydrogen content of the i layer.

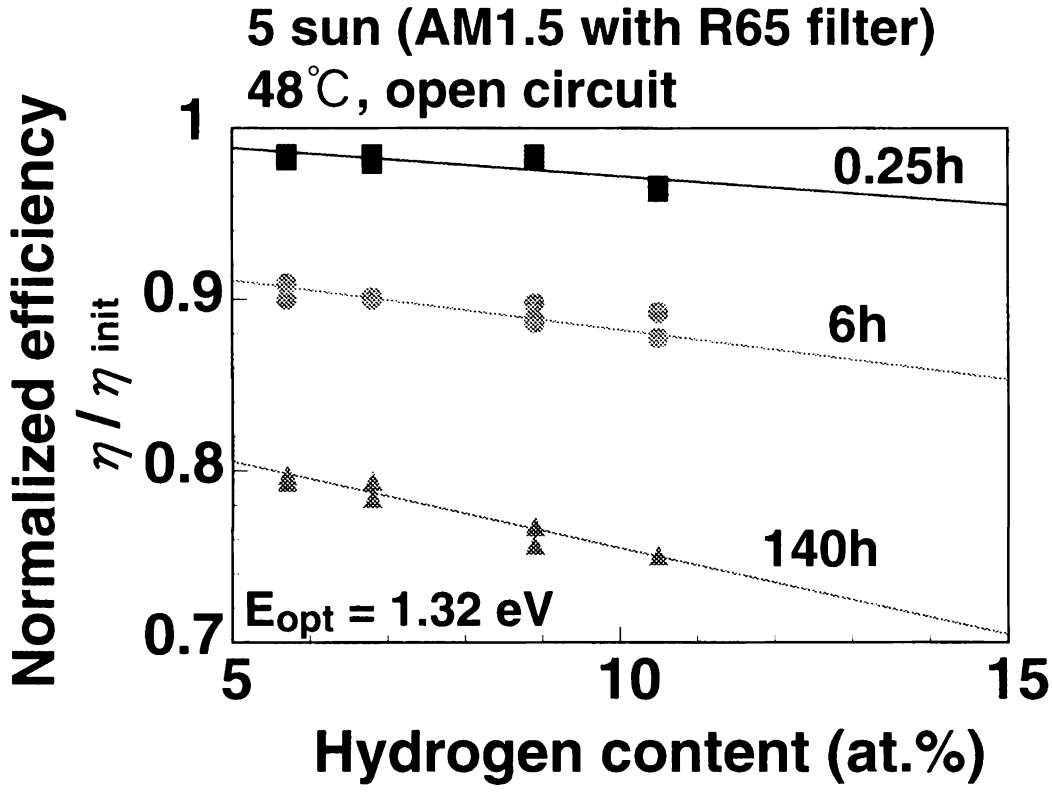

Fig. 2.13 Normalized conversion efficiency, which is the value divided by the initial conversion efficiency, of a-SiGe single-junction solar cells after red light soaking for 0.25, 6 and 140 hours (5 sun, AM-1.5 with R65 filter at 48°C under open circuit condition) as a function of C_H of the i layer.

assists the creation of light-induced defects, although the effect of Ge is not revealed yet. More details of the effects of compositions on the stability are discussed in Chapter 4. Consequently, the optimum compositions are believed to shift to the lower C_H region, though the amount of the shift depends on the degradation conditions such as the light intensity, light soaking time, temperature and i-layer thickness. The world's most efficient solar cells applied this concept to cell design are introduced in Chapter 5.

2.6 Summary

A detailed study of a-SiGe:H films deposited by a plasma-CVD method using SiH_4, GeH_4, and H_2 gas mixtures has been demonstrated with paying careful attention to its composition: both C_H and C_{Ge}. Furthermore, the properties have been compared among a-SiGe:H films and solar cells with a constant optical gap of 1.32 eV and different combinations of C_H and C_{Ge}.

(1) Concerning the correlation of film properties with deposition conditions, (a) C_{Ge} depends only slightly on T_s and decreases with a rise in rf power, (b) C_H increases with a decrease in T_s or an upturn of R_D, (c) the optimum R_D, which corresponds to the maximum photo-sensitivity, depends on T_s.

(2) E_{opt} is controllable by changing T_s and R_D, in addition to the $[GeH_4]/[SiH_4]$ source gas mixture ratio, and can be expressed by a linear function of C_H and C_{Ge}. As a result, films with different compositions can have the same E_{opt}.

(3) The optimum composition for initial properties, such as the Urbach tail characteristic energy, defect density, and conversion efficiency of solar cells, was determined for a certain E_{opt} (= 1.32 eV). These tendencies can be explained in terms of the hydrogen bonding configuration.

(4) The optimum composition for a certain E_{opt} shifts to the lower C_H region after light soaking due to the larger degradation for higher C_H samples. This suggests that hydrogen or $Si\text{-}H_2$ plays an important role in light-induced degradation.

References

1. W. Paul, D.K. Paul, B.Von Roedern, J. Blake and S. Oguz, Phys. Rev. Lett. **46**, 1016 (1981).
2. L. Yang, J. Newton and B. Fieselmann, Mater. Res. Soc. Symp. Proc. **149** , 497 (1989).
3. A. Matsuda, M. Koyama, N. Ikuchi, Y. Imanishi and K. Tanaka, Jpn. J. Appl. Phys. **25**, L54 (1986).
4. H. Haku, K. Sayama, Y. Nakashima, T. Takahama, M. Isomura, H. Tarui, Y. Hishikawa, S. Tsuda, S. Nakano, M. Ohnishi and Y. Kuwano, Jpn. J. Appl. Phys. **26**, 1978 (1987).
5. J. Chevalier, H. Wieder, A. Onton and C.R. Guarnieri, Solid State Commu. **24**, 867 (1977).
6. L. Tichy and A. Trisk, Solid State Commu. **41**, 751 (1982).
7. K.D. Mackenzie, J.H. Burnette, J.R. Eggert, Y.M. Li and W. Paul, Phys. Rev. B **38**, 6120 (1988).
8. L. Chen, J. Tauc, T.K. Lee and E.A. Sciff, J. Non-Cryst. Solids **114**, 585 (1989).
9. S. Wagner, V. Chu, J.P. Conde and J.Z. Liu, J. Non-Cryst. Solids **114**, 453 (1989).
10. E. Lotter and G.H. Bauer, J. Non-Cryst. Solids **114**, 322 (1989).
11. M. Stutzmann, R.A. Street, C.C. Tsai, J.B. Boyce and S.E. Ready, J. Appl. Phys. **66**, 569 (1989).
12. Z.E. Smith, A. Matsuda, H. Matsuura, H. Oheda, M. Tanaka and S. Yokoyama, J. Non-Cryst. Solids **114**, 48 (1989).
13. D.A. Papaconstantopoulos and E.N. Economou, Phys. Rev. B **24**, 7233 (1981).
14. G.D. Cody, C.R. Wronski, B. Abeles, R.B. Stephens and B. Brooks, Solar Cells **2**, 227 (1980).
15. A. Matsuda, M. Matsumura, S. Yamasaki, H. Yamamoto, T. Imura, H. Okushi, S. Iizuma and K. Tanaka, Jpn. J. Appl. Phys. **20**, 183 (1981).
16. R.C. Ross and J. Jaklik,Jr., J. Appl. Phys. **55**, 3785 (1984).
17. Y. Hishikawa, S. Tsuda, K. Wakisaka and Y. Kuwano, J. Appl. Phys. **73**, 4227 (1993).
18. Y. Hishikawa, M. Sasaki, S. Tsuge, S. Okamoto and S. Tsuda, Mater. Res. Soc. Symp. Proc. **297**, 779 (1993).
19. S. Tsuda, T. Takahama, M. Isomura, H. Tarui, Y. Nakashima, Y. Hishikawa, N. Nakamura, T. Matsuoka, H. Nishikuni, S. Nakano, M. Ohnishi and Y. Kuwano, Jpn. J. Appl. Phys. **26**, 33 (1987).
20. Y. Hishikawa, S. Tsuge, N. Nakamura, S. Tsuda, S. Nakano and Y. Kuwano, Appl. Phys. Lett. **57**, 771 (1990).
21. Y. Hishikawa, N. Nakamura, S. Tsuda, S. Nakano, Y. Kishi and Y. Kuwano, Jpn. J. Appl. Phys. **30**, 1008 (1991).
22. V. Vorlicek, M. Zavetova, S.K. Pavlov and L. Pajasova, J. Non-Cryst. Solids **45**, 289 (1981).
23. M. Vanecek, J. Kocka, J. Stuclik and A. Triska, Solid State Commun. **39**, 1199 (1981).
24. M. Sasaki, S. Okamoto, Y. Hishikawa, S. Tsuda and S. Nakano, Sol. Energy Mater. & Sol.

Cells **34**, 541 (1994).

25. J.H. Scofield, J. Electron Spectrosc. **8**, 129 (1976).
26. C.J. Fung, K.J. Gruntz, L. Ley, M. Cardona, F.J. Demond, G. Muller and S. Kalbitzer, J. Non-Cryst. Solids **35 & 36**, 255 (1980).
27. S.Z. Weisz, M. Gomez, J.A. Muir, O. Restro, R. Perez, Y. Goldstein and B. Abeles, Appl. Phys. Lett. **44**, 634 (1984).
28. K.D. Mackenzie, J.R. Effert, D.J. Leopold, Y.M. Li, S. Lin and W. Paul, Phys. Rev.B **31**, 2198 (1985).
29. F.J. Kampas and R.W. Grittith, Appl. Phys. Lett. **39**, 407 (1981).
30. Y.S. Tsuo, Y. Xu, E.A. Ramsay, R.S. Crandall, S.J. Salamon, I. Balberg, B.P. Nelson Y. Xiao and Y. Chen, Mater. Res. Soc. Symp. Proc.**219**, 769 (1991).
31. J. Tauc, R. Grigorovici and A. Vancu, Phys. Status Solidi B **15**, 627 (1966).
32. A. Morimoto, T. Miura, M. Kumeda and T. Shimizu, Jpn. J. Appl. Phys. **20**, L833 (1981).
33. W. Beyer, J. Non-Cryst. Solids **97&98**, 1027 (1987).
34. L. Pauling, *The Nature of the Chemical Bond* (Cornell University Press, Ithaca, New York, 1960) 3rd ed., p.78.
35. F.A. Cotton and G. Wilkinson, *Advenced Inorganic Chemistry* (Interscience, New York, 1972) 3rd ed., p.113.
36. J.E.Huheey, *InorganicChemistry* (Harper and Row, New York, 1978) 2nd ed., p.848.
37. M. Stutzmann, Philos. Mag. B **60**, 531 (1989).
38. Y. Hishikawa, M. Isomura, S. Okamoto, H. Hashimoto and S. Tsuda, Sol. Energy Mater. & Sol. Cells **34**, 303 (1994).
39. E. Maruyama, A. Terakawa, K. Sayama, K. Ninomiya, Y. Hishikawa, H. Tarui, S. Tsuda, S. Nakano and Y. Kuwano, *Proc. 23rd IEEE Photovoltaic Specialists Conf.* (Louisville, 1993) p.827.

Chapter 3
Inhomogeneous Hydrogen Bonding Structures in a-SiGe:H

3.1 Background

Incorporated H atoms and their bonding structures are important for determining the properties of a-Si alloys. It has been often reported that material qualities such as photo-conductivity, defect density and photo-stability of a-Si related materials deteriorate with increasing dihydride concentration ([Si–H_2]), evaluated by the decomposition of IR absorption peaks centered at ~2000 and ~2100 cm^{-1}.[1-6] The H content ,C_H, in the material is one of the key factors determining the H bonding structure in a-Si:H deposited by plasma CVD, partly because the probability of multiple H atoms bonding to one Si atom increases with C_H. Indeed, many previous studies have already reported that [Si–H_2]/[Si–H] has a 1 on 1 positive correlation to C_H for a-Si:H deposited by various deposition systems such as plasma CVD or magnetron sputtering method.[2,7-10] Another important factor is the process condition. For example, it is known that [Si–H_2] can be reduced independently from C_H by the use of highly H_2-diluted SiH_4 plasma or post H-plasma treatment.[3,6] In this way, quantitative comprehension of the H bonding configurations in a-Si:H has been steadily progressing.

a-SiGe:H is a tetrahedrally bonding semiconductor as well as a-Si:H. It has also been suggested that Si–H_2 configurations in a-SiGe:H films cause the deterioration of the photoelectric properties of the materials and solar cell performances including stability against light exposure.[4,11] However, the H bonding structure in a-SiGe:H is much less understood than that of a-Si:H due to the feature of H atoms selectively bonding to Si rather than to Ge, so-called "preferential attachment."[12-14] This feature is believed to cause a microscopic inhomogeneity in the network and to deteriorate the electronic properties of the alloys. The preferential attachment is probably due to the smaller binding energy of H–Ge than that of H–Si. However, the detailed mechanisms determining the preference of H bonding and the deterioration of material properties are not clear yet.

The purpose of the study in this chapter is to reveal the principle of H bonding in device-quality

a-SiGe:H alloys deposited by rf plasma CVD from SiH_4, GeH_4 and H_2 mixture gas. The correlations between the H bonding configurations and C_H of a-SiGe:H alloys with various compositions were systematically investigated. In order to separately consider the microstructures around Si and Ge, the author focuses on the C_H per host atom, namely Si or Ge. The results of a-SiGe:H are discussed by comparing with those of a-Si:H and hydrogenated amorphous germanium (a-Ge:H). The origin of H bonding preference is also mentioned in connection with the deposition kinetics. Furthermore, the construction mechanism of H–Si bonding structures is also discussed.

3.2 Experimental

a-SiGe:H films with various compositions were prepared in a UHV (ultra high vacuum) rf plasma reactor from a gas mixture of SiH_4, GeH_4 and H_2. The deposition conditions are shown in Table 3.1. The a-SiGe:H films of 2000-5000 Å thick were deposited simultaneously on Corning #7059 glass substrates for optical and compositional measurements, and on silver-coated glass substrates for infrared reflectance absorption spectroscopy (IR-RAS) measurement. C_{Ge} (= [Ge]/([Si]+[Ge]) atomic ratio) was determined by the X-ray photoelectron spectroscopy (XPS) method. C_H was evaluated by combining the XPS and secondary ion mass spectroscopy (SIMS) methods. The H bonding configurations were observed using the reflectance IR absorption spectra measured for the samples on the silver-coated glass substrates and subtracted from the silver reflectance spectra. The details of these composition analysis were shown in Chapter 2 (see 2.2.

Table 3.1 Deposition conditions of samples.

Substrate temperature	80-350	℃
Reaction pressure	~20	Pa
Background pressure	10^{-5}-10^{-6}	Pa
RF power density	20-50	mW/cm^2
Hydrogen dilution ratio		
$[H_2]/([GeH_4]+[SiH_4])$	0-30 for a-Si:H	
	10 for a-Ge:H	
	2.5-40 for a-SiGe:H	

Experimental).

3.3 Composition dependence of hydrogen bonding configurations

3.3.1 H–Si bonding configurations in a-Si:H and a-Ge:H

Figure 3.1 shows the microstructure factor of a-Si:H, [Si–H_2]/[Si–H], deposited from low-diluted ([H_2]/[SiH_4] < 2.5) and high-diluted ([H_2]/[SiH_4] > 10) source gases plotted against C_H. [Si–H_2]/[Si–H] for the low-diluted a-Si:H samples has 1 on 1 correlations to C_H, as previously reported.[5, 10-13] The [Si–H_2]/[Si–H] ratio can be reduced independently from C_H by the use of high dilution. Figure 3.2 shows the microstructure factor of a-Ge:H, [Ge–H_2]/[Ge–H], deposited from diluted source gases ([H_2]/[GeH_4] = 10) plotted against C_H. [Ge–H_2]/[Ge–H] in a-Ge:H also has 1 on 1 correlations to C_H and increases more drastically with C_H than that of a-Si:H, in spite of the higher dilution ratio. This is partly because the a-Ge:H samples with high C_H (> 7 at.%) should have been deposited at very low temperatures (< 100℃). When deposited at higher temperatures than 150 ℃, the C_H and [Ge–H_2]/[Ge–H] of a-Ge:H are less than 8 at.% and 0.2, respectively.

3.3.2 H–Si bonding configurations in a-SiGe:H

The bonding H contents per host atom for Si and Ge in a-SiGe:H were defined respectively as follows,

$$C_{H(Si)} = ([Si–H_2]+[Si–H])/[Si], \tag{3.1}$$

$$C_{H(Ge)} = [Ge–H]/[Ge]. \tag{3.2}$$

Here, the relation, $C_H = (1-C_{Ge})\times C_{H(Si)}+C_{Ge}\times C_{H(Ge)}$, follows. Figure 3.3 shows the relationship between $C_{H(Si)}$ and $C_{H(Ge)}$ in a-SiGe:H with various compositions. C_H in the films were widely varied by changing the substrate temperature from 80 to 350℃. One can see that only $C_{H(Si)}$ increases with increasing C_H, and $C_{H(Ge)}$ is almost constant at 2-4 at.%. The results in Fig. 3.3 suggest that the differences of H–Si bonding structure are more dominant than H–Ge when

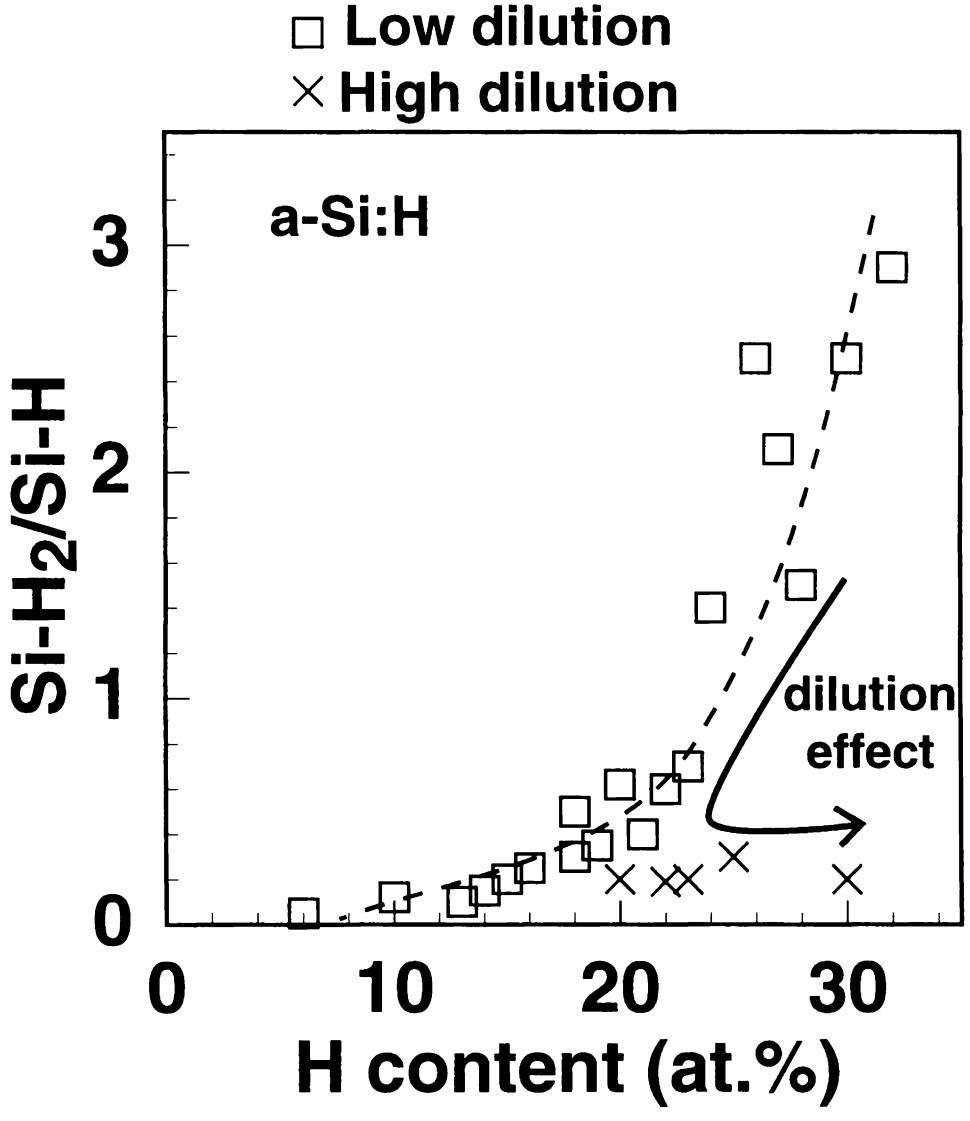

Fig. 3.1 [Si-H_2]/[Si-H] plotted against C_H for a-Si:H deposited from low-diluted ([H_2]/[SiH_4] < 2.5) and highly diluted ([H_2]/[SiH_4] > 10) source gases. The arrow indicates a schematic trend when increasing dilution ratio.

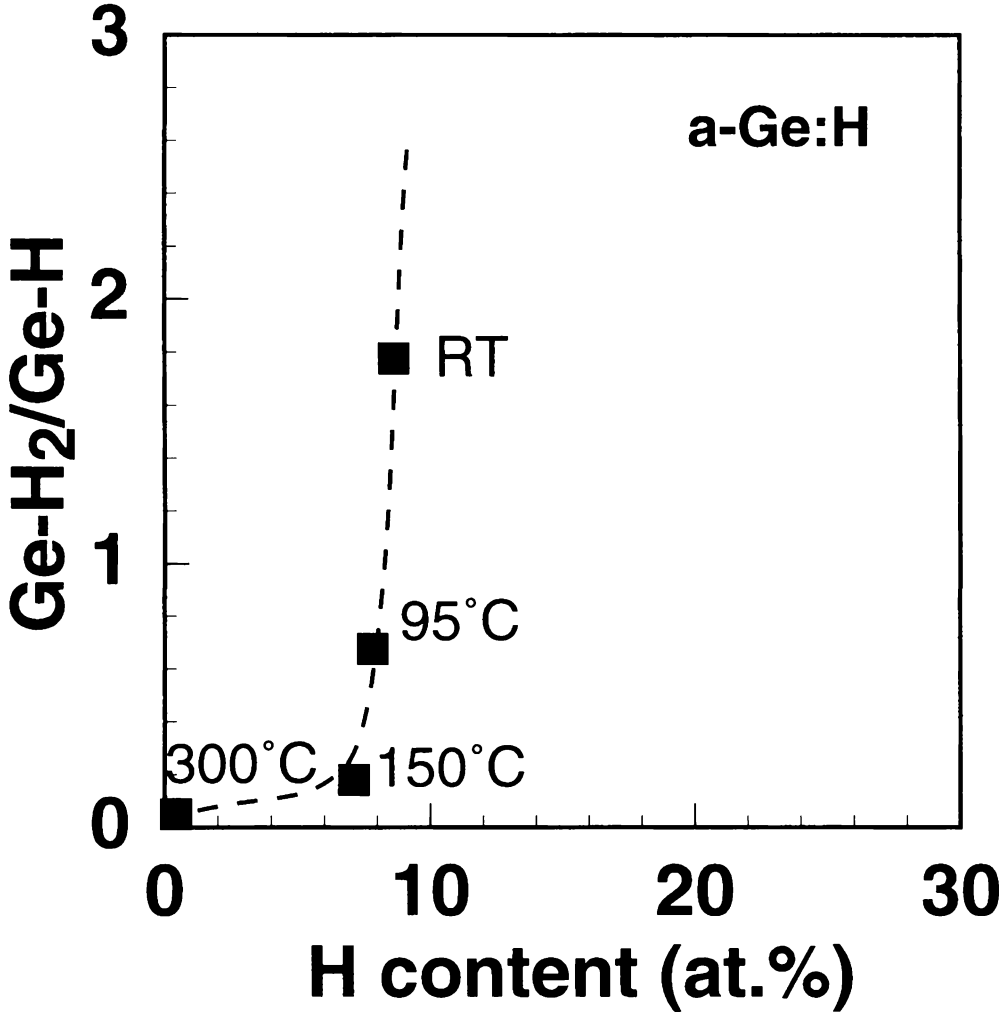

Fig. 3.2 [Ge-H_2]/[Ge-H] plotted against C_H for a-Ge:H deposited from diluted source gases ([H_2]/[GeH_4] = 10). C_H was controlled by varying the process temperature from room temperature to 300℃.

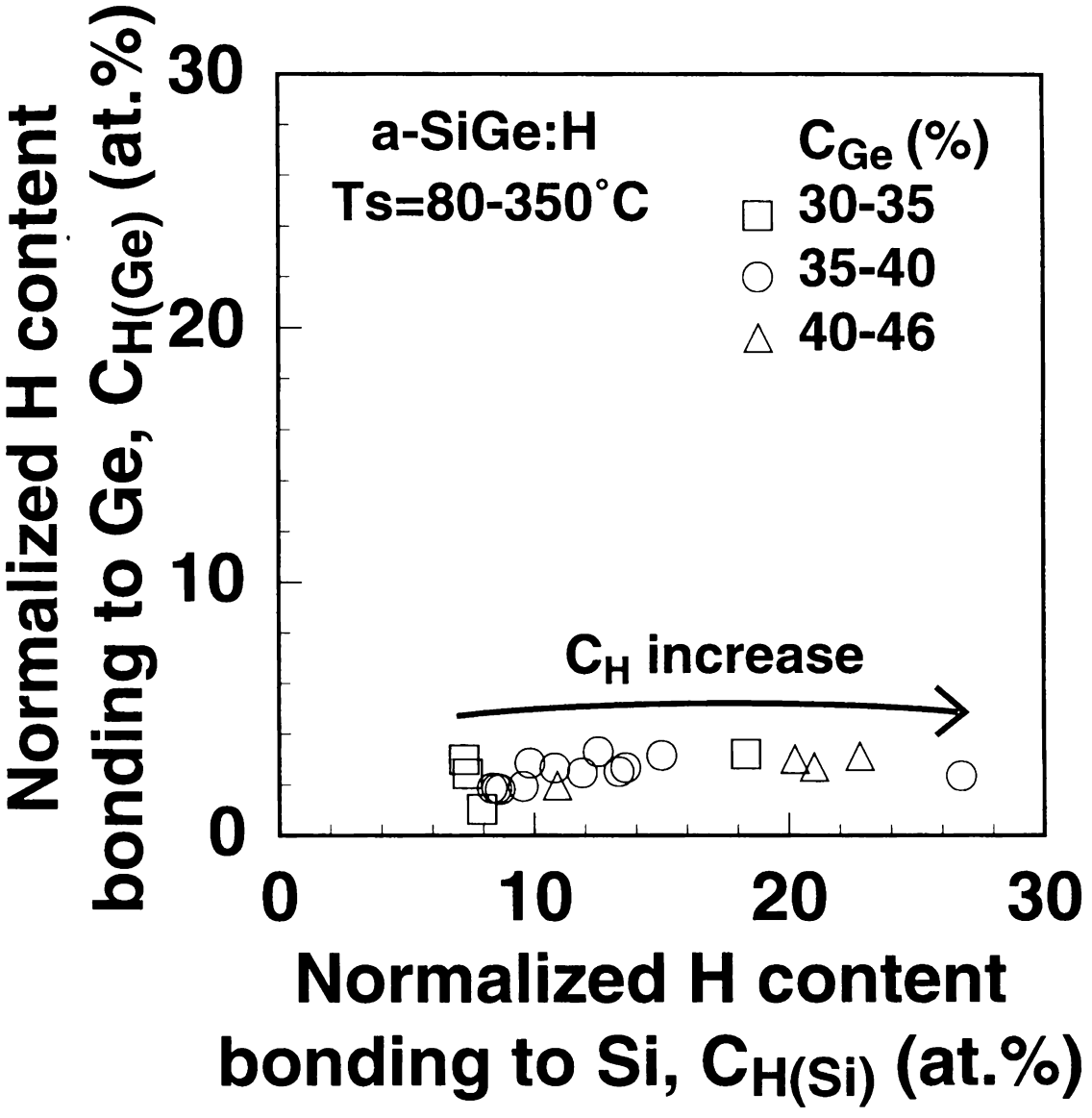

Fig. 3.3 The relationship between $C_{H(Si)}$ (=([Si-H_2]+[Si-H])/[Si]) and $C_{H(Ge)}$ (= [Ge-H]/[Ge]) in a-SiGe:H with C_{Ge} = 30-60 at.%.

comparing the a-SiGe:H samples with various C_H. The author thus focused on the H–Si bonding configurations in a-SiGe:H. Figure 3.4 shows the [Si–H_2]/[Si–H] of a-SiGe:H samples deposited from low-diluted ([H_2]/([SiH_4]+[GeH_4] = 2.5) and high-diluted ([H_2]/([SiH_4]+[GeH_4] = 20-40) mixture gases as a function of $C_{H(Si)}$. The broken line in Fig. 3.4 indicates the [Si–H_2]/[Si–H]-C_H trend of low-diluted a-Si:H replotted from Fig. 3.1. The [Si–H_2]/[Si–H]-$C_{H(Si)}$ correlation of the low-diluted a-SiGe:H is similar to the [Si–H_2]/[Si–H]-C_H correlation of a-Si:H. In addition, [Si–H_2]/[Si–H] of a-SiGe:H can be reduced by the high H_2-dilution of the source gas as well as a-Si:H.

For H–Si bonds in a-SiGe:H alloys, the [Si–H_2]/[Si–H]-$C_{H(Si)}$ correlation of both low- and high-diluted samples is similar to the [Si–H_2]/[Si–H]-C_H correlation in a-Si:H, as shown in Fig. 3.4. This suggests that the construction mechanism of the H–Si bonding structure of a-SiGe:H during deposition, including the effect of high H_2 dilution, is approximately the same as that of a-Si:H. There also exists, however, a minor quantitative difference. The H–Si configurations in a-SiGe:H are more insensitive to the H_2-dilution than that of a-Si:H. In order to obtain the dilution effect on the [Si–H_2]/[Si–H] shown in Fig. 3.4, larger dilution ratios (>20) and higher rf power density (>300 mW/cm^2) were needed, although the dilution ratios of ~5, and the rf power density of ~30 mW/cm^2 are effective enough for a-Si:H.[2] This is consistent with previous studies which have reported that the optimum dilution-ratio[14,15] and process temperature[2,16] for a-SiGe:H are higher than those for a-Si:H. The IR absorption peak at ~2100 cm^{-1} is generally attributed to the stretching vibration mode of dihydride (Si–H_2) bonds including (Si–H_2)$_n$ chains, although there is still another opinion that ascribes the origin of the peak to the surface-like configuration which consists of H atoms terminating the inner wall of voids.[2] However, the similarity of the [Si–H_2]/[Si–H]-$C_{H(Si)}$ correlation of a-SiGe:H to the [Si–H_2]/[Si–H]-C_H correlation of a-Si:H suggests that the peak is mainly caused by the Si–H_2 configuration rather than by the voids.

3.3.3 Origin of material deterioration with alloying

Figure 3.5 shows C_H, $C_{H(Si)}$ and $C_{H(Ge)}$ for a-SiGe:H plotted against C_{Ge}. C_{Ge} was controlled by varying GeH_4 flow ratio with keeping the process temperature constant at 230℃. Figure 3.6 shows the change in the [Si–H_2]/[Si–H]-$C_{H(Si)}$ correlation as C_{Ge} increases.

The deterioration of electronic properties when adding Ge has been often attributed to the

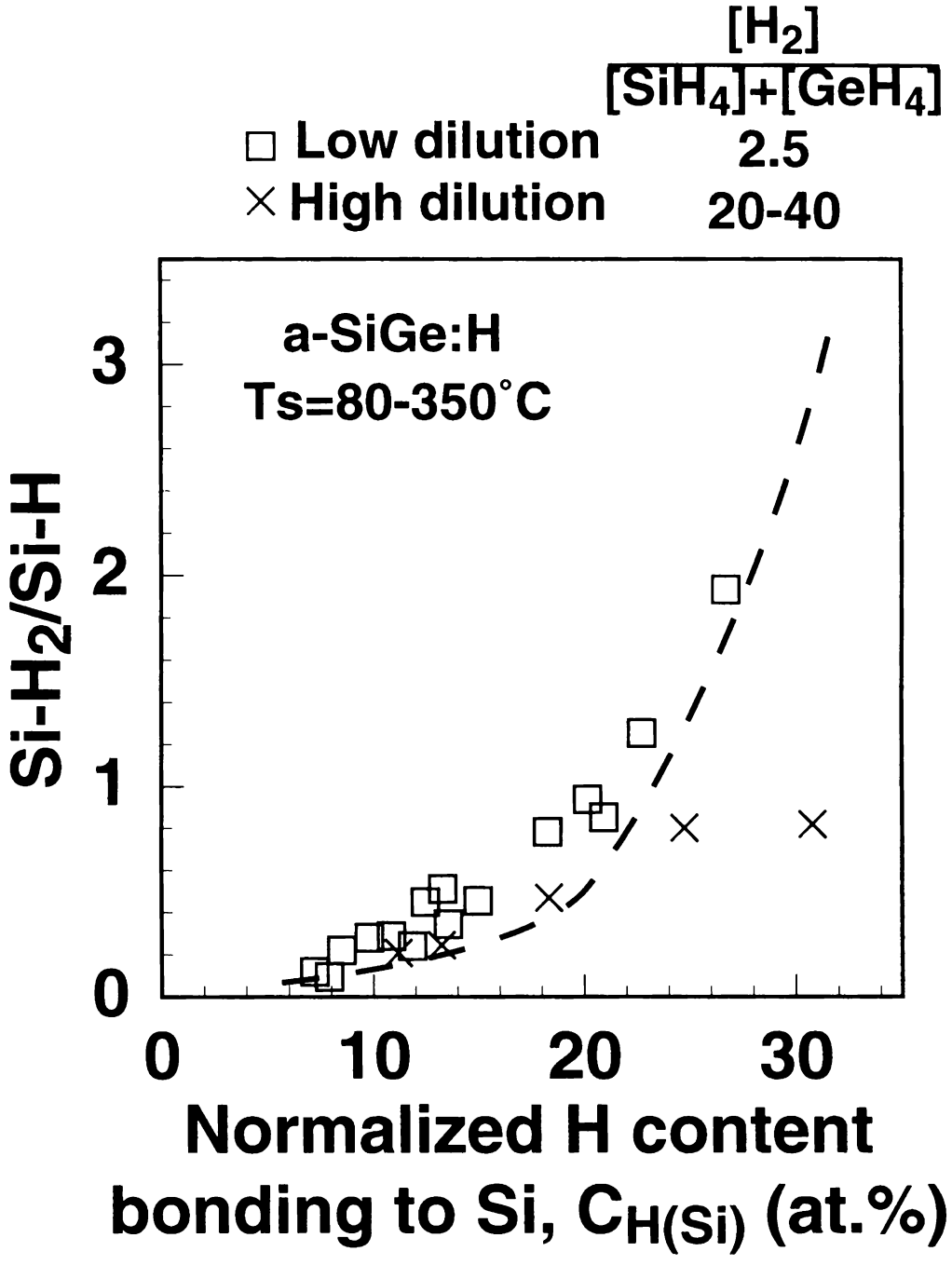

Fig. 3.4 [Si-H_2]/[Si-H] plotted against $C_{H(Si)}$ for a-SiGe:H samples deposited from low-diluted ([H_2]/([SiH_4]+[GeH_4] = 2.5) and highly-diluted ([H_2]/([SiH_4]+[GeH_4] = 20-40) mixture gases. The broken line indicates the [Si-H_2]/[Si-H]-C_H trend of low-diluted a-Si:H replotted from Fig. 3.1.

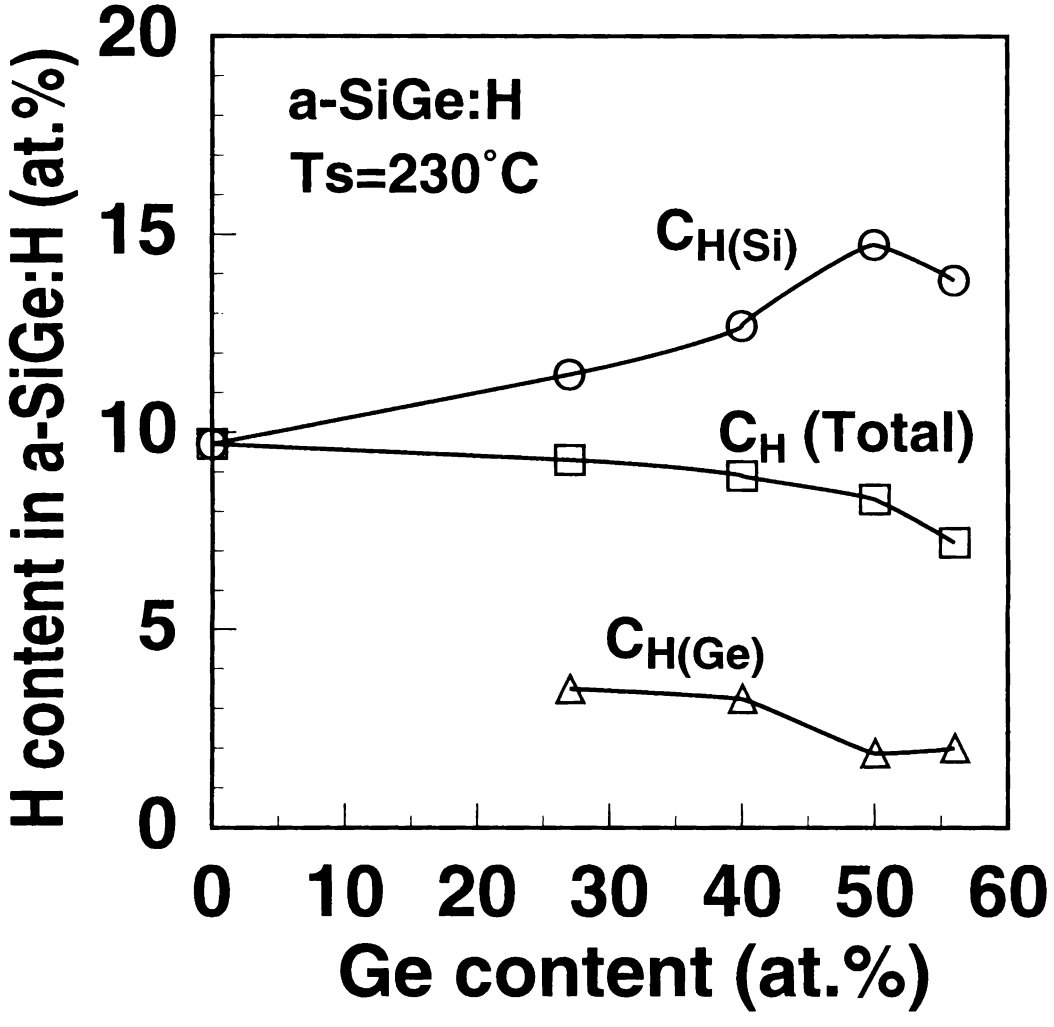

Fig. 3.5 C_H, $C_{H(Si)}$ and $C_{H(Ge)}$ of a-SiGe:H plotted against C_{Ge}. C_{Ge} was controlled from 0 to 60 at.% by varying GeH_4 flow ratio with keeping the process temperature constant at 230℃.

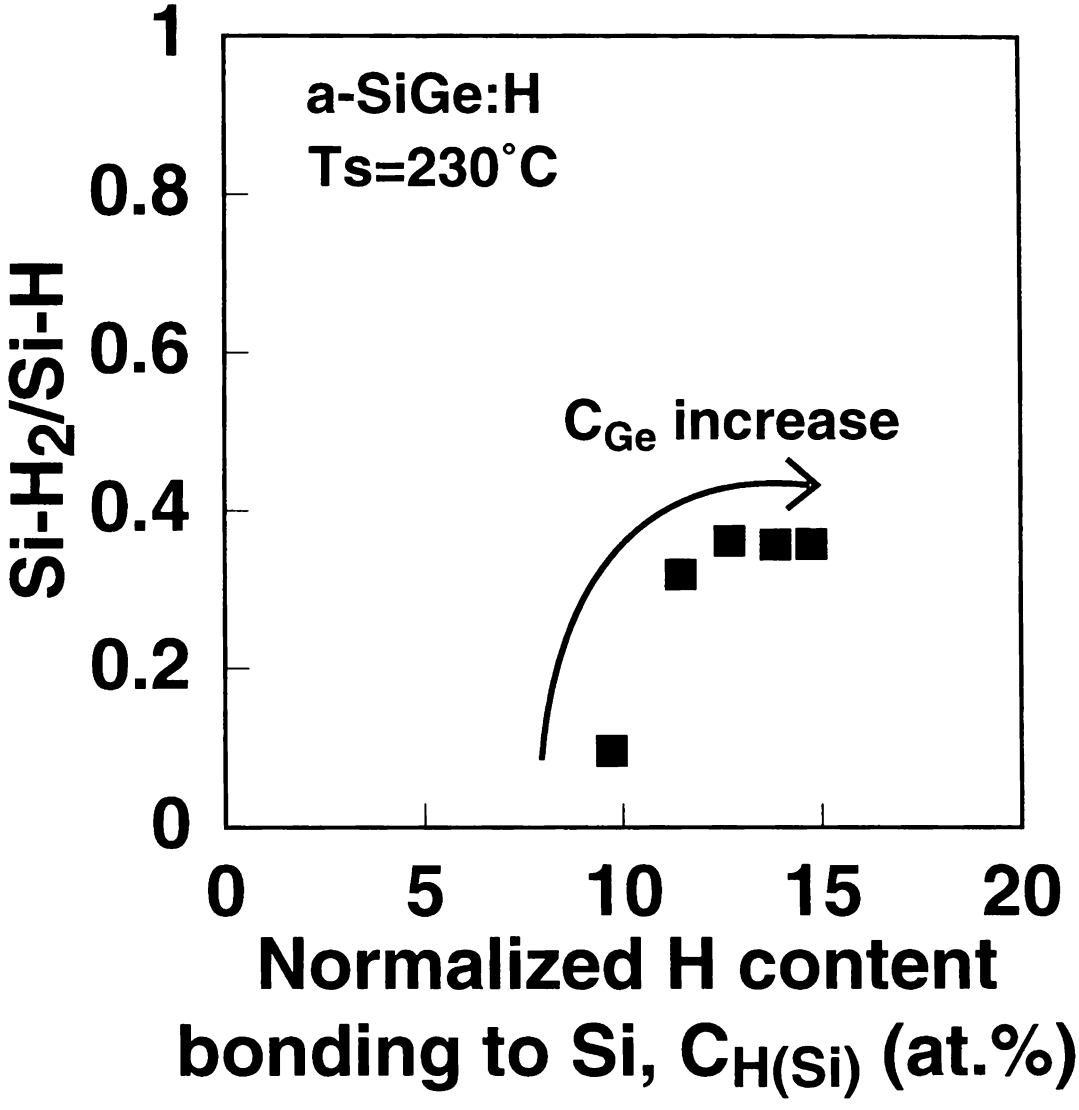

Fig. 3.6 [Si-H_2]/[Si-H] plotted against $C_{H(Si)}$ for a-SiGe:H with various C_{Ge} (0-60 at.%) deposited from low-diluted source gases ([H_2]/([SiH_4]+[GeH_4] = 2.5). The arrow indicates a schematic trend when increasing C_{Ge}.

preferential H attachment to Si,[12-14] which causes a lack of H–Ge bonds and the insufficient termination of Ge dangling bonds. However, when increasing C_{Ge}, $C_{H(Si)}$ and [Si–H_2]/[Si–H] increase in contrast to the slight decrease of C_H as shown in Figs. 3.5 and 3.6. Thus, the increase in Si–H_2 bonds is thought to also partly cause the deterioration of film properties. Concerning the photo-stability, Stutzmann *et al.* reported that the metastable dangling bond (DB) defects created by exposing prolonged illumination are mainly Si oriented DB, although most of the initial defects are Ge oriented DB.[17,19] This selective creation of the metastable Si DB is also explainable by the increasing Si–H_2 bonds. This is because the Si–H_2 introduced by alloying reduces the average network coordination of Si and seems to enhance the structural flexibility selectively around Si atoms.

$C_{H(Si)}$ and [Si–H_2]/[Si–H] in a-SiGe:H are thought to be determined by the H-elimination reactions during film growth as well as a-Si:H, which have been reported to be not simple H–Si breaking but a combined reaction to Si–Si or H_2 formation because its activation energy is much smaller than the H–Si binding energy.[17] The increasing $C_{H(Si)}$ and [Si–H_2]/[Si–H] with C_{Ge} as shown in Figs. 3.5 and 3.6 suggest that the existence of Ge atoms, bonding to less H, prevents the H-elimination reactions between H–Si bonds. The suppressed H-elimination reactions consequently retain more H–Si bonds in the bulk and cause Si–H_2 structures with increasing C_{Ge}. This is also probably the reason why additional energy for surface reactions is demanded for high-quality a-SiGe:H via higher process temperatures, or higher ratios of H_2 dilution than for a-Si:H, as mentioned previously.[1,4]

3.3.4 Origin of preferential attachment

The preferential H attachment coefficient, P, is defined by the following equation,[12,13]

$$P = C_{H(Si)}/C_{H(Ge)} = \{([Si–H_2]+[Si–H])\times[Ge]\}/\{[Ge–H]\times[Si]\}. \quad (3.3)$$

Figure 3.7 shows the P of a-SiGe:H deposited at various substrate temperatures (replotted data from Fig. 3.3) plotted against C_H. P increases from 3 to 11 with an increase in C_H from 5 to 17 at.%. Figure 3.8 shows the P of a-SiGe:H deposited at 230℃ (replotted data from Fig. 3.5) plotted against C_{Ge}. P increases again from 3 to 8 with an increase in C_{Ge} from 2 to 56 at.%.

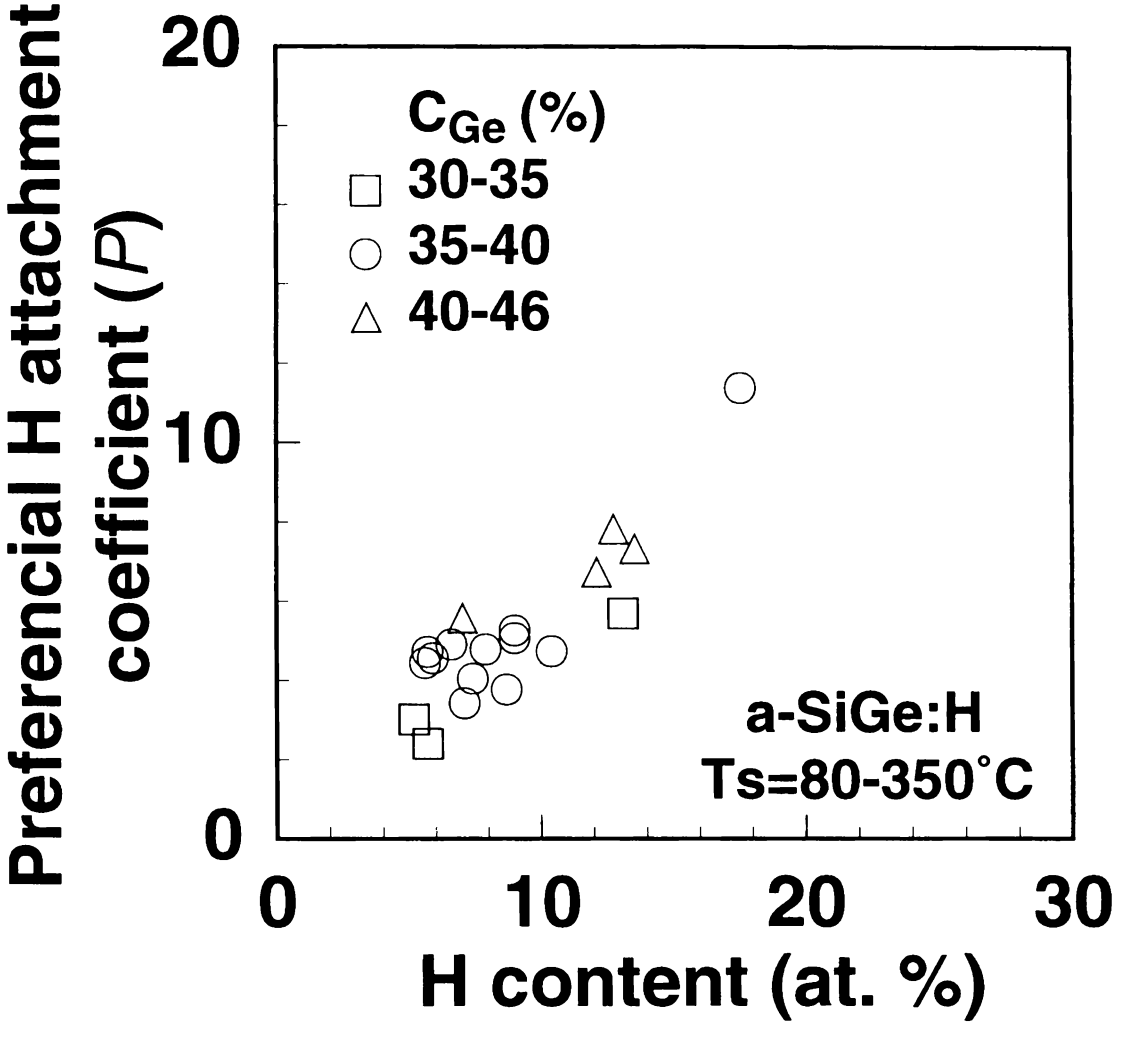

Fig. 3.7 P of a-SiGe:H deposited at various substrate temperatures (replotted data from Fig. 3.3) plotted against C_H. C_H was controlled by changing the substrate temperature from 80 to 350℃.

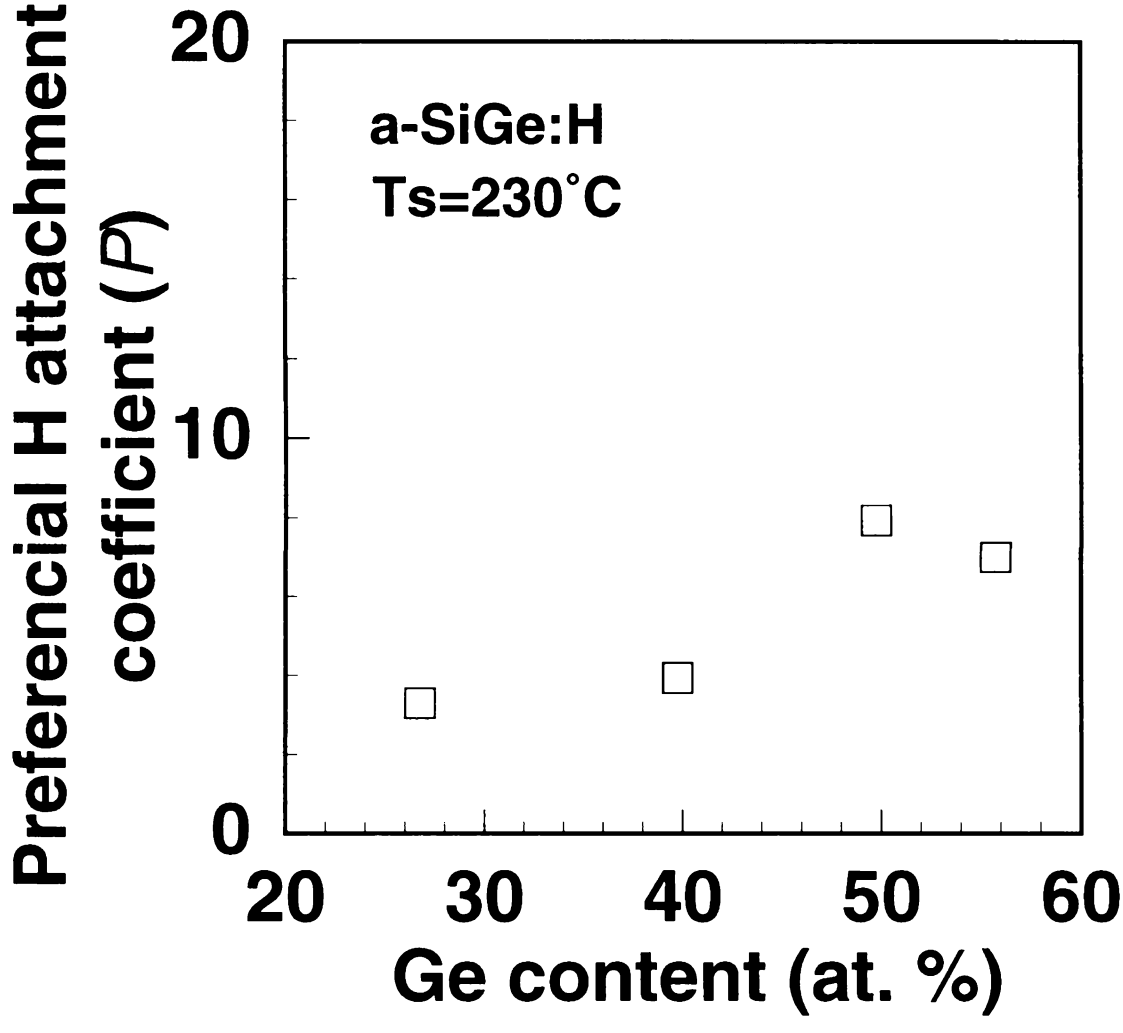

Fig. 3.8 P of a-SiGe:H deposited at 230℃ (replotted data from Fig. 3.5) plotted against C_{Ge}. C_{Ge} was controlled by changing $[GeH_4]/[SiH_4]$ flow ratio.

P of a-SiGe:H prepared by rf plasma CVD or rf sputtering has been previously reported to be ~10 by Paul *et al*,[12] ~5 by Stutzmann *et al*,[19] ~3-6 by Wakagi *et al*,[20] ~2-4 by Rudder *et al*,[21] and to be ~3 by Schroeder *et al.*[22] P is a well normalized value to remove the effect of the difference in Ge/Si ratio, and indicates that how many times H atoms are statistically more easily bonded to Si over Ge in the alloy. Therefore, they argued that a certain P value exists independently of the compositions.[22] In other words, there seemed to be a constant difference between the statistical bonding probability of H atoms to Si and to Ge. However, according to the results shown in Figs. 3.7 and 3.8, P values have positive correlations to both C_H and C_{Ge}. In addition, $C_{H(Ge)}$ is almost constant at 2-4 at.% independently of both C_H and C_{Ge}, as shown in Figs. 3.3 and 3.5. Thus, it might be an error to assume the existence of the critical P value determined simply by the difference of H bonding probabilities. These results suggest that the critical value determining the preferential attachment is not P but $C_{H(Ge)}$.

The author interprets the origin of the preference of H bonding from the viewpoint of the film growth kinetics as follows. Figure 3.9 shows schematic illustrations of the growing surface of a-SiGe:H (left) and the depth profiles of $C_{H(Ge)}$ and $C_{H(Si)}$ (right). (1) The main precursors contributing to a-SiGe:H film deposition are polyhydride radicals such as SiH_3^* and GeH_3^*. Thus, the topmost surface of the growing film is covered by H atoms supplied by those radicals.[17] (2) During several atomic-layer growth, surplus H atoms are eliminated from H–Si bonds in the layers under the topmost surface, so-called "growth zone", and $C_{H(Si)}$ decreases with film growth to reach a value of the bulk a-SiGe:H as well as suggested for a-Si:H.[23] As a result, $C_{H(Si)}$ strongly reflects growing conditions such as the process temperature. (3) H is eliminated much faster from H–Ge bonds at the growing surface because of the smaller binding energy (which means a shorter time constant for chemical reaction) than that of H–Si bonds.[24] Thus, $C_{H(Ge)}$ rapidly reaches to the steady-state value for the bulk, independently of the growing conditions. (4) Consequently only $C_{H(Si)}$ changes with C_H, and P is strongly dependent on C_H and C_{Ge}. The points of this model are that the H-elimination reaction around Ge atoms occurs quickly to minimize $C_{H(Ge)}$, and the reactions in the growth zone such as H elimination and H rebinding mainly occur only around Si atoms. In other words, the thickness of the growth zone for Ge is much smaller than that for Si (Fig. 3.9).

This model is consistent to recent experimental observations by *in-situ* reflective IR absorption

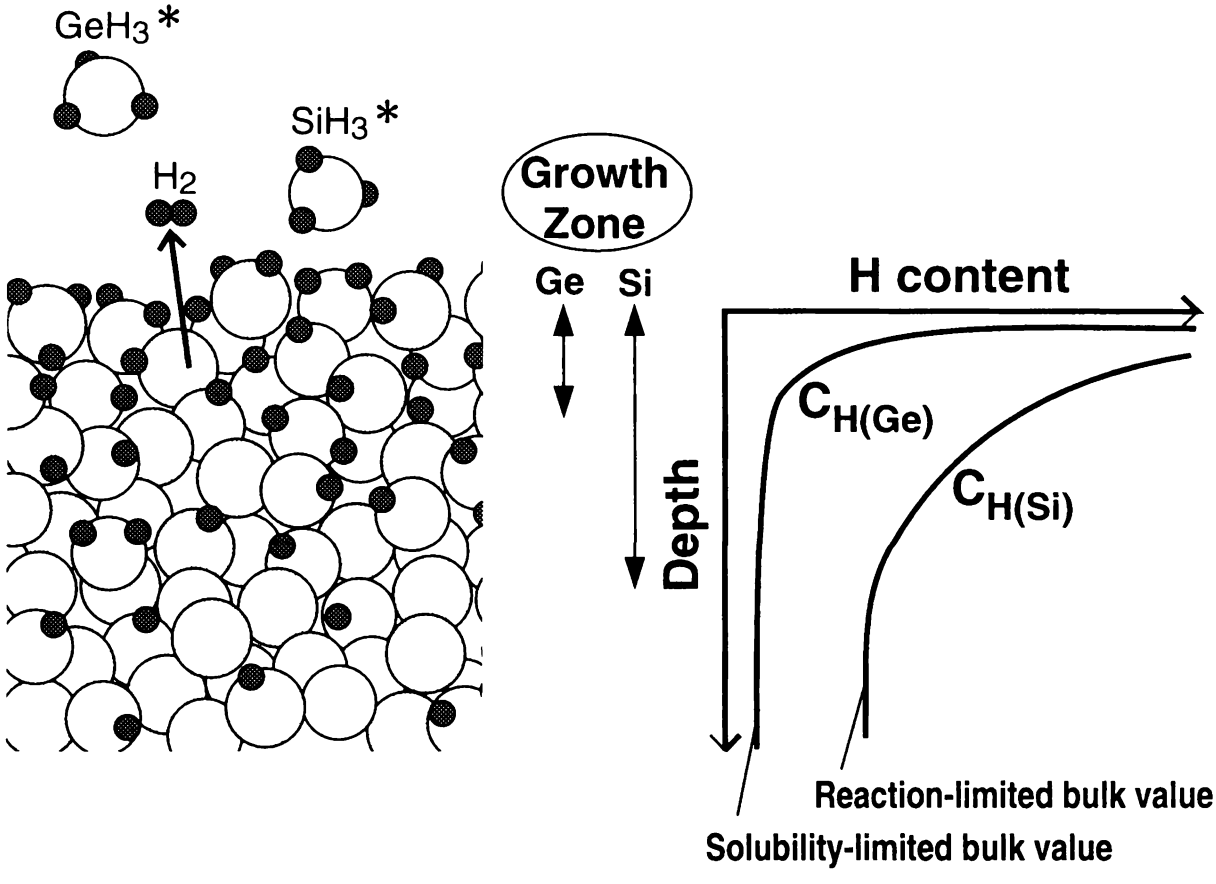

Fig. 3.9 Schematic illustration of the a-SiGe:H film growth deposited by rf plasma CVD. SiH_3^* and GeH_3^* radicals flying from source gas plasma regions stick to the surface of the growing film and become bulk via H elimination and network construction in the growth zone. H atoms bonding to Ge are released faster than those to Si, which means that the growth zone of Ge is thinner than that of Si. Therefore, $C_{H(Ge)}$ rapidly reaches to solubility-limited value below 5 at.%. (See text.)

spectroscopy on growing a-SiGe:H film.[25,26] Toyoshima *et al.* reported that the behavior of thermal H desorption from surface Si–hydride species of Si rich alloys is similar to that of a-Si:H.[25] Nakagawa *et al.* also suggested that $C_{H(Ge)}$ is determined in a much shorter time (or much thinner zone from the topmost surface) than that of Si–H.[26] Turning now to the origin of the constant $C_{H(Ge)}$, Jackson *et al.* and Acco *et al.* suggested that there exists a solubility-limited C_H in a-Si:H, which is associated with the concentration of defect-related deep H trap. They reported the solubility-limited C_H values of ~5 at.%[27] and 3-4 at.%[28], respectively, by H evolution experiments. These values for a-Si:H are consistent to 2-4 at.% of $C_{H(Ge)}$ for the bulk a-SiGe:H. The solubility-limited C_H values (< 5 at.%) is a minimum C_H in order to maintain a rigid amorphous network (with less dihydride bonds or void structures) in a mixture of the fourfold Si or Ge and univalent H atoms. This is supposed to be the reason why $C_{H(Ge)}$ in a-SiGe:H is determined independently from deposition conditions.

3.4 Are H–Si bonding structures random ?

The similarity of the [Si–H_2]/[Si–H]-$C_{H(Si)}$ correlation of a-SiGe:H (Fig. 3.4) to the [Si–H_2]/[Si–H]-C_H correlation of a-Si:H (Fig. 3.1) was pointed out in *3.3.2.* This suggests that there exists a common rule determining H–Si bonding structures in both a-Si:H and a-SiGe:H.

"Randomness" was traditionally considered to be a useful model to describe a-Si structure. Because the non-equilibrium structure of amorphous materials seems to be determined by the atomic arrangement corresponding to the maximum entropy. Schubert *et al.* compared the relative concentrations of Si–Si, Si–Ge and Ge–Ge bonds, and suggested that the tetrahedral matrix arrangement of Si–Ge is approximately random in a-SiGe:H.[29] Lucovski *et al.* and Gaspari *et al.* have respectively tried to describe H bonding structures as a function of C_H by statistical considerations assuming the random arrangement of H and Si atoms in the solid.[7,10] Although these random models have succeeded to qualitatively explain the increase in [Si–H_2] with C_H, there still remains a quantitative missing link. For example, it is well known that [Si–H_2] can be reduced independently from C_H by the use of deposition techniques such as highly H_2-diluted SiH_4 plasma or post H-plasma treatment.[3,6] The previous random models could not explain these transitions in

H structures depending on the deposition conditions. Randomness probably stands up for materials fabricated by rapid cooling from its liquid-phase. However, at most ~300℃ of the a-Si:H deposition temperature is much less than its melting point of 1412℃. Under these non-equilibrium conditions, the structure of a-Si:H is affected not only by the randomness but also by the growth kinetic. The purpose of this section is to discuss the construction mechanism of H–Si bonding structures.

3.4.1 Two numerical random models

Figure 3.10 schematically illustrates the growth process of a-Si:H film. SiH_3^* and H^* radicals generated in the plasma come flying and stick to the growing surface. Then, the topmost of the growing film is covered by H atoms, and C_H of this region is 200-300 at.%. After several atomic-layer growth, C_H reached a steady state value of bulk at 10-20 at.% and H configurations were fixed. Important reactions in the growth zone are (a) the distortion of excess H atoms and (b) the reconstruction of H bonding structures including H insertion from the hydrogen-rich surface. In order to analytically describe the construction kinetics of H–Si bonding structures, the author proposes two random models simulating these two reactions. One is based on the assumptions of (A) random H-elimination from SiH_3 radicals, and the other on (B) random H-insertion and mixing reaction into Si network, respectively. These random models are compared to the experimental results given in *3.3.2*.

***Model A:** Random H-elimination*

It was assumed that each Si atom on the growing topmost is bonding to three H atoms and H bonding configurations are determined simply by H-elimination reaction from H–Si bonds with atomic unit. There are three possible H-elimination reactions as follows,

$$Si\text{–}H_x \rightarrow Si\text{–}H_{x-1} + H \quad (x=1, 2, 3). \tag{3.4}$$

If H atoms randomly eliminate from each configuration, the possibility of that a certain H-detachment reaction occurs following each x value in Eq. (3.4) can be represented as $C_{Si\text{–}H_x}/C_H$ (x=1, 2, 3). Where $C_{Si\text{–}H_x}$ is H content of $Si\text{–}H_x$ configuration and $\Sigma C_{Si\text{–}H_x} = C_H$. In these

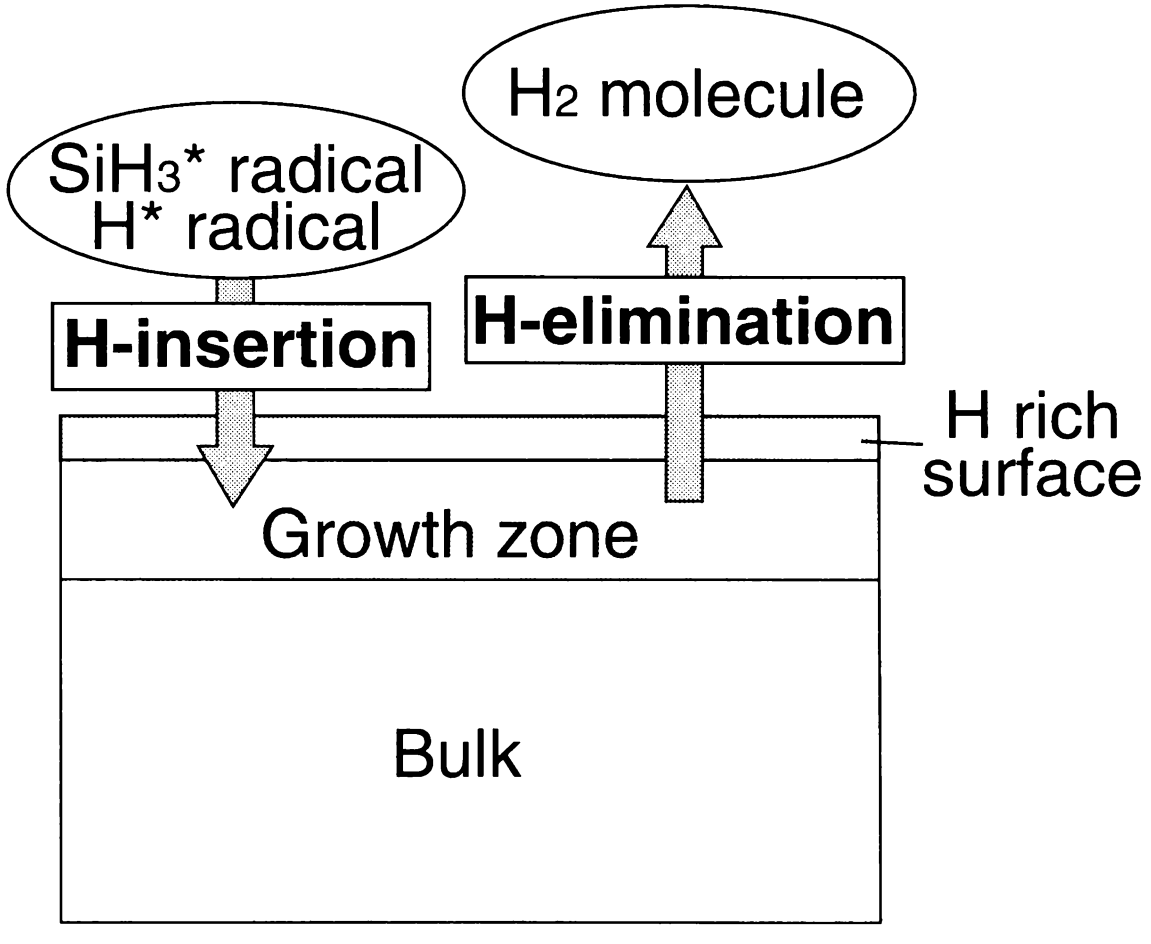

Fig. 3.10 Schematic illustration of H reactions in the growing a-Si:H surface. The hydrogen content (C_H) and bonding configurations in a-Si:H are considered to be determined by the hydrogen elimination and insertion reactions.

reactions, when Si–H_x vanishes Si–H_{x-1} is simultaneously created. The decreasing ratios of C_{Si-H_x} (x=1, 2, 3) with decreasing C_H can be represented as follows, respectively,

$$dC_{Si-H_3}/dC_H = 3C_{Si-H_3}/C_H, \tag{3.5}$$

$$dC_{Si-H_2}/dC_H = 2C_{Si-H_2}/C_H - 2C_{Si-H_3}/C_H, \tag{3.6}$$

$$dC_{Si-H}/dC_H = C_{Si-H}/C_H - C_{Si-H_2}/C_H. \tag{3.7}$$

These simultaneous differential equations, Eq. (3.5)-(3.7), can be solved under the following boundary conditions,

$$C_{Si-H_x} \mid_{C_H=3} = 0 \ (x = 1, 2), \ C_{Si-H_3} \mid_{C_H=3} = 3, \tag{3.8}$$

$$C_{Si-H_x} \mid_{C_H=0} = 0 \ (x = 1, 2, 3). \tag{3.9}$$

C_H=3 in Eq. (3.8) indicates the topmost condition of the growing film where SiH_3 radicals pour on. The solutions can be represented as follows,

$$C_{Si-H_3} = C_H^3/9, \tag{3.10}$$

$$C_{Si-H_2} = -2C_H^2(C_H - 3)/9, \tag{3.11}$$

$$C_{Si-H} = C_H(C_H - 3)^2/9. \tag{3.12}$$

Thus, the [polyhydride]/[monohydride] ratio of this random H-elimination model can be represented as a function of C_H as follows,

$$(C_{Si-H_3} + C_{Si-H_2})/C_{Si-H} = -C_H(C_H - 6)/(C_H - 3)^2. \tag{3.13}$$

Model B: *random H-insertion*

H-Si bonding structure in a-Si:H network is assumed to be determined by randomly driving H atoms into Si network and/or by randomly mixing of Si and H atoms. In this random network composed of M fourfold Si atoms and L univalent H atoms, assuming that all H atoms combine with Si atoms and the number of dangling bonds is negligible compared to M and L, the number of Si–H bonds, N_{Si-H}, and Si–Si bonds, N_{Si-Si}, can be represented as

$$N_{Si-H} = L = M\, C_H, \tag{3.14}$$

$$N_{Si-Si} = (4M-L)/2 = M(4-C_H)/2, \tag{3.15}$$

where $C_H = L/M$. The probability of a bond sampled from the network at random being a Si–Si bond, p_{Si-Si}, and a H–Si bond, p_{H-Si}, is represented as follows, respectively,

$$p_{Si-Si} = N_{Si-Si}/(N_{Si-H} + N_{Si-Si}) = (4-C_H)/(4+C_H), \tag{3.16}$$

$$p_{H-Si} = 1-p_{Si-Si} = 1-N_{Si-Si}/(N_{Si-H} + N_{Si-Si}) = 2C_H/(4+C_H). \tag{3.17}$$

When a H atom is sampled from the network at random, the probability of the configuration of the H–Si bond being the mono-hydride—in other words, the rest three folds of the Si atom connected with the neighboring Si—is p_{Si-Si}^3. In the similar consideration, H content in different configurations can be represented as,

$$C_{Si-H} = C_H\, p_{Si-Si}^3 = C_H(4-C_H)^3/(4+C_H)^3, \tag{3.18}$$

$$C_{Si-H_2} = 3C_H\, p_{H-Si}\, p_{Si-Si}^2 = 6C_H^2(4-C_H)^2/(4+C_H)^3, \tag{3.19}$$

$$C_{Si-H_3} = 3C_H\, p_{H-Si}^2\, p_{Si-Si} = 12C_H^3(4-C_H)/(4+C_H)^3, \tag{3.20}$$

$$C_{Si-H_4} = C_H\, p_{H-Si}^3 = 8C_H^4/(4+C_H)^3. \tag{3.21}$$

Thus, [polyhydride]/[monohydride] ratio of this random H-insertion model can be represented as a function of C_H as follows,

$$(C_{Si-H_2} + C_{Si-H_3} + C_{Si-H_4}) / C_{Si-H} = (1-p_{Si-Si}{}^3)/p_{Si-Si}{}^3 = 2C_H(C_H{}^2 + 48)/(4-C_H)^3. \quad (3.22)$$

This result is quantitatively consistent with that obtained by Gaspari *et al.* through a statistical computer simulation.[10]

3.4.2 Comparison to the experimental results

Figures 3.11(a) and 11(b) show Si-H_x contents (x=1, 2 and 3) of the random H-elimination model (*Model A*) described by Eqs. (3.10)-(3.12) as functions of C_H. Figures 3.12(a) and 12(b) show Si-H_x contents (x=1, 2, 3 and 4) of the random H-insertion model (*Model B*) described by Eqs. (3.18)-(3.21) as functions of C_H. Although these two models brought qualitatively similar results, the random H-elimination causes less polyhydride structures than the random H-insertion model in the region with C_H less than 30 at.%. Figure 3.13 shows [polyhydride]/[monohydride] ratios of *Model A* and *Model B* described respectively by Eqs. (3.13) and (3.22) as functions of C_H. The hatched regions indicate the experimental results of high and low diluted a-Si:H samples, respectively, shown in Fig. 3.1. One can see that the low diluted samples selectively contain polyhydride bonds and that the high diluted samples approximately correspond to the random models (Fig. 3.14). Under the low diluted conditions, H-insertion is not significant and H-elimination is dominant. Although atomic-unit random reactions were assumed in *Model A*, the low diluted conditions are thought to allow only limited reactions with relatively small activation energy. The actual H abstraction reactions are not simple H–Si bond breaking but the combined reactions with Si–Si or H–H bond formation.[18]

Thus, the reaction rate of H distortion reaction is considered to depend on the network around the H-Si bond. The reactions from monohydride and dihydride configurations can be represented as follows,

$$Si_3\text{-}SiH + H \rightarrow Si_3\text{-}Si + H_2 \uparrow , \quad (3.23)$$

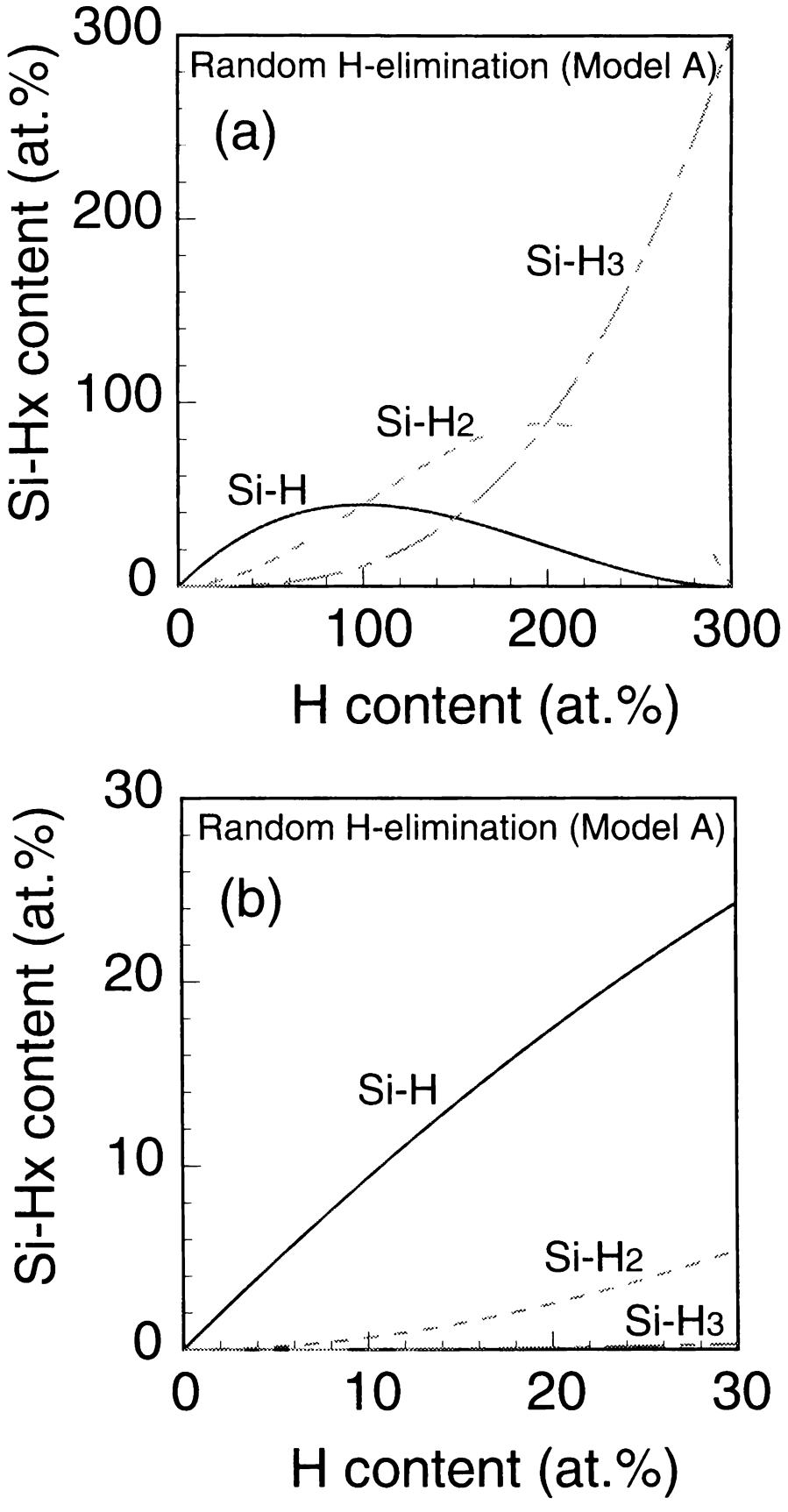

Fig. 3.11 Si-H_x contents (x=1, 2 and 3) of the random H-elimination model (*Model A*) described by Eqs. (3.10)-(3.12) as functions of C_H: (a) C_H = 0-30 at.%, (b) C_H = 0-300 at.%.

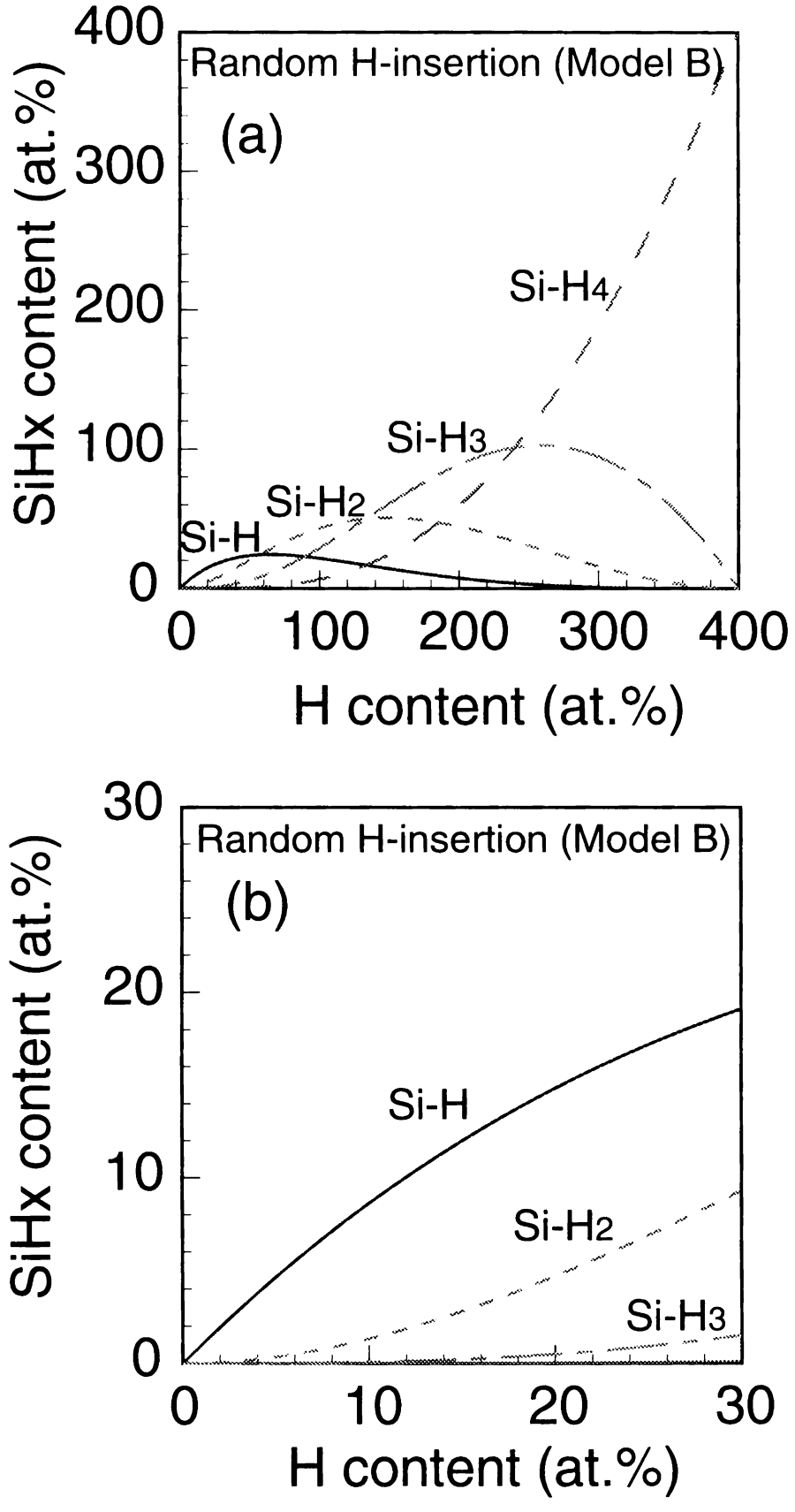

Fig. 3.12 Si-H_x contents (x=1, 2 and 3) of the random H-insertion model (*Model B*) described by Eqs. (3.18)-(3.21) as functions of C_H: (a) C_H = 0-30 at.%, (b) C_H = 0-300 at.%.

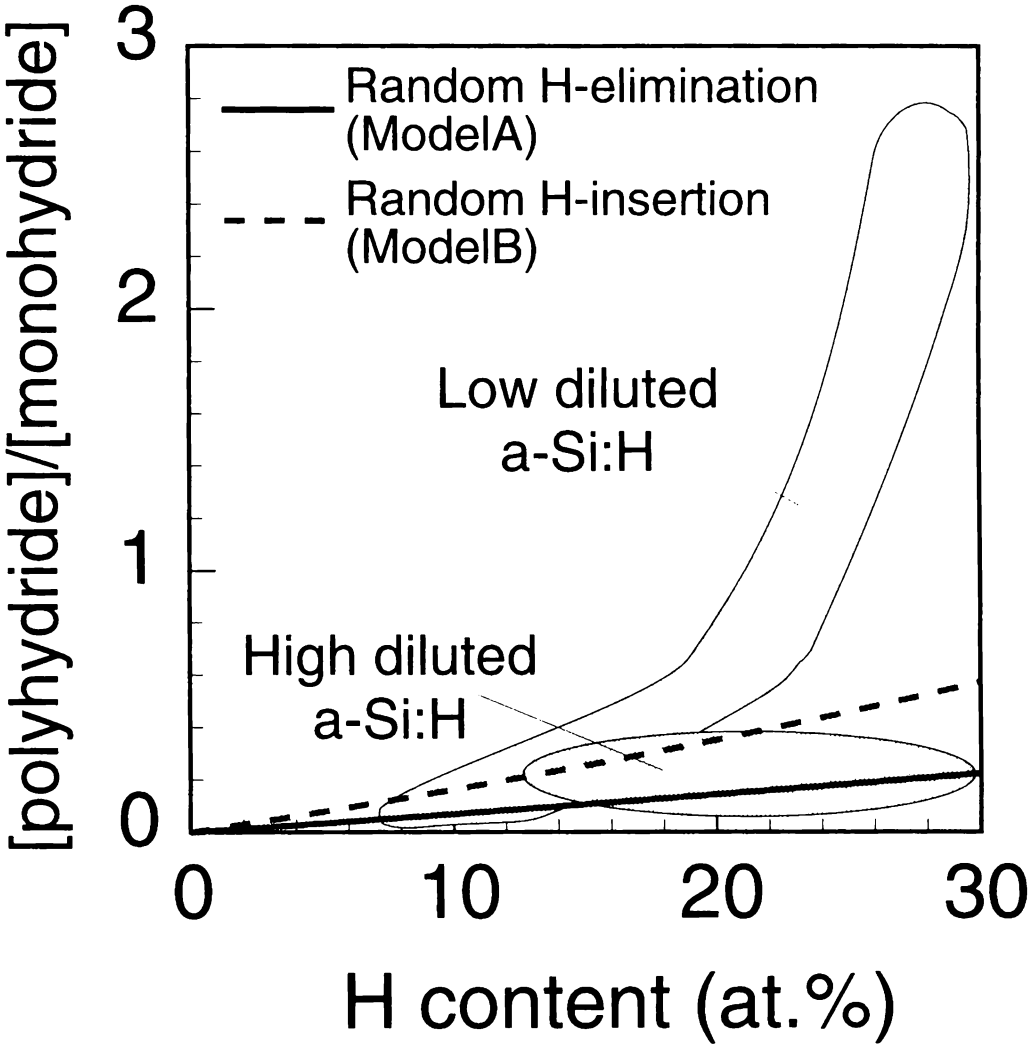

Fig. 3.13 [polyhydride]/[monohydride] ratios of *Model A* and *Model B* described respectively by Eqs. (3.13) and (3.22) as functions of C_H. The hatched regions indicate the experimental results of high and low diluted a-Si:H samples, respectively, shown in Fig. 3.1.

Process Condition Dependence of H bonding Structures in a-Si:H

Deposition conditions	Energy for surface reaction	H bonding structures
Low dilution	Small	Selective SiH_2 formation
High dilution	Large	Random

The reason of selective SiH_2 formation

	Activation energy	Reaction rate
$SiH_2 \rightarrow SiH + H$	large	slow
$SiH \rightarrow Si + H$	small	fast

Fig. 3.14 A summary of process condition dependence of hydrogen bonding configurations in a-Si:H.

$$Si_2\text{-}SiH_2 + H \rightarrow Si_2\text{-}SiH + H_2 \uparrow . \quad (3.24)$$

Sato *et al.* and Srinivasan *et al.* respectively reported that the activation energy of H abstraction from monohydride (Eq. (3.23)) is smaller than that from dihydride (Eq. (3.24)) by *ab initio* simulations,[30,31] and the reaction rate of (Eq. (3.23)) is much faster than that of (Eq. (3.24)).[31] These are probably the reason of preferential polyhydride formation under low diluted process (Fig. 3.14).

On the other hand, the high diluted deposition processes are thought to apply enough energy to cause H-elimination and insertion reactions by the H radicals or ions pouring on. An active reconstruction of the amorphous network caused by these reactions results in the random H bonding configurations which give the largest entropy of the arrangement of H atoms.

3.5 Summary

The composition dependencies of H bonding configurations in a-SiGe:H alloy films with various compositions deposited by rf plasma CVD were systematically investigated by comparisons to a-Si:H and a-Ge:H. Conclusions drawn in this chapter are summarized below.

(1) As C_H increases from 7 to 27 at.% by varying the substrate temperature from 80 to 350℃, the normalized H content per Si atom ($C_{H(Si)}$) in a-SiGe:H drastically increases with C_H, while the normalized H content per Ge atom ($C_{H(Ge)}$) is almost constant at 2-4 at.%. This suggests that the structural differences of a-SiGe:H with C_H are mainly caused in the regions around Si atoms.

(2) When focusing on H–Si bonds, [Si–H_2]/[Si–H]-$C_{H(Si)}$ correlations in a-SiGe:H deposited from both low- and high- diluted source gases are equivalent with those in a-Si:H. This suggests that the construction mechanism of H bonding structures around Si atoms in a-SiGe:H is similar to that in a-Si:H.

(3) As C_{Ge} increases from 0 to 60 at.% at a constant substrate temperature of 230℃, only $C_{H(Si)}$ increases form 10 to 14 at.%. The increase in $C_{H(Si)}$ with C_{Ge} is considered to be caused by the existence of Ge atoms which prevent H-elimination reactions around Si atoms. This increase in $C_{H(Si)}$ indirectly causes an increase in [Si–H_2]/[Si–H] and a material deterioration by alloying.

(4) The preferential attachment coefficient, $P = C_{H(Ge)}/C_{H(Si)}$, has positive correlations to both C_H and C_{Ge}. The P value is considered to be determined not simply by the statistical difference of the bonding probabilities of H to Si and to Ge, but by the kinetics of H elimination during film growth. The $C_{H(Ge)}$ value is supposed to be solubility limited, while the $C_{H(Si)}$ value is surface reaction limited.

(5) Two random models were proposed to describe the construction kinetics of H–Si bonding structures, and these models were compared to the experimental results. H-bonding configurations of high-diluted samples are almost random. On the other hand, H-bonding configurations of low-diluted samples are not random but selectively contains polyhydride bonds.

References

1. A. H. Mahan, P. Raboisson and R. Tsu, Appl. Phys. Lett. **50**, 335 (1987).
2. Y. Hishikawa, S. Tsuda, K. Wakisaka and Y. Kuwano, J. Appl. Phys. **73**, 4227 (1993).
3. Y. Hishikawa, K. Ninomiya, E. Maruyama, S. Kuroda, A. Terakawa, K. Sayama, H. Tarui, M. Sasaki, S. Tsuda and S. Nakano, *Proc. 1st World Conference on the Photovoltaic Energy Conversion* (1994, Waikoloa) p.386.
4. A. Terakawa, M.Shima, K. Sayama, H. Tarui, H. Nishiwaki and S. Tsuda, Jpn. J. Appl. Phys. **34**, 1741(1995).
5. S. Okamoto, Y. Hishikawa and S. Tsuda, Jpn. J. Appl. Phys. **35**, 26 (1996).
6. S. Okamoto, Y. Hishikawa, S. Tsuge, M. Sasaki, K. Ninomiya, M. Nishikuni and S. Tsuda, Jpn. J. Appl. Phys. **33**, 1773 (1994).
7. G. Lucovsky and G. N. Parsons: *OPTOELECTRONICS-Device and Technologies* **4** (1989) 119.
8. F. Finger, V. Viret, A. Shah, X.-M. Tang, J. Weber and W. Beyer, Mater. Res. Soc. Symp. Proc. **192**, 583 (1990).
9. A. A. Langford, M. L. Fleet, P. B. Nelson, W. A. Lanford and N. Maley: Phys. Rev. B**45**, 13367 (1992).
10. F. Gaspari, S. K. O'Leary, S. Zukotynski and J. M. Perz, J. Non-Cryst. Solids **155**, 149 (1993).
11. A. Terakawa, M. Shima, K. Sayama, H. Tarui, S. Tsuda and S. Nakano, Jpn. J. Appl. Phys. **32**, 4849 (1993).
12. W. Paul, D. K. Paul, B. Von Roedern, J. Blake and S. Oguz, Phys. Rev. Lett. **46**, 1016 (1981).
13. B. Von Roedern, D. K. Paul, J. Blake, R.W. Collins, G. Moddel, and W. Paul, Phys. Rev. **B25**, 7678 (1982).
14. S. Z. Weisz, N. Gomes, J. A. Muir, O. Resto and R. Perez, Appl. Phys. Lett. **44**, 634 (1984).
15. L. Yang, L. Chen and A. Catalano, Mater. Res. Soc. Symp. Proc. **219**, 259 (1991).
16. M. Shima, A. Terakawa, M. Isomura, M. Tanaka, S. Kiyama and S. Tsuda, Appl. Phys. Lett. **71**, 84 (1997).
17. M. Stutzmann, R.A. Street, C.C. Tsai, J.B. Boyce and S.E. Ready, J. Appl. Phys. **66**, 569 (1989).
18. A. Matsuda and K. Tanaka, J. Appl. Phys. **60**, 2351 (1986).
19. M. Stutzmann, Tech. Dig. 5th Sunshine Workshop on Solar Cells (1992) p.23. 21.
20. M. Wakagi, M. Chigasaki, K. Tamahashi, T. Ohno, M. Naruse, M. Hanazono and E. Maruyama, J. Non-Cryst. Solids **77/78**, 889 (1985).
21. R.A. Rudder, J.W.Cook and G. Lucovski, J. Vac. Sci. Techn. **43**, 871 (1983).
22. S. Schroeder, M. Leidner and H. Oechsner, Mater. Res. Soc. Symp. Proc. **219**, 277 (1991).
23. M. Kawasaki, Y. Matsuzaki and H. Koinuma, Phys. Rev. B**39**, 13316 (1989).

24. J.W. Sharp and G. Eres, Appl. Phys. Lett. **62**, 2807 (1993).

25. Y. Toyoshima, G. Gangly, T. Ikeda, K. Saitoh, M. Kondo and A. Matsuda, Mater. Res. Soc. Symp. Proc. **467**, 567 (1997).

26. K. Nakagawa, Y. Yoshida, S. Miyazaki and M. Hirose, J. Non-Cryst. Solids **227**, 48 (1998).

27. W.B. Jackson, N.H. Nickel, N.M. Johnson, F. Pardo and P.V. Santos, Mater. Res. Soc. Symp. Proc. **336**, 311 (1994).

28. S. Acco, D.L. Williamson, P.A. Stolk, F.W. Saris, M.J. van den Boogaard, W.C. Sinke, W.F. van der Weg, S. Roorda and P.C. Zalm, Phys. Rev. B**53**, 4415 (1996).

29. M.B. Schubert, K. Eberhardt and G.H. Bauer, Mater. Res. Soc. Symp. Proc. **192**, 121 (1990).

30. K. Sato, Y. Sugiyama, A. Uchiyama, S. Iwabuchi, T. Hirano and H. Koinuma, Phys. Rev. B**46**, 1913 (1992).

31. E. Srinivasan, H. Yang and G.N. Parsons, J. Chem. Phys. **105**, 5467 (1996).

Chapter 4
Effects of i-layer Optical Gap and Compositions on a-SiGe Solar Cell Stability

4.1 Background

One of the main problems of a-Si based solar cells is a decline in efficiency due to an increase in the number of metastable defects in the photovoltaic layer during light irradiation, or the so-called Staebler-Wronski effect (SWE).[1] As mentioned in Chapter 1, multi-junction solar cells should relieve this problem because each photovoltaic layer is thinner than that of single-junction solar cells, and a strong internal electric field prevents carrier recombination and maintains a higher fill factor after illumination. In addition to the cell structure, the stability of the materials themselves must also be improved. It is thus necessary to clarify the origin of the light-induced changes in a-Si alloys. For instance, optical gap (E_{opt}), hydrogen and impurities are considered to play a role in the defect creation mechanism.[2]

The unstable kinetic behavior of a-Si alloys exposed to illumination is believed to be caused not by a direct optical excitation from bonding into antibonding states, but by the recombination of photo-generated carriers. This is because, for example, it has been confirmed that current injection also causes a degradation similar to light soaking.[2] Metastable dangling bonds are thought to be created by the breaking of weak bonds in amorphous networks. Here, the non-radiative recombination of photo-excited hole-electron pairs, via trapping in the valence- and conduction-band tails, provides the energy for breaking weak bonds. Thus, E_{opt} is probably a dominant factor in the light-induced defect creation process, because the recombination energy, a trigger for photo-induced structural change, should depend on E_{opt}. Indeed, many previous reports have suggested that a-Si:H and its alloy materials with narrower E_{opt} are more stable.[3-11] A research group from Princeton Univ. reported that the saturated defect density of a-Si:H and a-SiGe:H after prolonged illumination tends to decrease slightly with a decrease in E_{opt}.[3-5] Bauer *et al.* analyzed photodegradation behavior in the conductivity of a-Si:H, a-SiGe:H and a-SiC:H, and noted longer time decay for narrower E_{opt}.[7] Unold *et al.* theoretically predicted that no degradation should occur

in a-SiGe:H with E_{opt} less than a certain value.[10] In these previous studies, however, not enough attention was paid to the effect of compositions, such as hydrogen content (C_H) or germanium content (C_{Ge}), which are strongly correlated to E_{opt}.[12] a-Si:H with a narrower E_{opt} contains a smaller amount of hydrogen, and the E_{opt} of a-SiGe:H is generally reduced by increasing the germanium atomic ratio. Therefore, the effects of hydrogen and the energy gap on stability could not be separated clearly in experiments using a-Si:H system. In particular, C_H and hydrogen bonding configurations are considered to be an important factor affecting the light-induced degradation process.[13-18]

There is another uncertain factor concerning the origin of the effect of E_{opt} on photostability. This is the contributing effect of E_{opt} on annealing kinetics. The degradation behavior of a-Si alloys is determined by the balance of the defect creation and annealing processes. If the energy barrier from the metastable state to the annealed state becomes smaller with a decrease in E_{opt}, annealing may be activated and seemingly smaller degradation may result. The comprehension of defect annealing kinetics is thus as important as the comprehension of defect creation mentioned above. To the author's knowledge, studies have yet to be carried out on the E_{opt} dependence of the annealing process of a-SiGe:H alloys.

The purpose of this chapter is to clarify the effects of the i-layer E_{opt} on a-SiGe solar cell stability. a-SiGe single-junction solar cells with various E_{opt} and those with a constant E_{opt} and various combinations of C_H and C_{Ge} were prepared. The degradation behavior among the samples with various E_{opt} and those with constant E_{opt} and various compositions were systematically compared to distinguish the contribution of E_{opt} from the effect of compositions. Cells with various E_{opt} were recovered by annealing at various temperatures after light soaking. Their behavior during recovery was also systematically analyzed to separate the effects of E_{opt} on the creation and removal of metastable defects. The main focus was put on the variation of the decay time-constants of the degradation and recovery processes. Furthermore, the effect of E_{opt} on the temperature dependence of solar cell stability is also discussed together with connecting the effect to defect creation and annealing kinetics.

4.2 Experimental

a-SiGe single-junction solar cells with a constant E_{opt} and various combinations of C_H and C_{Ge} were used, as mentioned in Chapter 2. a-SiGe single-junction solar cells with various E_{opt} were also prepared. The cells consisted of a TCO/p(a-SiC:H)/i(a-SiGe:H)/n(a-Si:H)/metal structure. A-SiGe:H was deposited using a rf plasma reactor from a gas mixture of SiH_4, GeH_4 and H_2. The thickness of the i-layer was ~1000 Å. A-SiGe:H films of 2000-3000 Å thick were also prepared on Corning #7059 substrates to monitor the optical and compositional properties. More details of the sample preparation and evaluation are given in Chapter 2.

4.3 Degradation ratio

4.3.1 Composition dependence of light-induced degradation

Figure 4.1 schematically illustrates the E_{opt} contour map of a-SiGe:H as a function of C_H and C_{Ge}. Following Eq. (2.4), the correlation among C_H, C_{Ge} and E_{opt} is represented as a plate painted with various tones, shown in Fig. 4.1. Each tone on the plate indicates a region in which E_{opt} is close. The three arrows on the plate show the directions in which the materials are supposed to become more stable.

Arrow I shows the direction along which E_{opt} decreases when C_{Ge} increases. In this case, C_H does not strongly depend on C_{Ge} if the substrate temperature is constant, as shown in Chapter 3. Arrow II shows the direction along which E_{opt} decreases by reducing C_H in a-Si:H. As mentioned above, materials have been reported to become more stable in the directions of both arrows I and II. However, it has not yet been confirmed that hydrogen is a dominant factor in the case of arrow I, because E_{opt} also decreases. The C_H dependence of the degradation behavior of a-SiGe solar cells with constant E_{opt} and different compositions was shown in Fig. 2.10. Arrow III shows the direction in which C_H decreases while E_{opt} was kept constant, as shown in Fig. 2.10. The fact that the materials become more stable in the direction of arrow III, in which the effect of E_{opt} is free, supports the assumption that decrease in C_H contributes to at least partly stabilizing the materials in arrow I also. This also confirms the contributing effect of incorporated hydrogen or its bonding

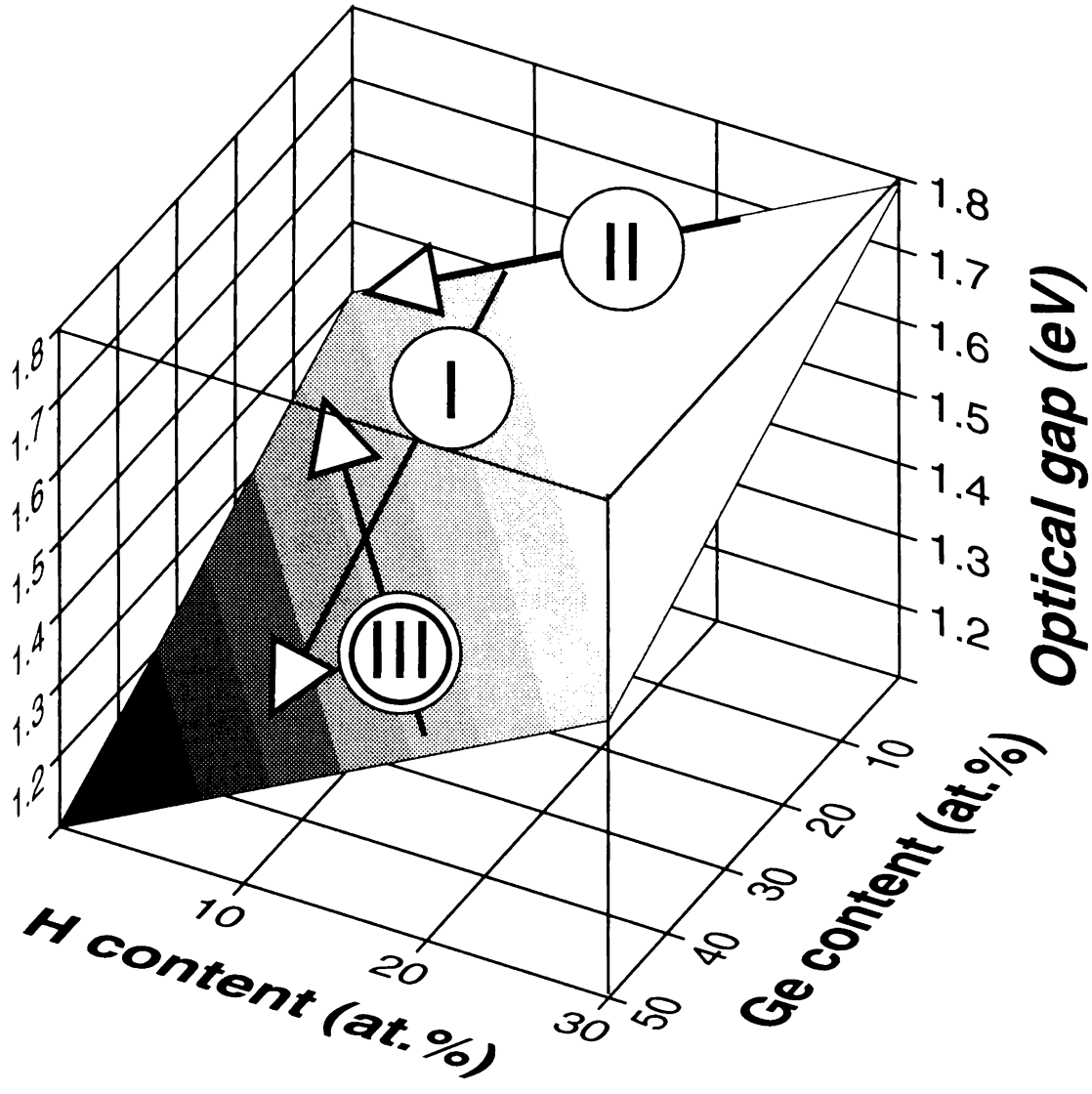

Fig. 4.1 Schematic illustration of E_{opt} contour map of a-SiGe:H as a function of C_H and C_{Ge}. Three arrows show the directions in which materials are considered to become more stable. (See text.)

structure to the creation of metastable defects. In other words, metastable defect density can be reduced by decreasing C_H.

There is still the possibility of the participation of C_{Ge}, which increases with C_H in the direction of arrow III, because the Ge–Ge or Ge–H bonds are weaker and break easier than Si–Si or Si–H bonds. However, this kind of effect from increasing C_{Ge} would seem to be relatively small — at least smaller than the effect of the band gap — if a-SiGe:H alloys with higher C_{Ge} and lower E_{opt} are more stable, as was previously suggested.

A number of kinetic models[2] which were proposed to explain the Staebler-Wronski effects of a-Si have linked to the motion of incorporated hydrogen, which is a small, univalent atom and is considered to move easily within the tetrahedral network. The likeliest suggestion is that the hydrogen moves to and stabilizes metastable defects, which arise from the breakage of weak Si-Si bonds during light exposure, by attaching itself to one of a pair of dangling bonds or by coordinating a three-centered Si-H-Si configuration (Fig. 4.2).[13,19-21] Thus, too many hydrogen atoms or Si–H_2 configurations are supposed to enhance the motion of hydrogen atoms during light soaking, besides they decrease the average fold number of Si networks, and consequently cause more metastable defects.

4.3.2 Optical gap dependence of light-induced degradation and thermally-induced recovery

Figure 4.3 shows the cell efficiency normalized by the initial efficiency after white light soaking. The efficiency is plotted against the E_{opt} of i-layers. After 70 minutes, the cells with E_{opt} = 1.4-1.5 eV showed the most degradation. However, after 7500 minutes, the minimum normalized efficiency shifted to the region of E_{opt}=1.2-1.3 eV. Here, we should note that, in the i-layer with narrower E_{opt}, (1) the carrier generation rate is larger, and (2) the concentration of carrier generation on the incident side is more radical, because of the higher photon absorption coefficient. To cancel the influence of these factors, the same set of cells was also degraded under filtered light. Filters sharply cut the short-wavelength part of the 5 sun, AM-1.5 light, and a cut wavelength was selected for each E_{opt} of the i-layers in order to keep the short-circuit current at 35-40 mA/cm^2. Figure 4.4 shows the cell efficiency normalized by the initial efficiency after filtered light soaking. The minimum again shifted to the narrower E_{opt} region during the filtered light soaking, as in Fig. 4.3. The minimum shifts shown in Figs. 4.3 and 4.4 mean that cells with narrower E_{opt} degrade

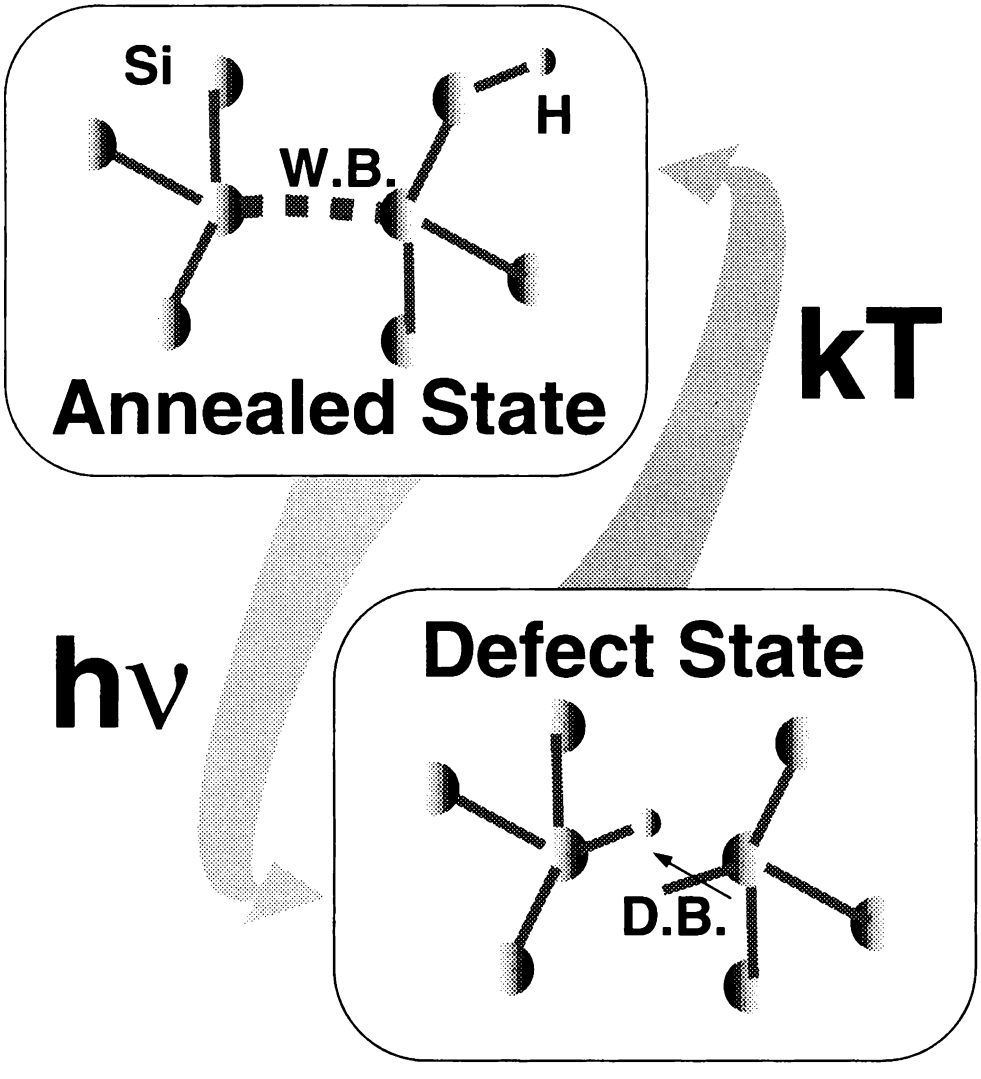

Fig. 4.2 Schematic illustrations of a hydrogen-mediated model of the reversible Staebler-Wronski effects.

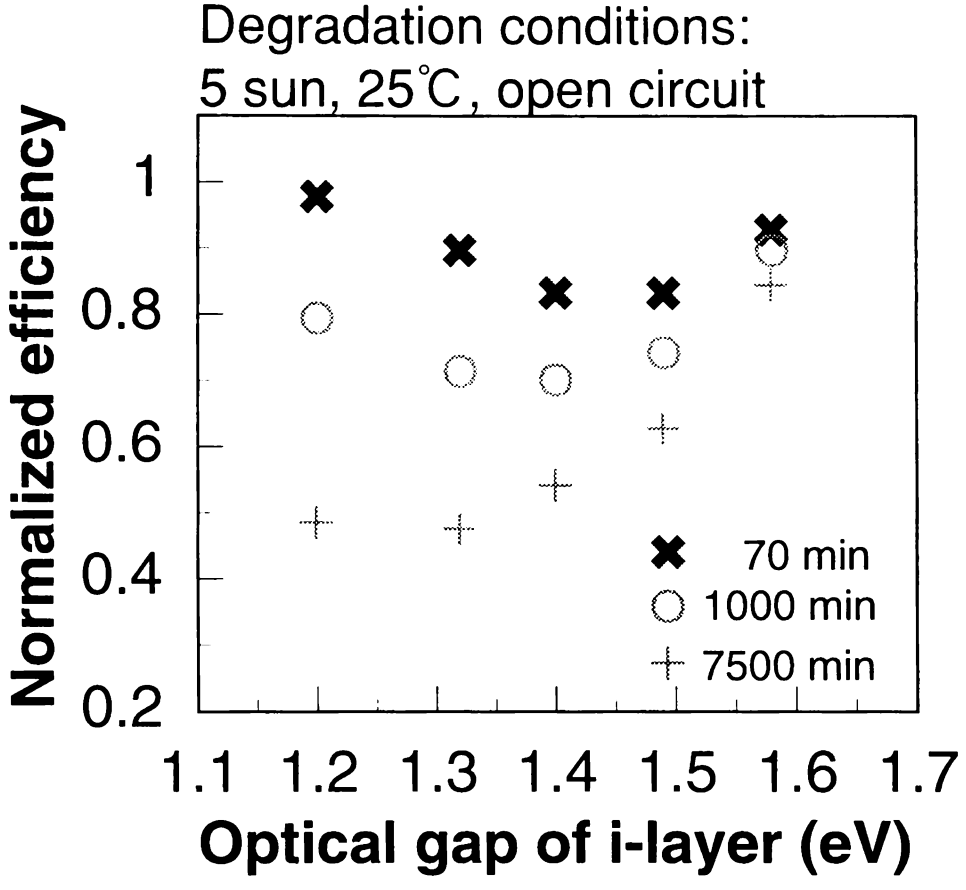

Fig. 4.3 The normalized efficiency of a-SiGe single-junction cells after 70, 1000 and 7500 minutes of white light soaking (5 sun, AM-1.5 light with open circuit conditions at 25 ℃) plotted against the E_{opt} of i-layers.

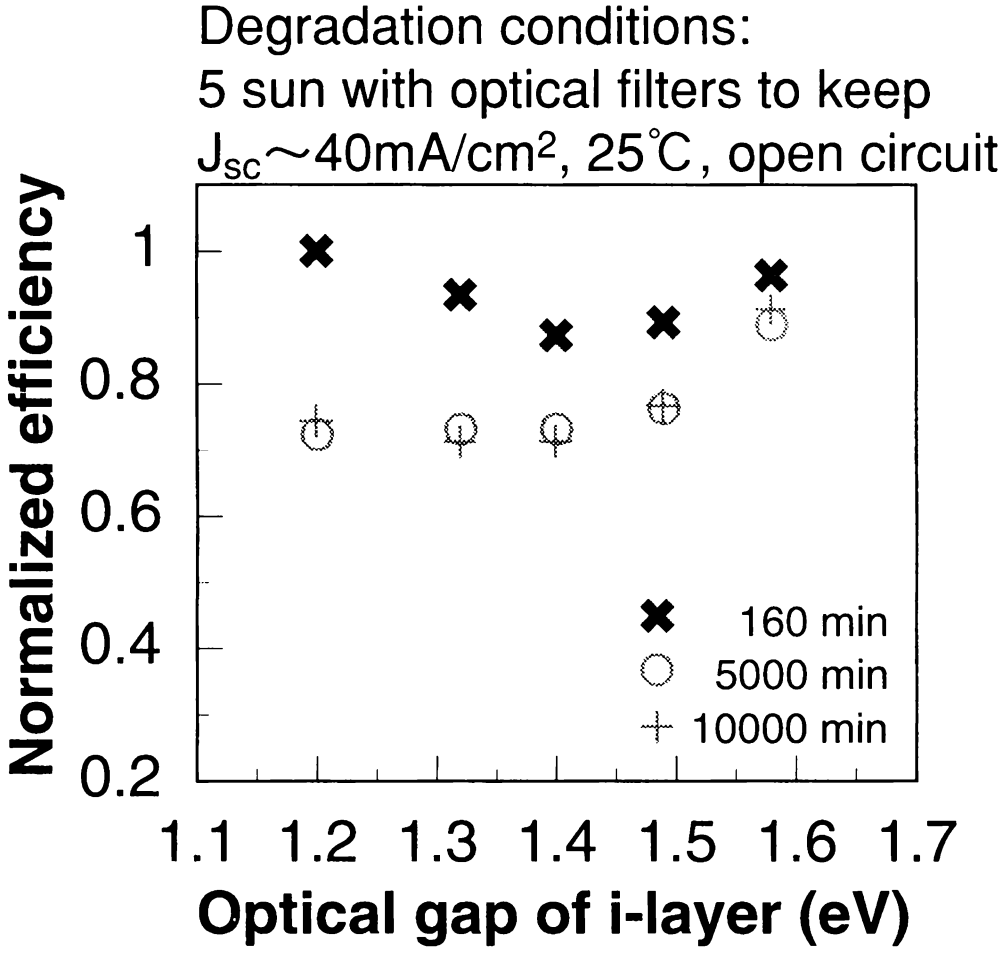

Fig. 4.4 The normalized efficiency of a-SiGe single-junction cells after 160, 5000 and 10000 minutes of filtered light soaking plotted against E_{opt} of i-layers. The filters sharply cut the short-wavelength part of the 5 sun, AM-1.5 light, and a cut wavelength was selected for each E_{opt} of i-layers to keep the short-circuit current at 35-40 mA/cm^2.

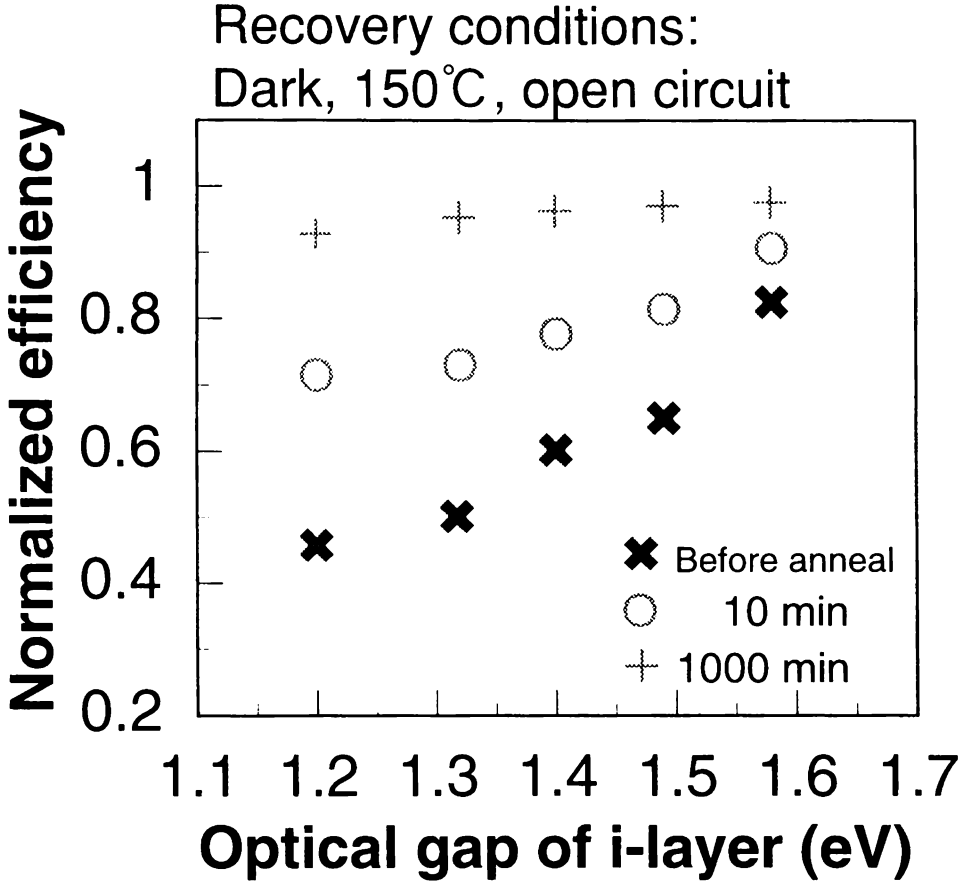

Fig. 4.5 The normalized efficiency of a-SiGe single-junction cells during dark annealing at 150℃, plotted against E_{opt} of i-layers.

slower.

The cells degraded under white light were recovered by thermal annealing at 150 ℃. Figure 4.5 shows the cell efficiency normalized by the initial efficiency during annealing, plotted against annealing time. In contrast to the case of degradation, no peak shift was observed. After 1000 minutes of annealing, the efficiency of all samples recovered to more than 95% of their initial values.

4.4 Time constant analysis for defect creation and annealing

The degradation and recovery of the solar cell efficiency are thought to occur due to the creation and removal, respectively, of metastable defects in the i layers. To clearly understand the degradation and recovery behavior in cell performance, the time-dependent data of cell efficiency were related to the change of defect density.

4.4.1 Definition of time constant

Previous experimental results suggested that the cell efficiency or fill factor during light-induced degradation has a linear relationship to the logarithm of the defect density.[22-24] For example, Chen and Yang reported the following empirical relation,[24]

$$\eta \propto 1 - A \log N, \tag{4.1}$$

where η, A and N are, respectively, the efficiency, constant depending on the cell structure and defect density of i-layer.

The term "degradation ratio," meaning the ratio of decreasing conversion efficiency, is generally used to describe the stability of a-Si materials. However, the "degradation ratio" not only reflects the stability of materials, but also the stability of the device structure. For example, cells with thinner i-layers exhibit smaller degradation. The differences of cell structure appear as variations in "A" in Eq. (4.1). In order to extract the effect of the material factor by canceling A, the normalized efficiency (η_N) was defined as follows using Eq. (4.1),

$$\eta_N = (\eta - \eta_{sat})/(\eta_{init} - \eta_{sat})$$

$$= \log (N/N_{sat})/\log (N_{init}/N_{sat}), \quad (4.2)$$

where η_{init}, η_{sat}, N_{init} and N_{sat} are the initial and saturated efficiency and defect density, respectively.

Figure 4.6 shows a kinetic model of the creation and removal of metastable defects during light-soaking and thermal-annealing. The changing rate of defect density is believed to be determined by a trade-off among the following four processes: light-induced creation (LIC), light-induced annealing (LIA), thermal-induced creation (TIC), and thermal-induced annealing (TIA). Redfield proposed the following relationship to describe defect creation kinetics,[25,26]

$$dN/dt = C_1 (N_t - N) R - C_2 N R + \nu_1 (N_t - N) - \nu_2 N, \quad (4.3)$$

where N_t and R are, respectively, the total density of potential defect sites and the recombination rate of light-generated carriers, and C_1, C_2, ν_1 and ν_2 are constants corresponding to LIC, LIA, TIC, and TIA. The time dependence of N can be represented by the following stretched-exponential function,

$$N = N_{sat} - (N_{sat} - N_{init}) \exp (-(t/\tau)^{\beta}), \quad (4.4)$$

where τ and β are constants. Although $\beta=1$ is the solution of Eq. (4.3), the values $0<\beta<1$ have been reported previously from an experimental fitting.[26] When assuming $R=0$, Eqs. (4.3) and (4.4) respectively become the rate equation and its solution, which were proposed by Kakalios *et al*,[27] expressing the reduction of defect density during annealing in the dark. Thus, Eq. (4.3) can represent the saturation behavior that not only increases defect density during light-soaking, but also decreases defect density during annealing.

Using Eqs. (4.2) and (4.4), the time dependence of η_N during light-soaking or dark annealing can be represented as,

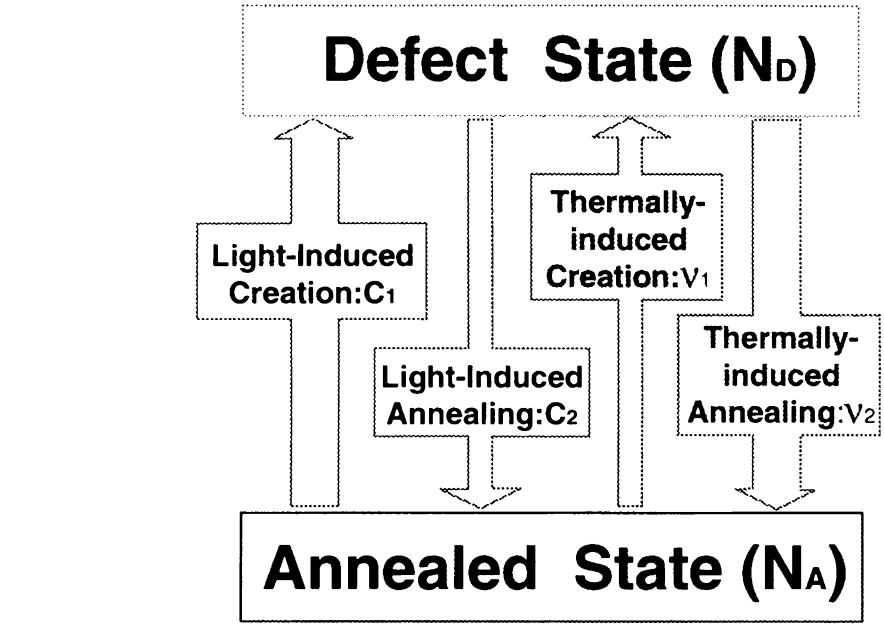

$$\frac{dN}{dt} = C_1(N_t - N)R - C_2NR + \nu_1(N_t - N) - \nu_2N$$

$$\text{Solution: } N(t) = N_{sat} - (N_{sat} - N_{init})\exp(-(t/\tau)^{\beta})$$

$$\tau = \frac{1}{(C_1 + C_2)R + \nu_1 + \nu_2}$$

$$N_{sat} = \frac{N_t(C_1R + \nu_1)}{(C_1 + C_2)R + \nu_1 + \nu_2}$$

Fig. 4.6 A kinetic model of the creation and removal of metastable defects during light-soaking and thermal-annealing. (See text.)

$$\eta_N = (\eta - \eta_{sat})/(\eta_{init} - \eta_{sat}) = -(1/n)\log[1-(1-1/10^n)\exp\{-(t/\tau)^{\beta}\}], \quad (4.5)$$

where n = log (N_{sat}/N_{init}). To quantitatively discuss the photostability of i-layer materials, the main focus is put on the time constant, τ, in which the cell-structure constant "A" is canceled, as shown in Eq. (4.5).

4.4.2 Effect of optical gap and composition on the time constant for degradation

Figure 4.7 shows the efficiency normalized by the initial and saturated values of a-SiGe solar cells with constant E_{opt} and different compositions plotted against the AM 1.5, 5 sun light soaking time at 25°C. The solid lines in Fig. 4.7 are the fitting curves of Eq. (4.5). Here, we assumed n = 2, which corresponds to the increase in defect density from 10^{15} to 10^{17}cm^{-3} to be saturated during light soaking. η_{sat} and τ_{LIC} (τ for light-induced defect creation) and β for each E_{opt} were estimated from the fitting curves. There are about 1.5 orders of magnitude difference in τ_{LIC} between 1.20 eV and 1.58 eV cells, even taking into account the fitting errors. The larger τ_{LIC} for the narrower E_{opt} cell is consistent with the results in the previous report which indicates that the rate of decrease in photo-conductivity becomes lower with the narrowing of E_{opt}.[6]

A clear correlation has been observed between the degradation time constant, τ_{LIC}, and the i-layer E_{opt}, as shown in Fig. 4.7. However, while E_{opt} changes, the compositions also change. To clarify the effect of the difference in C_H and C_{Ge} on τ_{LIC}, the degradation behavior of a-SiGe solar cells with a constant E_{opt} (~1.32 eV) and various combinations of C_H and C_{Ge} were also compared. Figure 4.8 shows the efficiency of these cells normalized by the initial and saturated values, plotted against light soaking time. When C_H, $C_{H(Si\text{-}H2)}$ and C_{Ge} were changed while E_{opt} was kept constant, no composition dependence of τ_{LIC} for light-induced degradation was observed. This result indicates that difference in C_H, $C_{H(Si\text{-}H2)}$ and C_{Ge} has very little effect on the degradation time constant, τ_{LIC}.

4.4.3 Effect of optical gap on the time constant for recovery

Cells with various E_{opt} i-layers were recovered by thermal annealing at various temperatures after 1000 minutes of light-soaking. Figure 4.9 shows cell efficiency normalized by the values

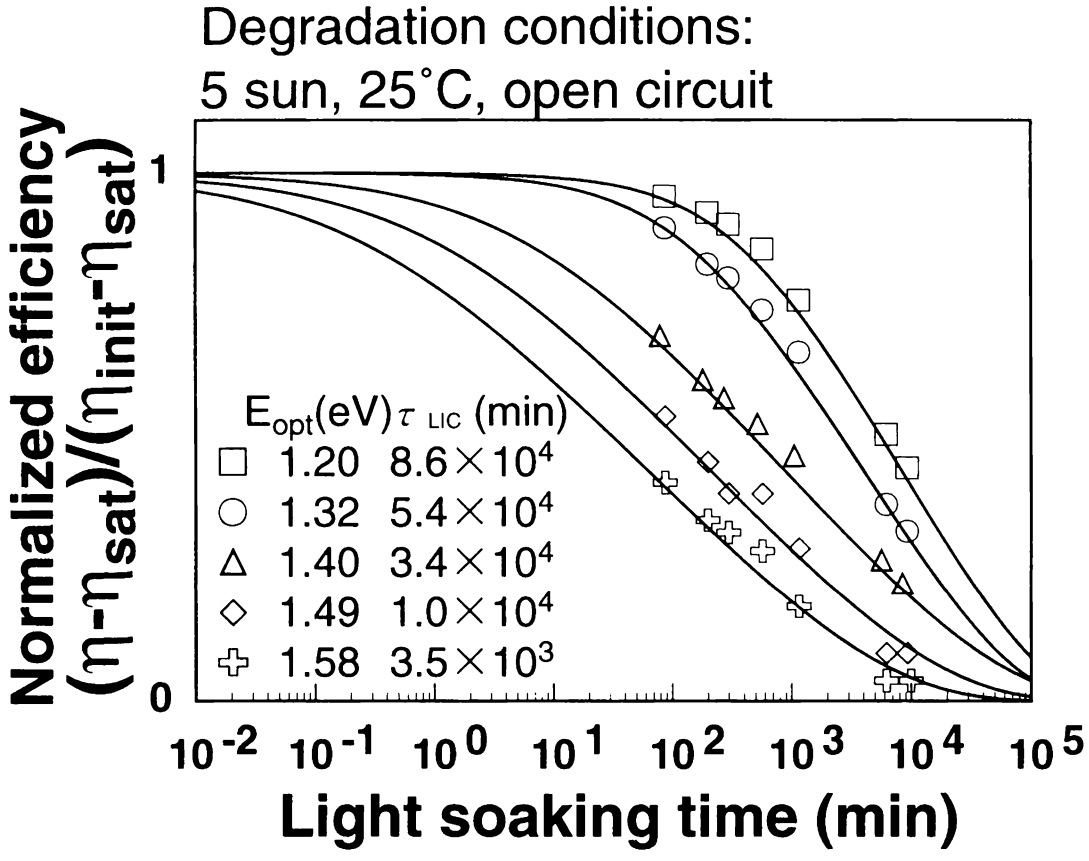

Fig. 4.7 The degradation of the efficiency of a-SiGe single-junction solar cells with various E_{opt} i-layers during ligh soaking (5 sun, AM-1.5 light, open circuit conditions, 25 °C), normalized by the initial and saturated values, plotted against the light-soaking time. The solid lines are fitting curves, where n=2 in Eq. (4.5) was assumed.

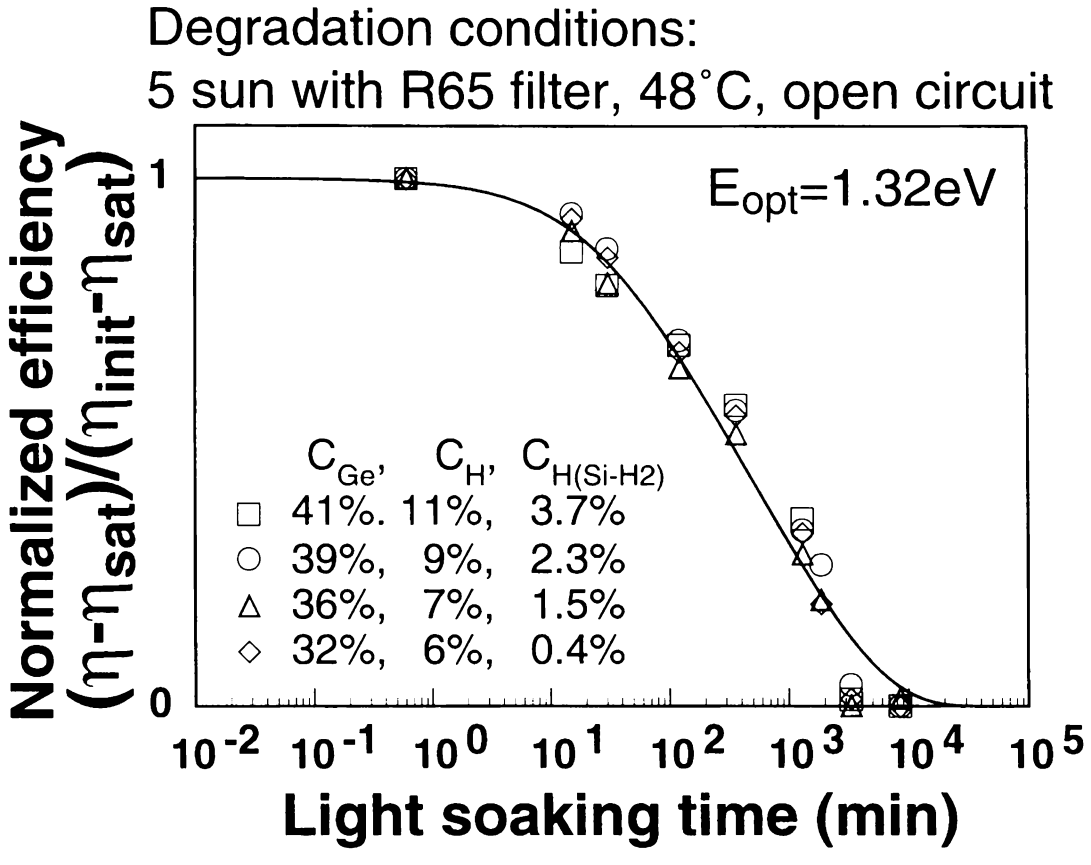

Fig. 4.8 The degradation of the efficiency of a-SiGe single-junction cells with constant E_{opt} during red light soaking (5 sun, AM-1.5 light through R65 optical filter with open circuit conditions at 25 ℃), normalized by the initial (η_{init}) and saturated (η_{sat}) values. The solid lines are the fitting curves of Eq. (4.5).

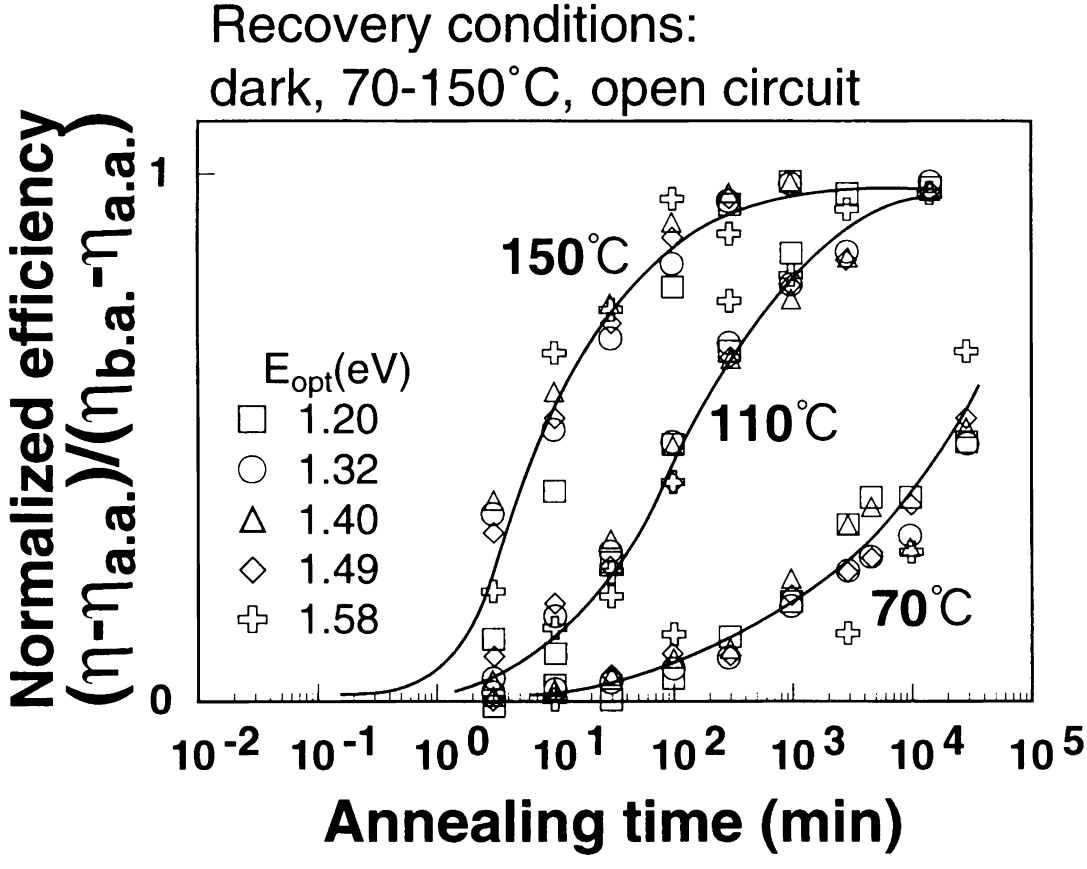

Fig. 4.9 The recovery of the efficiency of a-SiGe single-junction solar cells with various E_{opt} i-layers during annealing (in dark, open circuit conditions at 70, 110 and 150 °C), by the initial and saturated values of annealing, plotted against the annealing time. $\eta_{b.a.}$ and $\eta_{a.a.}$ are the efficiency before annealing and the saturated efficiency after annealing, respectively. $\eta_{a.a.}$ for 70 °C was estimated from curve fitting by Eq. (4.5).

before and after 300 minutes of annealing at 70, 110 and 150 ℃, plotted against annealing time. At higher temperatures, efficiency recovers more rapidly. At a certain temperature, however, no variation in time-dependence data was observed among samples with different E_{opt}.

The time constants for degradation and annealing were evaluated for various E_{opt} and annealing temperatures by fitting the time-dependence data from Figs. 4.7 and 4.9 to Eq. (4.5). The solid lines in Figs. 4.7 and 4.9 are fitting curves.[28] Figure 4.10 shows the time constant for degradation during 5 sun light soaking at 25℃ (τ_{LIC}), and the time constant for annealing in dark (τ_{TIA}) at various temperatures plotted against E_{opt}. τ_{TIA} becomes smaller with the increase in annealing temperature for each E_{opt}. This results in an increase in the annealing velocity, $1/\tau_{TIA}$, which is a thermally activated factor. It is possible to see that τ_{TIA} does not depend on E_{opt}, in contrast to the negative dependence of τ_{LIC} on E_{opt}. The activation energy for the annealing of metastable defects (ΔE_a) was evaluated using an Arrhenius plot of the temperature dependence data of τ_{TIA}. Figure 4.11 shows ΔE_a as a function of E_{opt}. ΔE_a is also not strongly dependent on E_{opt}

4.4.4 Discussions

In this section, the origin of the E_{opt} effects on the time constants (τ_{LIC} and τ_{TIA}) is discussed. According to Eqs. (4.3) and (4.4), τ and the N_{sat} are, respectively, represented as,

$$\tau \propto \{(C_1+C_2)R+\nu_1+\nu_2\}^{-1}, \tag{4.6}$$

$$N_{sat} \propto (C_1R+\nu_1)/\{(C_1+C_2)R+\nu_1+\nu_2\}. \tag{4.7}$$

In a light-soaking experiment at room temperature, TIC and TIA were not significant compared with LIC and LIA. Therefore, the time constant for light-induced degradation, τ_{LIC}, becomes,

$$\tau_{LIC} \propto \{(C_1+C_2)R\}^{-1}. \tag{4.8}$$

On the other hand, in an annealing experiment in the dark, R~0. Therefore, the time constant for annealing, τ_{TIA}, becomes,

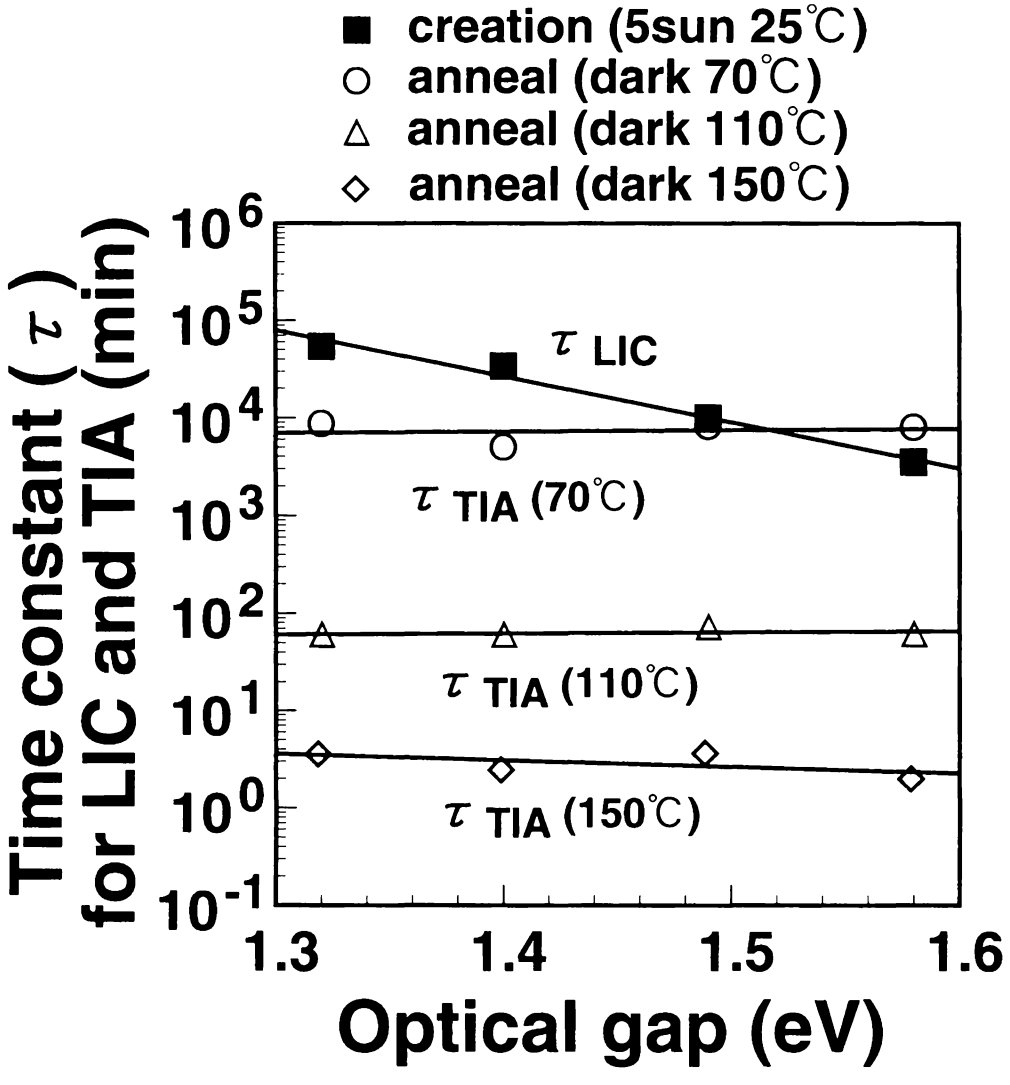

Fig. 4.10 The time constant for degradation during 5 sun ligh soaking at 25℃ (τ_{LIC}) and annealing in dark at various temperatures (τ_{TIA}) plotted against E_{opt}.

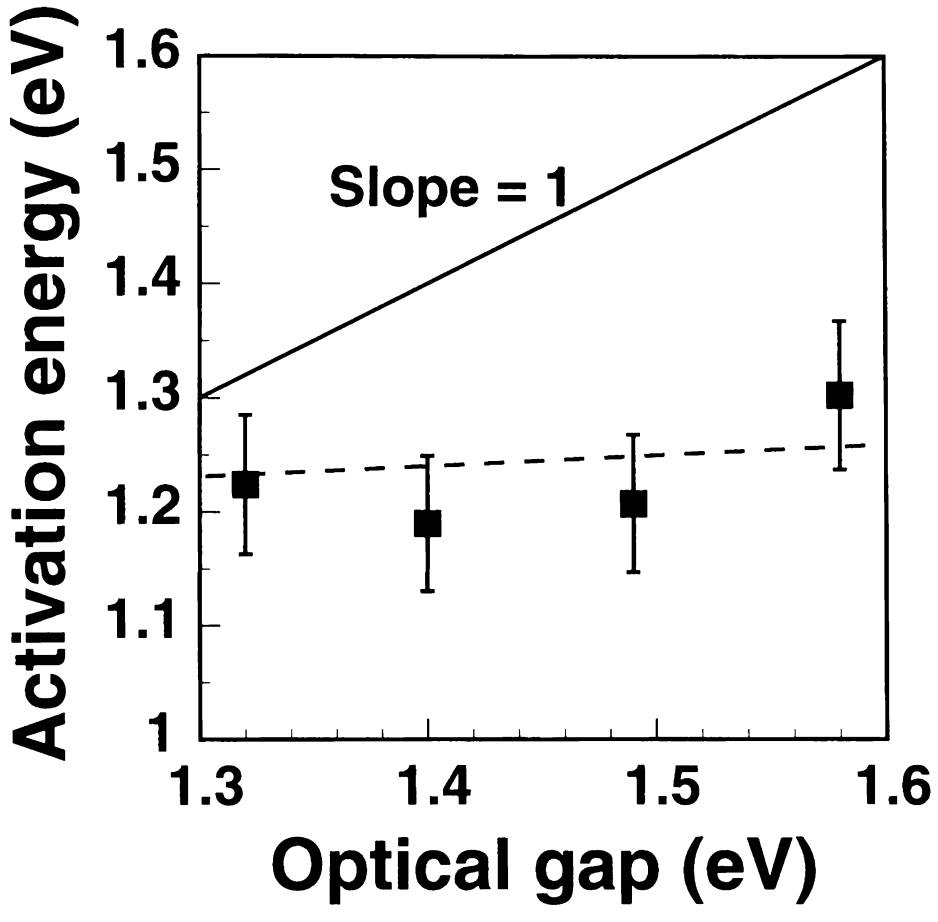

Fig. 4.11 The activation energy for the annealing of metastable defects, evaluated by an Arrhenius plot, as a function of E_{opt}. The dashed and solid lines indicate a linear fitting line and slope=1, respectively.

$$\tau_{TIA} \propto (\nu_1 + \nu_2)^{-1}. \quad (4.9)$$

In Eqs. (4.8) and (4.9), it is possible to see that τ_{LIC} is determined only by the light-induced factors, C_1 and C_2, and τ_{TIA} only by the thermally-induced factors, ν_1 and ν_2 (Fig. 4.12).

The increase in τ_{LIC} with the decrease in E_{opt}, as shown in Fig. 4.10, results in the decrease of the light-induced factors, C_1 and C_2. It has already been confirmed that the E_{opt} dependence of τ_{LIC} is not due to the variations in the compositions, such as C_H or C_{Ge}, but the variations in E_{opt} itself, as mentioned in *4.4.2.* Figure 4.13 shows an energy-configuration diagram representing the metastability of a-Si:H alloys. The deeper and shallower minima indicate the annealed and light-soaked (defect) states, respectively. The upward arrows in the figure show the energies arising from the nonradiative recombination of hole-electron pairs, which is a driving force of the light-induced processes. The most possible explanation for the suppression of the light-induced processes in cells with a narrower E_{opt} is a decrease in the recombination energy as shown in Fig. 4.13, which means the diminished energy available from hole-electron recombination for structural changes of amorphous networks. However, there is another possible cause for the E_{opt} dependence of τ_{LIC}. This is the change in the potential barrier between the annealed states and metastable states when E_{opt} is reduced. However, the missing dependence of τ_{TIA} and of ΔE_a on E_{opt}, as shown in Figs. 4.10 and 4.11, rules out the participation of the barrier height or thermal annealing processes in the variation in τ_{LIC}.

The decrease of defect density during annealing is thought to be due to the structural relaxation in the amorphous network via the diffusion of hydrogen atoms.[29-33] Thus, the E_{opt} independence of ΔE_a in Fig. 4.11 suggests that the variation of E_{opt} causes little energy difference in the trap depth for hydrogen atoms, which should diffuse to remove metastable defects during annealing. This may appear strange when first considering the facts: (1) the energy level of germanium dangling bonds is shallower than that of Si dangling bonds, and (2) the binding energy of H–Ge bonds is smaller than that of H–Si bonds. However, this is consistent with previously reported results for a-SiGe:H alloys: (1) a majority of light-induced metastable defects are Si oriented despite the existence of a considerable amount of germanium oriented defects,[8,34] (2) most hydrogen atoms are bonded to Si atoms,[34-37] as mentioned in Chapter 3, and (3) the activation energy for hydrogen diffusion does not depend strongly on C_{Ge}.[37] The activation energy of 1.2-1.3

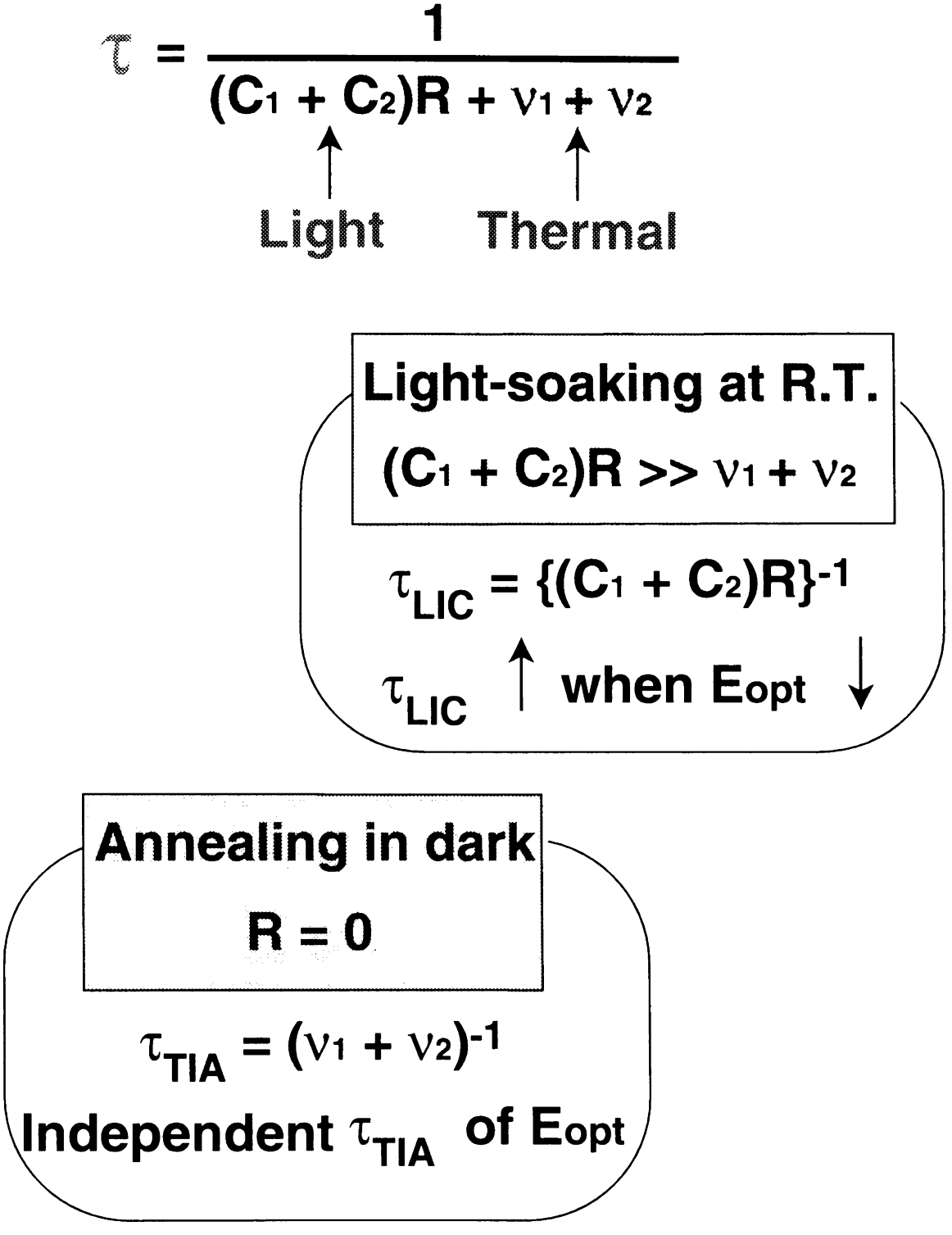

Fig. 4.12 Explanation of the E_{opt} dependence of the degradation time constant (τ_{LIC}) and annealing time constant (τ_{TIA}).

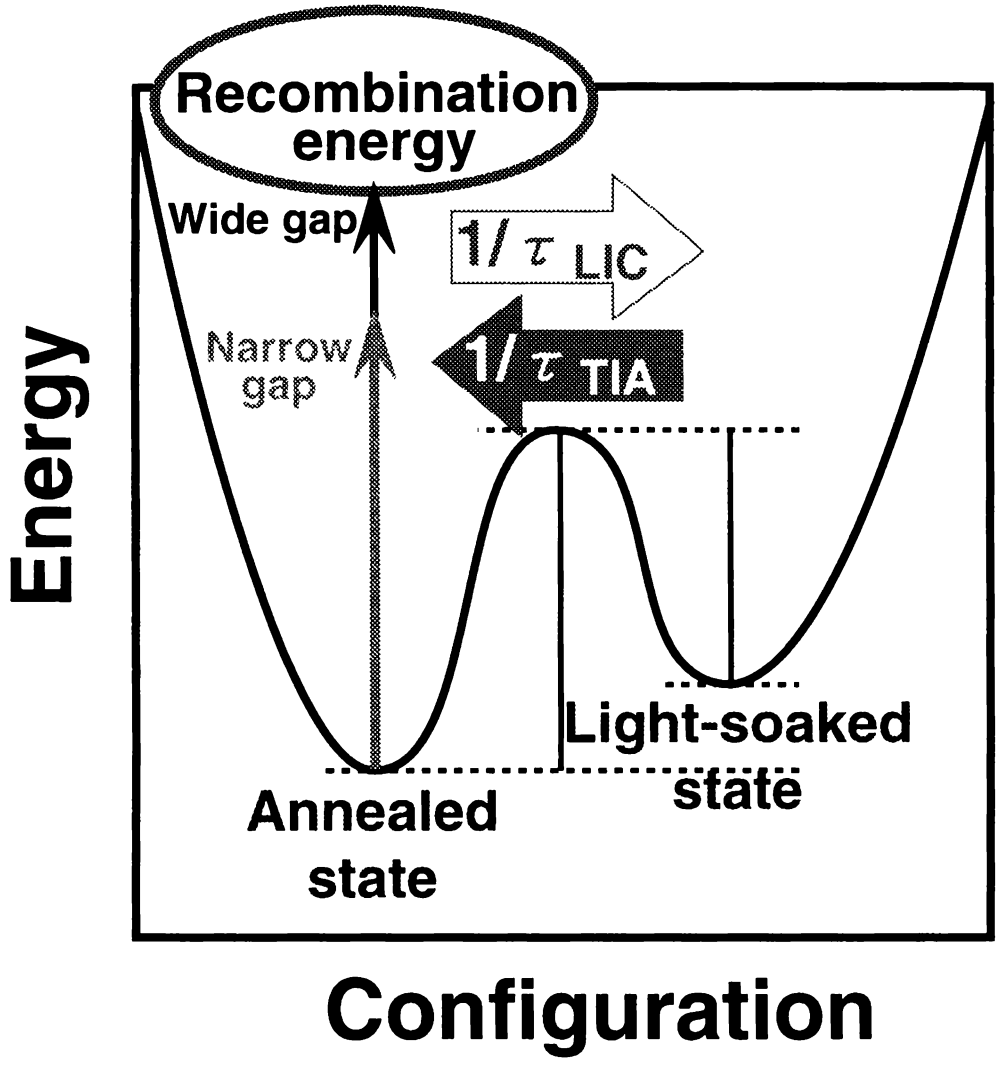

Fig. 4.13 An energy-configuration diagram representing the metastability of a-Si:H alloys. The upward arrows indicate recombination energies which depend on E_{opt}.

eV for annealing of metastable defects in a-SiGe cells with various E_{opt}, as shown in Fig. 4.11, is comparable to the previously reported activation energies for hydrogen diffusion and annealing of metastable defects in a-Si:H.[29-34,38]

4.5 Influence of optical gap on the temperature dependence of cell stability

4.5.1 Temperature dependence of degradation

The degradation behavior of a-Si based solar cells is strongly affected by the temperature during light soaking. When estimating the output power of a-Si solar cells for outdoor use, the effect of temperature must be taken into account. Figures 4.14(a) and 4.14(b) show the normalized conversion efficiency of (a) a-Si single and (b) a-SiGe single cells during 5 sun, AM-1.5 light soaking at various temperatures. At room temperature, the a-SiGe single cell shows greater degradation than the a-Si single cell under continuous illumination, respectively, shown as × in Figs. 4.14(a) and 4.14(b). However, the a-SiGe cells become more stable under higher temperatures and exhibit a much greater temperature dependence compared with cells without a-SiGe i-layers. It is necessary to investigate whether this tendency explains the E_{opt} dependence of activation energy for annealing metastable defects.[39]

4.5.2 Optical gap dependence of temperature factor

The same set of cells with various E_{opt} was degraded under 5 sun light soaking at 25-75 ℃. The degradation ratio in the efficiency after light soaking is defined as,

$$\Delta \eta (t, T_{LS}) = 1 - \eta (t, T_{LS}) / \eta_{init}, \tag{4.10}$$

where t, T_{LS} and $\eta (t, T_{LS})$) are the light-soaking time, the temperature during light soaking and the degraded efficiency, respectively. Figures 4.15 (a) and 4.15 (b) show $\Delta \eta (t, T_{LS})$ after (a) 1000 minutes and (b) 7500 minutes of light soaking plotted against the temperature during degradation. The solid lines in Figs. 4.15 (a) and 4.15 (b) were obtained by linear fitting. Here, the incline of $\Delta \eta (t, T_{LS})$ against the temperature is defined as a temperature factor, $f_T(t)$. $f_T(t)$, indicating the

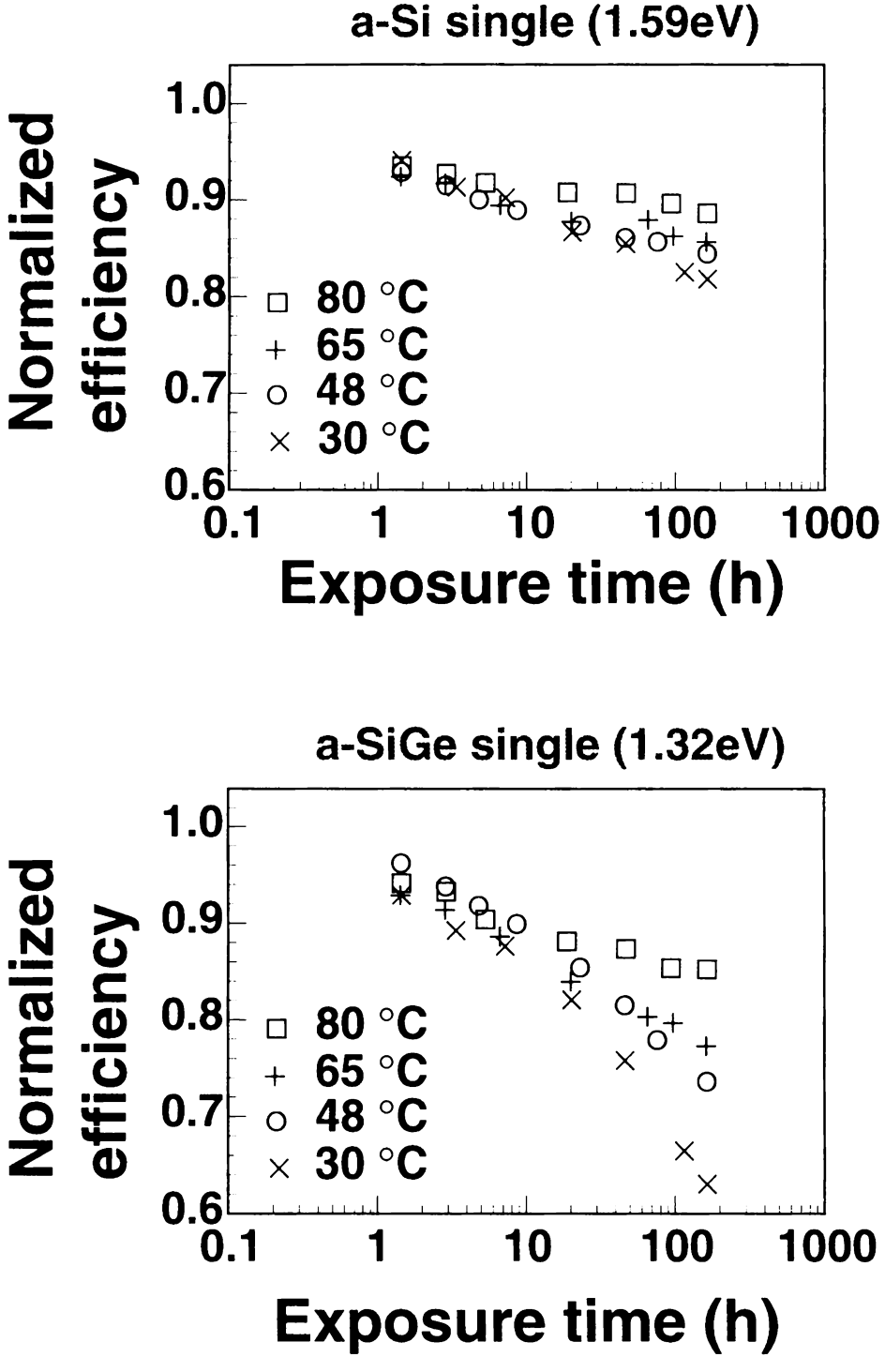

Fig. 4.14 The normalized efficiency of (a) a-Si and (b) a-SiGe cells during 5 sun, AM-1.5 light soaking at various temperatures.

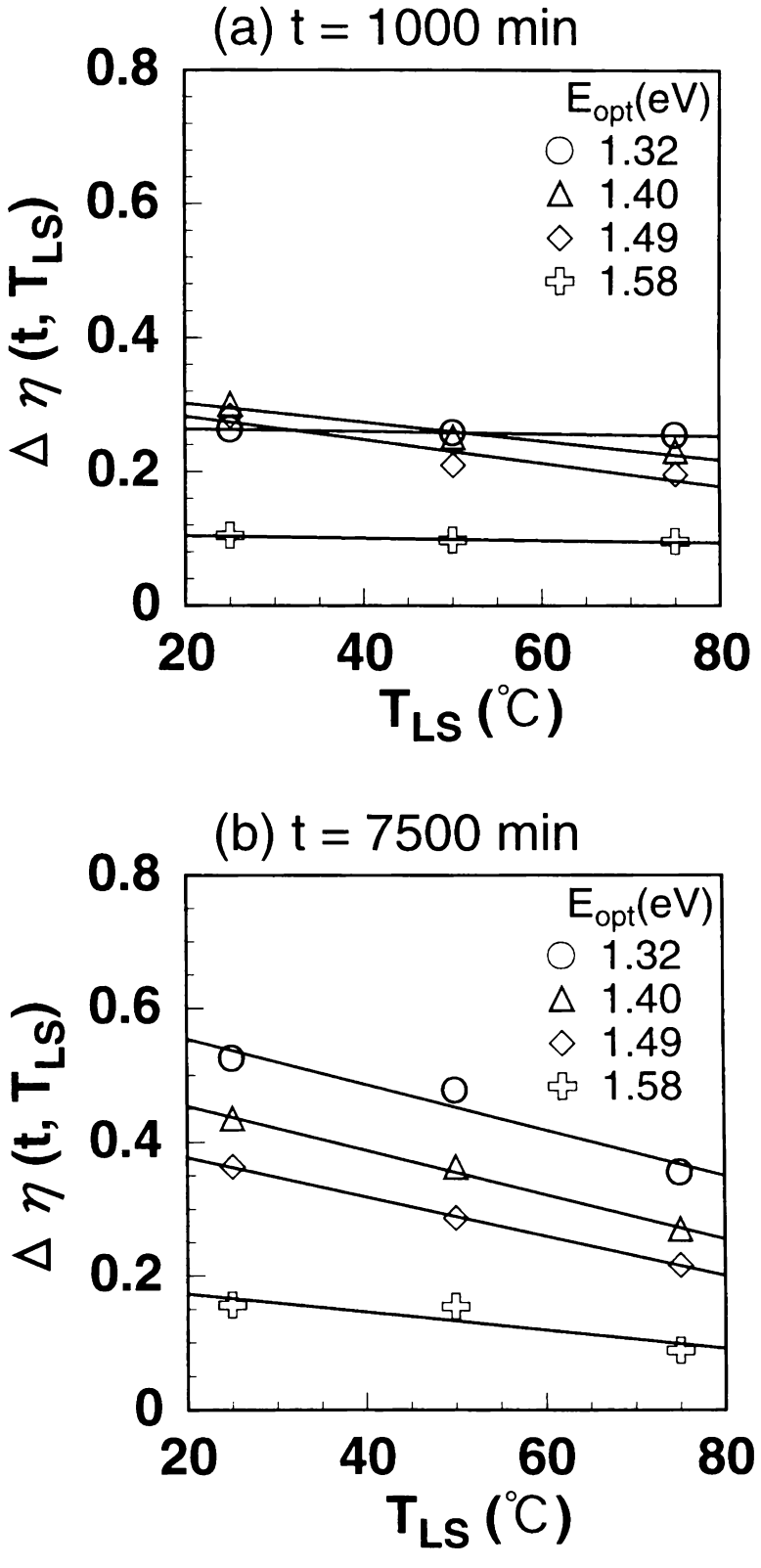

Fig. 4.15 The degradation ratio ($\Delta \eta$ (t, T_{LS})) for t=1000 min and (b) t=7500 min plotted against the temperature during light soaking.

temperature dependence of the cell stability, can be represented as follows,

$$f_T(t) = -(d/dT_{LS})\,\Delta\,\eta\,(t, T_{LS}), \tag{4.11}$$

where $f_T(t) > 0$ because of the negative dependence of $\Delta\,\eta$ on T_{LS}.

Figure 4.16 shows $f_T(t)$ for 1000 and 7500 minutes of light soaking plotted against E_{opt}. The temperature factor for 7500 minutes, f_T(7500 min), has a negative dependence on E_{opt}. This means that the stability of cells with a narrower E_{opt} is more strongly dependent on the degradation temperature after sufficiently long light soaking. On the other hand, the temperature factor for 1000 minutes, f_T(1000 min), has a peaks at 1.4-1.5 eV. This is because 1000 minutes of light soaking is not sufficient for narrower E_{opt} cells to reach N_{sat} due to the slower progress of degradation, as shown in Fig. 4.7.

4.5.3 Origin of the effect of optical gap on the temperature dependence of stability

Cells with narrower E_{opt} show a stronger temperature dependence of cell efficiency after prolonged illumination (Fig. 4.16). However, it is erroneous to believe that this temperature dependence is due to the smaller activation energy for narrower E_{opt}, because the independence of the activation energy for annealing from E_{opt} has already been shown in Fig. 4.11.

The E_{opt} dependence of the temperature factor f_T in Fig. 4.16 can be roughly explained using the following intuitive considerations (as shown in Fig. 4.17). Using Eqs. (4.7)-(4.9), N_{sat} can be represented as follows,

$$N_{sat} \propto (p/\tau_{LIC} + q/\tau_{TIA})/(1/\tau_{LIC} + 1/\tau_{TIA}), \tag{4.12}$$

where $p = C_1/(C_1+C_2) \sim 1$, $q = \nu_1/(\nu_1+\nu_2) << 1$, because the light-induced and thermally-induced processes are mainly the defect creation ($C_1 >> C_2$) and annealing reactions ($\nu_1 << \nu_2$), respectively. N_{sat} is a function of both a light-induced term, $1/\tau_{LIC}$, and a thermally induced term, $1/\tau_{TIA}$, as shown in Eq. (4.12). When decreasing E_{opt}, τ_{LIC} increases while τ_{TIA} remains constant as shown in Fig. 4.10. Thus, the contribution to N_{sat} of τ_{TIA} in Eq. (4.12), which is a thermally activated factor, becomes larger. Consequently, N_{sat} for narrower E_{opt} cells exhibit

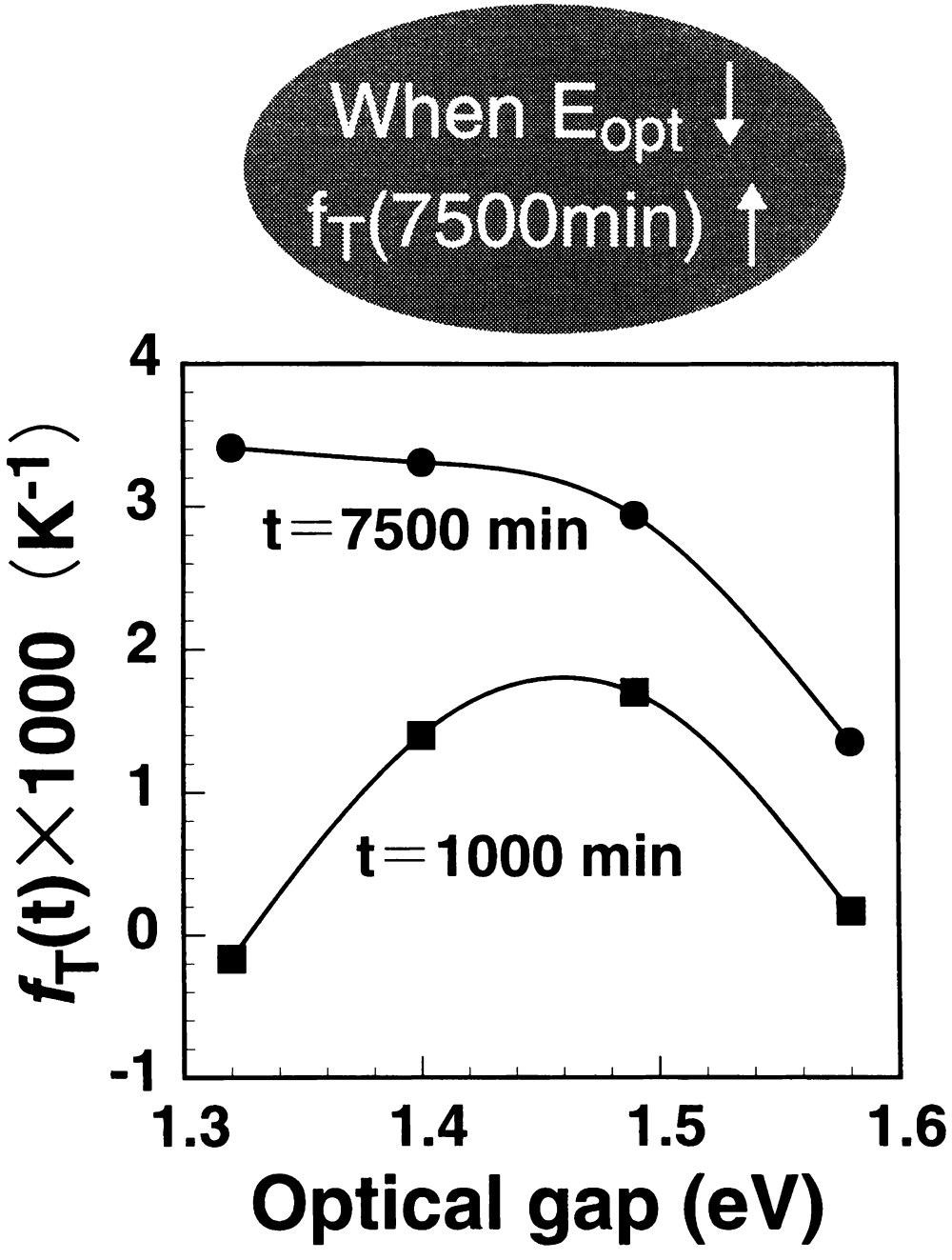

Fig. 4.16 The factors of the temperature dependence of the degraded efficiency (f_T(t)) for t=1000 min and t=7500 min of light soaking plotted against E_{opt}.

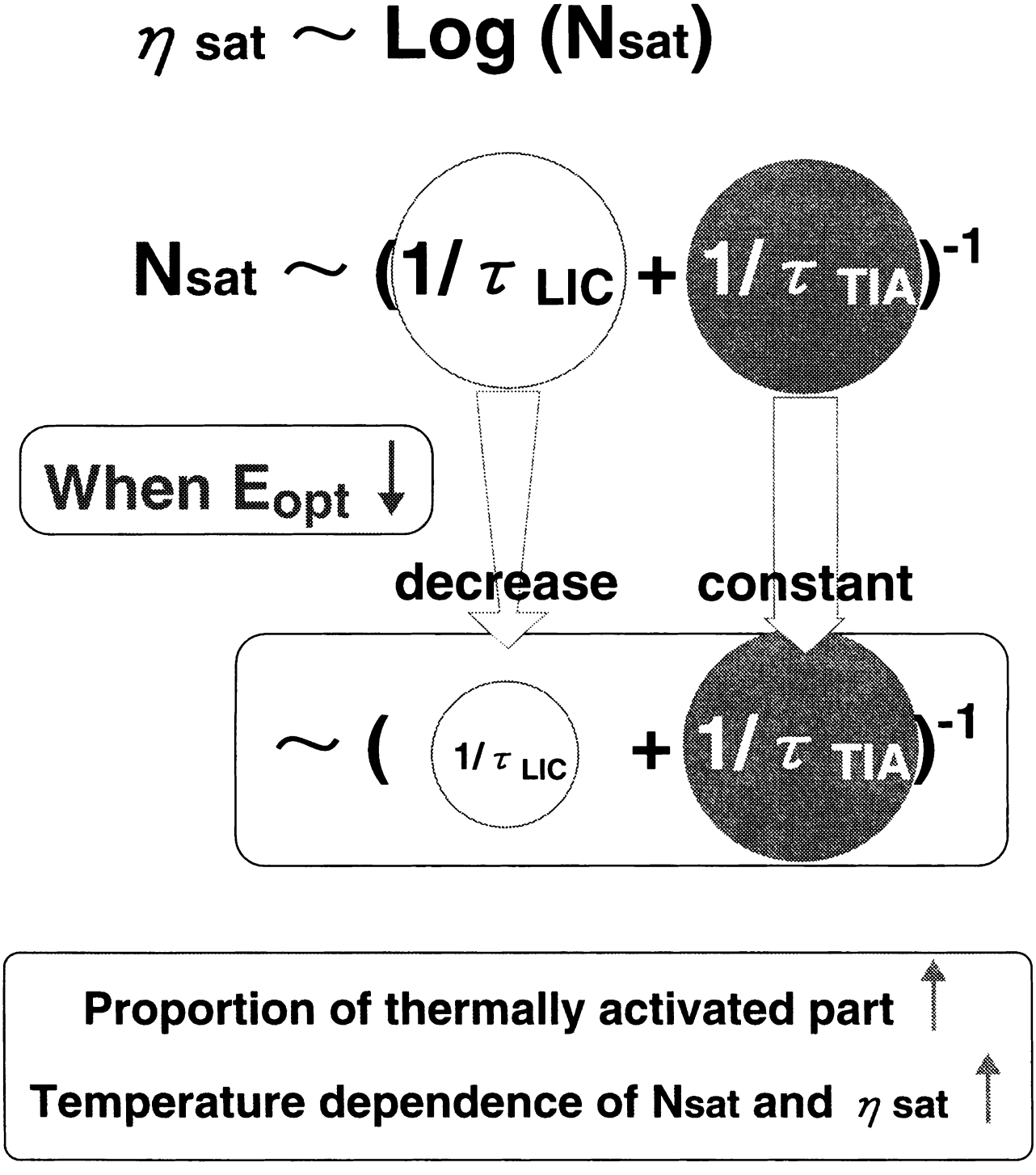

Fig. 4.17 An intuitive explanation of the E_{opt} dependence of the temperature factor. (See text.)

greater temperature dependence.

This can also be demonstrated more rigorously. The negative dependence of f_T(7500 min) to E_{opt}, as shown in Fig. 4.16, can be represented as follows, using Eq. (4.11),

$$(d/dE_{opt})f_T(7500\ \text{min}) = -(d/dE_{opt})(d/dT)\,\Delta\,\eta\,(7500\ \text{min}, T_{LS}) < 0. \tag{4.13}$$

This equality can be proven using the previous assumption. Since $\Delta\,\eta$ has a monotonous positive dependence to N_{sat} after extended light soaking, the meaning of Eq. (4.13) is qualitatively almost equivalent to,

$$(d/dE_{opt})(d/dT_{LS})N_{sat} > 0. \tag{4.14}$$

This inequality has yet to be proven. When differentiating both sides of Eq. (4.12) by T_{LS} and E_{opt}, considering that τ_{LIC} only depends on E_{opt} and τ_{TIA} only on T_{LS}, the following relation can be obtained,

$$(d/dE_{opt})(d/dT_{LS})N_{sat} \propto (d\,\tau_{LIC}/dE_{opt})(d\,\tau_{TIA}/dT_{LS})(p-q)(\tau_{TIA}-\tau_{LIC})/(\tau_{TIA}+\tau_{LIC})^3. \tag{4.15}$$

Where, $d\,\tau_{LIC}/dE_{opt} < 0$, $d\,\tau_{TIA}/dT_{LS} < 0$ (see Fig. 4.10), $(p-q) \sim 1 > 0$, $(\tau_{TIA}-\tau_{LIC}) < 0$ (because the velocity of the light-induced process, $1/\tau_{LIC}$, is larger than that of the thermally-induced process, $1/\tau_{TIA}$, under conditions causing degradation), and $(\tau_{LIC}+\tau_{TIA}) > 0$. In this way, Eq. (4.14) is confirmed.

Although a-SiGe:H alloys have considerable potential for improving initial conversion efficiency, a-SiGe cells have unfortunately exhibited relatively large degradation. However, it was suggested that solar cells with a-SiGe:H offer a greater advantage for operating at high temperatures than cells with a-Si:H due to the E_{opt} dependence of the defect creation process and the independence of the defect annealing process. Operating conditions should thus be considered in the design of highly-efficient solar cell submodules.

4.6 Summary

In order to reveal the effects of the i-layer E_{opt} and the composition of a-SiGe solar cells on stability against light soaking, the light-induced degradation and thermally-induced recovery behavior of a-SiGe cells with a constant E_{opt} and different compositions and those with various E_{opt} were systematically investigated.

(1) There are at least two aspects that should be considered for stability against light exposure. One is the saturated defect density, N_{sat}, and the other is the degradation time constant. It was shown that compositional factors such as C_H mainly affect N_{sat}, and E_{opt} affects the time constant (Fig. 4.18).

(2) It was clearly shown that a-SiGe cells with lower C_H and/or Si-H_2 content were more stable in a constant E_{opt} system. This result confirms the contribution of incorporated hydrogen atoms on metastable defect creation. The investigation of the light-induced degradation behavior of a-SiGe:H alloys in a constant E_{opt} system is significant, not only for improving the performance of these alloys themselves, but also for verifying the kinetic models proposed for a-Si materials.

(3) a-SiGe solar cells with a narrower E_{opt} degrade more slowly than, but recover as fast as, cells with a wider E_{opt}. This is because light-induced processes, such as LIC and LIA, are suppressed in materials with a narrower E_{opt}, while thermally-induced processes, such as TIC and TIA, do not depend on E_{opt}.

(4) Both the time constant (τ_{TIA}) and the activation energy (ΔE_a) for thermal annealing of metastable defects do not depend strongly on E_{opt}. These results suggest that the variation of E_{opt} causes little energetic difference in the trap depth preventing hydrogen diffusion for removing metastable defects during network relaxation by annealing, and indirectly reconfirm the suppression of the light-induced defect creation process in narrower E_{opt} alloys due to the smaller recombination energy.

(5) The degree of degradation for narrower E_{opt} cells exhibits a greater temperature dependence after sufficient long time light-soaking. This suggests that the saturated defect density, N_{sat}, which is determined by the balance of light induced and thermally-induced processes, depends on the temperature more strongly for narrower E_{opt} alloys. Because, when E_{opt} is decreased the contribution of the thermally activated factor to N_{sat} becomes relatively larger due to the E_{opt}

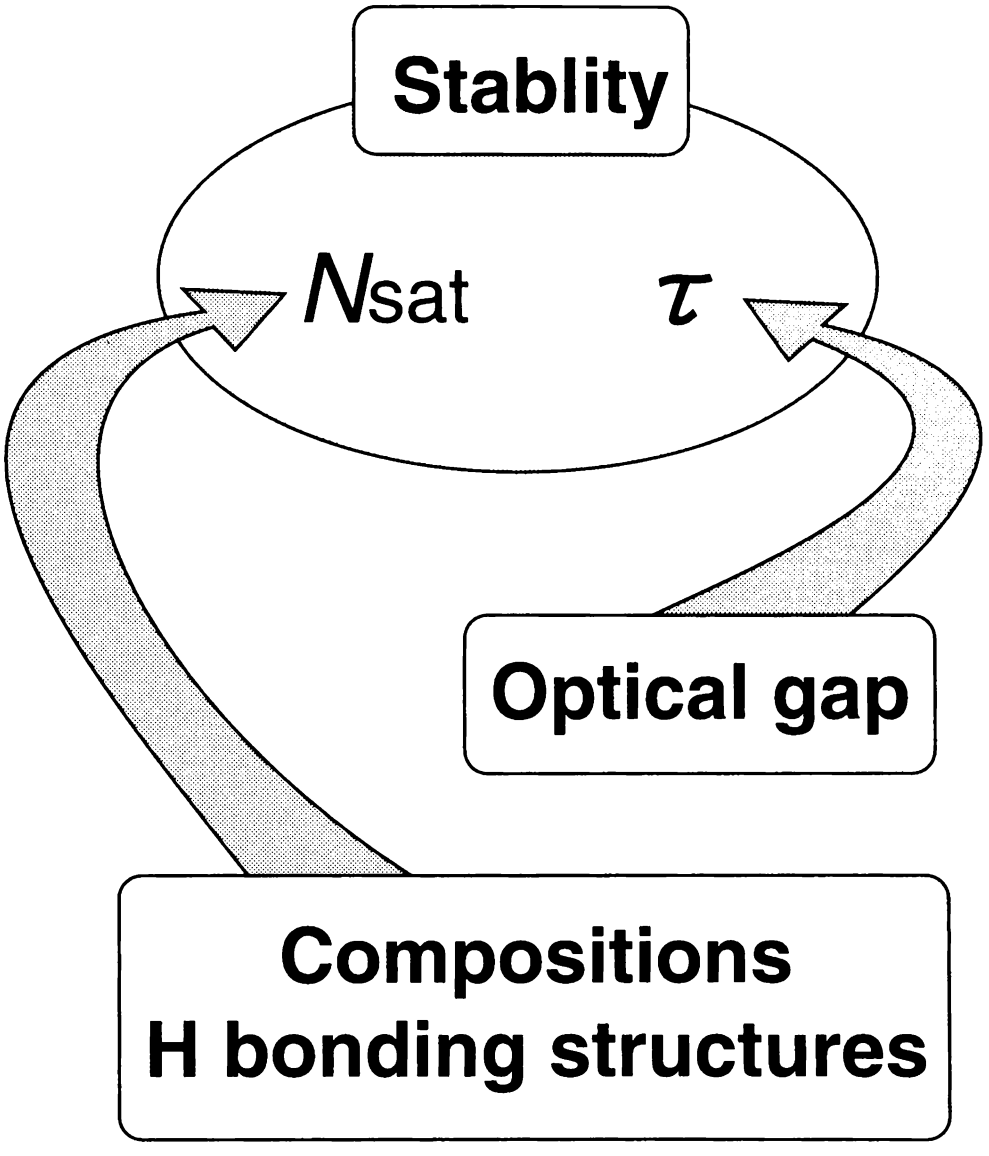

Fig. 4.18 Effects of E_{opt} and compositions of a-SiGe:H on stability against light-soaking. Compositional factors such as C_H mainly affect N_{sat}, and E_{opt} affects the time constant.

dependence of the light-induced defect creation process and the E_{opt} independence of the thermally-induced annealing process. Operating conditions should thus be considered in the design of highly-efficient solar cell submodules.

References

1. D. L. Staebler and C. R Wronsky, Appl. Phys. Lett. **31**, 292 (1977).
2. R. A. Street, *Hydrogenated Amorphous Silicon* (Cambridge University Press, 1991) p.213.
3. S. Ajishi, Z.E. Smith, V. Chu, J. Kolodzey, D. Slobodin, J.P. Conde, D.S. Shen and S. Wagner, AIP Conf. Proc. **157**, 25 (1987).
4. X. Xu, M. Kotharay, N. Hata, J. Bullock and S. Wagner, AIP Conf. Proc. **234**, 282 (1987).
5. P.A. Morin, N.W. Wang and S. Wagner, Mater. Res. Soc. Symp. Proc. **228**, 577 (1992).
6. A. Skumanich and N.M. Amer, Appl. Phys. Lett. **52**, 643 (1988).
7. G.H. Bauer, G. Schumm and C.-D. Abel, *Proc. 11th E.C. Photovoltaic Solar Energy Conf.* (Montreux, 1992) p. 672.
8. M. Stutzmann, *Tech. Dig. 5th Sunshine Workshop on Solar Cells* (1992) p. 23.
9. P. Papadopulos, A. Scholz, S. Bauer, B. Schroder and H. Oechsner, J. Non-Cryst. Solids **164-166**, 87 (1993).
10. T. Unold and J.D. Cohen, J. Non-Cryst. Solids **164-166**, 23 (1993).
11. G. Schumm, Phys. Rev. B **49**, 2427 (1994).
12. A. Terakawa, M. Shima, K. Sayama, H. Tarui, S. Tsuda, S. Nakano and Y. Kuwano, Jpn. J. Appl. Phys. **32**, 4849 (1993).
13. R. A. Street, *Hydrogenated Amorphous Silicon* (Cambridge University Press, 1991) p.211.
14. N. Nakamura, T. Takahama, M. Isomura, M. Nishikuni, K. Yoshida, S. Tsuda, S. Nakano, M. Ohnishi and Y. Kuwano, Jpn. J. Appl. Phys. **28**, 1762 (1989).
15. E. Bhattacharya and A.H. Mahan, Appl. Phys. Lett. **52**, 1587 (1988).
16. M. Osawa, T. Hama, T. Akasaka, T. Ichimura, H. Sakai, S. Ishida and Y. Uchida, Jpn. J. Appl. Phys. **24**, L838 (1985).
17. A. Terakawa, M Shima, K. Sayama, H. Tarui, H. Nishiwaki and S. Tsuda, Mater. Res. Soc. Symp. Proc. **336**, 487 (1994).
18. A. Terakawa, M Shima, K. Sayama, H. Tarui, H. Nishiwaki and S. Tsuda, Jpn. J. Appl. Phys. **34**, 1741 (1995).
19. W.B. Jackson, Phys. Rev. B **41**, 10257 (1990).
20. L.E. Mosley, M.A. Paesler and I. Shimizu, Philos. Mag. B **51**, L27 (1985).
21. H. Dersch, J. Stuke and J. Beichler, Appl. Phys. Lett. **38**, 456 (1981).
22. Z.E. Smith and S. Wagner, Mater. Res. Soc. Symp. Proc. **49**, 331 (1985).
23. N. Nakamura, T. Takahama, M. Isomura, M. Nishikuni, K. Yoshida, S. Tsuda, S. Nakano, M. Ohnishi and Y. Kuwano, Jpn. J. Appl. Phys. **28**, 1762 (1989).
24. L. Chen and L. Yang, J. Non-Cryst. Solids **137 & 138**, 1185 (1991).
25. D. Redfield, Appl. Phys. Lett. **52**, 492 (1988).

26. D. Redfield, *Proc. 11th EC Photovoltaic Solar Energy Conf.* (Montreux, 1992) p.179.

27. Kakalios, R.A. Street and W.B. Jackson, Phys. Rev. Lett. **59**, 1037 (1987).

28. n = log (N_{sat}/N_{init}) =2 in Eq. (4.5) was assumed for the fitting of degradation data in Fig. 4.7. On the other hand, n=1 was assumed for the fitting of annealing data in Fig. 4.9, because the 1000-minute light soaking, carried out before annealing, was not sufficient to reach N_{sat}.

29. M. Stutzmann, W.B. Jackson and C.C. Tsai, Phys. Rev. **B32**, 23 (1985).

30. W.B. Jackson and J. Kakalios, Phys. Rev. **B37**, 1020 (1988).

31. R. A. Street and K. Winer, Phys. Rev. **B40**, 6236 (1989).

32. R. A. Street, AIP Conf. Proc. **234** (1991) p. 21.

33. Q. Li and R. Biswas, Phys. Rev. **B52**, 10705 (1995).

34. M. Stutzmann, R.A. Street, C.C. Tsai, J.B. Boyce and S.E. Ready, J. Appl. Phys. **66**, 569 (1989).

35. W. Paul, D. K. Paul, B. Von Roedern, J. Blake and S. Oguz, Phys. Rev. Lett. **46**, 1016 (1981).

36. S. Z. Weisz, N. Gomes, J. A. Muir, O. Resto and R. Perez, Appl. Phys. Lett. **44**, 634 (1984).

37. S. Schroeder, M. Leidner and H. Oechsner, Mater. Res. Soc. Symp. Proc. **219**, 277 (1991).

38. W. Beyer, H.C. Weller and U. Zastrow, J. Non-Cryst. Solids **137 & 138**, 37 (1991).

39. A. Terakawa, M. Shima, T. Kinoshita, M. Isomura, M. Tanaka, S. Kiyama, S. Tsuda and H. Matsunami, *Proc. 14th EU Photovoltaic Solar Energy Conf.* (Barcelona, 1997), pp. 2359-2362.

Chapter 5
Applications to Efficient and Stable Solar Cells

5.1 Background

Multi-junction structures using a-SiGe:H alloys as the bottom photovoltaic materials are the most candidate of a-Si solar cells in outdoor-use power generators. In this chapter, the recent progresses in the performance of a-SiGe single and a-Si/a-SiGe tandem solar cells fabricated by the author's research group are reviewed, to which the knowledge of the present study was applied in the material design.

5.2 New concept of band-gap tailoring for a-SiGe:H i-layers

In a-Si based p-i-n solar cells, holes are the limiting carriers of the device performance. It has been, thus, generally considered that the improvement in the hole transportation is important in designing a-SiGe solar cells in which the hole mobility is smaller than in a-Si:H cells. Figure 5.1 shows the band diagram for the i-layer of previous conventional a-SiGe solar cells.[1,2] E_{opt} is continuously graded in the direction of the film thickness, and the narrowest E_{opt} portion is arranged near the p-layer. This is so-called "double graded structure (DGS)" and can be fabricated by varying GeH_4 flow ratio during deposition. DGS was developed to efficiently correct holes arising in the deep portion of the i-layer, in exchange for a little sacrifice in the electron transportation, by enhancing the field slope in the valence band and simultaneously by relieving the band off-sets between doped layers and i-layer.[1,2] Many research groups, have been focused their efforts to optimizing the DGS for a long time.[1-5] However, they faced to a dilemma. Although, in order to improve the stability it was demanded to reduce the i-layer thickness of ~300 nm, narrowing E_{opt} by adding more Ge to keep the photon absorption drastically deteriorated the collection efficiency of carriers.

In 1992, the author's group arrived at an alternative conclusion, called "strong field structure

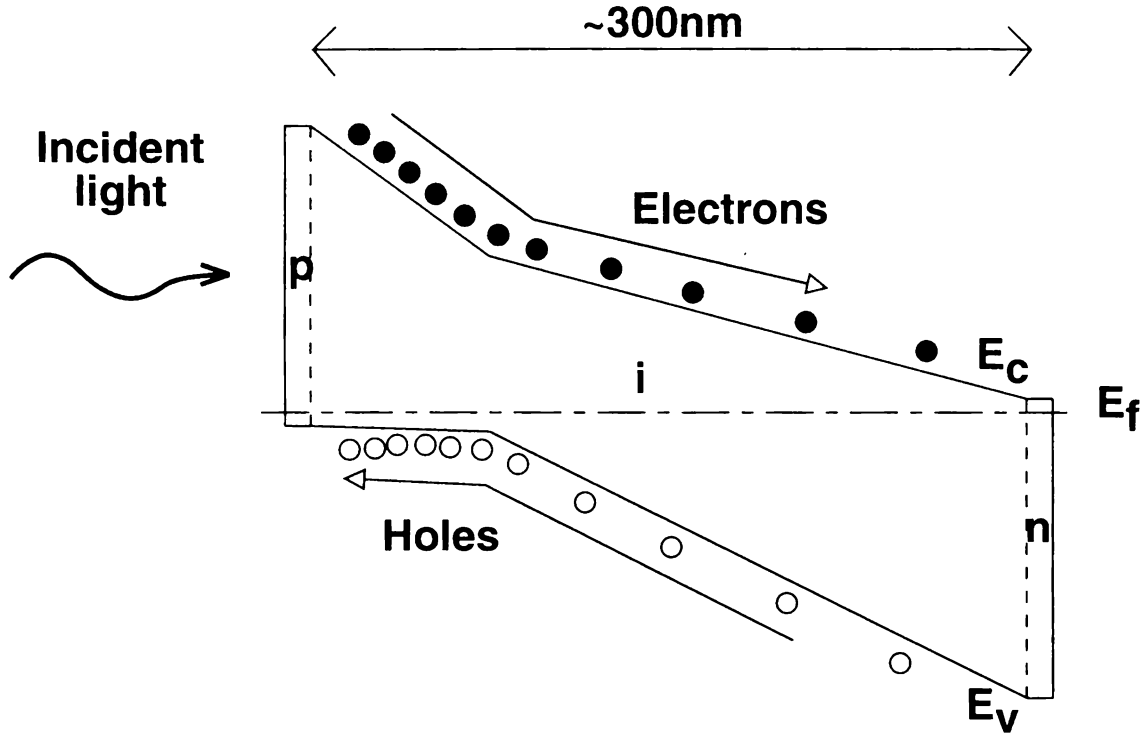

Fig. 5.1. The band diagram of an a-SiGe DGS (double graded structure) cell under I_{sc} condition.

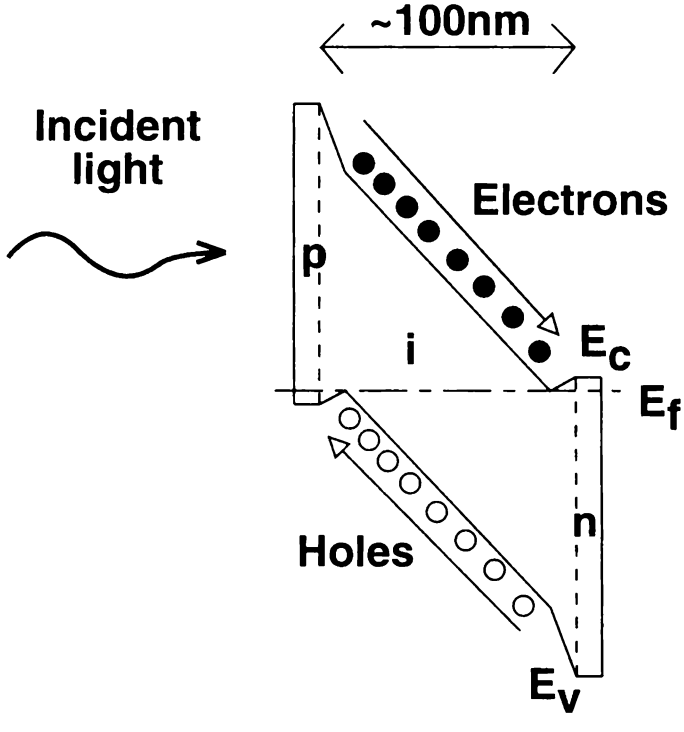

Fig. 5.2. The band diagram of an a-SiGe SFS (strong field structure) cell under I_{sc} condition.

(SFS)," as shown its band diagram in Fig. 5.2.[6] The design concepts of SFS were as follows; (1) The thickness of the i-layer was reduced to ~100 nm to enhance the internal electric field, while remaining the minimum graded portions of p/i and i/n interfaces to relieve the off-set effects. (2) It was found that the electronic properties of a-SiGe:H show drastic deterioration with C_{Ge} over ~40 at.%.[7-8] Thus, the very narrowest E_{opt} within a critical value was carefully chosen, and the region was thickened to 60-100 nm to maintain a photocurrent with a thinner i-layer. SFS solved the dilemma of DGS and realized a very high collection efficiency after light-induced degradation.[6] From the view point of the productivity in manufacturing, also SFS seems to excel DGS because the thinner i-layer can reduce the process time for deposition.

SFS also changed the status of material design for a-SiGe:H alloys. The cell performance of DGS was considered to be more sensitive to the band profiles rather than to the material properties of the narrowest E_{opt} region, because its proportion was relatively small. Besides, it was practically difficult to optimize the properties of whole region of i layer with variety of compositions. In contrary, the greater part of i layer of SFS is occupied by the narrowest E_{opt} region. Furthermore, the device performances became possible to be directly connected to the characteristics of bulk films as described in Chapters 2-4. Therefore, the properties of the narrowest E_{opt} a-SiGe:H became significantly important for SFS. These are other aspects of the background of the present study.

5.3 Material design for efficient solar cells and modules

5.3.1 A concept for optimizing i-layer compositions

The criteria for optimizing compositions of a-SiGe:H with a constant E_{opt}, concluded in Chapter 2, was applied to the i-layer material design of SFS cells. Figure 5.3 schematically illustrates the initial performance, stability and stabilized performance of a-SiGe solar cells with a constant E_{opt} as functions of C_H of the i layer. An optimum C_H exists for the initial state, while the stability against light exposure has an inverse relationship with C_H. Consequently, the best composition for the stabilized efficiency, which can be represented as the product of the initial performance and stability, slightly shifts to the lower C_H region than that for the initial state.

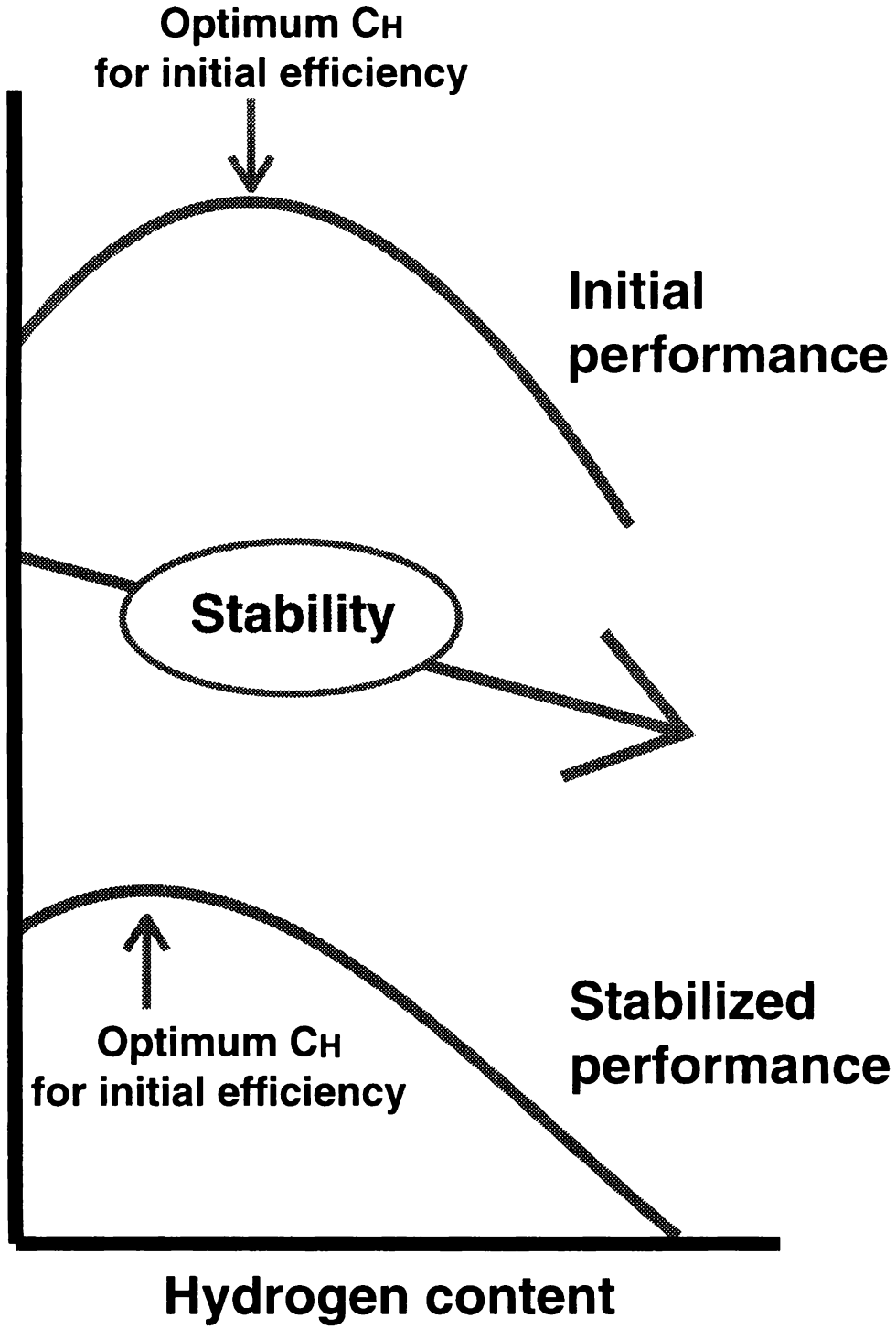

Fig. 5.3. Schematic illustrations of the initial performance, stability and stabilized performance of a-SiGe solar cells with constant E_{opt} as functions of C_H of the i layer. An optimum composition slightly shifts to the lower C_H region than that for the initial state.

5.3.2 a-SiGe single- and a-Si/a-SiGe tandem cells

Based on this concept, efficient a-SiGe single- and a-Si/a-SiGe tandem solar cells (area: 1 cm^2) were designed. a-SiGe single and a-Si/a-SiGe tandem cells consisted of TCO/ p(a-SiC:H)/ i(a-SiGe:H)/ n(a-Si:H)/ metal, and TCO/ p(a-SiC:H)/ i(a-Si:H)/ n(a-Si:H)/ p(a-SiC:H)/ i(a-SiGe:H)/ n(a-Si:H)/ metal, respectively. The thickness and E_{opt} of the a-SiGe:H i-layers are 130 nm and 1.32 eV, and those of the top a-Si:H i-layer of the tandem cell are 150 nm and 1.57 eV, respectively.

Figure 5.4 shows the initial and stabilized conversion efficiencies of an a-SiGe single-junction solar cell under red light (1sun AM-1.5 through R65 optical filter) plotted against C_H of a-SiGe:H layer.. The R65 filter was selected to evaluate a-SiGe solar cells under similar conditions to the bottom of tandem cells. The light-irradiation conditions for stabilization were AM-1.5, 5 sun light through a red optical filter (R65) at 48 ℃ for 6 hours with the open circuit condition. Figures 5.5 shows the initial and stabilized conversion efficiencies of an a-Si/a-SiGe tandem solar cell under 1 sun AM-1.5 light plotted against C_H of a-SiGe:H layer. The light-irradiation conditions for stabilization were AM-1.5, 5 sun light at 48 ℃ for 6 hours with the open circuit condition. These stabilizing conditions were corresponding to the one-year outdoor use. The shifts of optimum compositions for a-SiGe single- and a-Si/a-SiGe tandem solar cells agree well, as shown in Figs 5.4 and 5.5. Figures 5.6 (a) and 5.6 (b) show the efficiencies after prolonged illumination normalized by the initial values of (a) an a-SiGe single, and (b) an a-Si/a-SiGe tandem solar cells plotted against C_H of a-SiGe:H layer. The incline of light-induced degradation ratios of a-SiGe single- and a-Si/a-SiGe tandem solar cells also agree well. These results in Figs. 5.4-5.6 indicate that the performance of tandem cell is very sensitive to the properties and stabilities of the a-SiGe:H bottom i-layer.

In this experiment series, very high efficiencies were achieved. Figures 5.7 (a) and 5.7 (b) show the initial and stabilized illuminated I-V characteristics of (a) an a-SiGe single-junction cell and (b) an a-Si/a-SiGe tandem cells, corresponding to the highest stabilized efficiencies. The initial conversion efficiencies of 3.7 % for the a-SiGe cell under red light and 11.6 % for the tandem cell under white light have been achieved. These efficiencies became 3.3 % and 10.6 % after intense light soaking corresponding to outdoor exposure for one year.[9] The degradation ratio was only 8.6 %. The stabilized efficiencies for single- and tandem cells are the highest values ever reported for this size (1 cm^2) of an a-Si-based solar cell.[10]

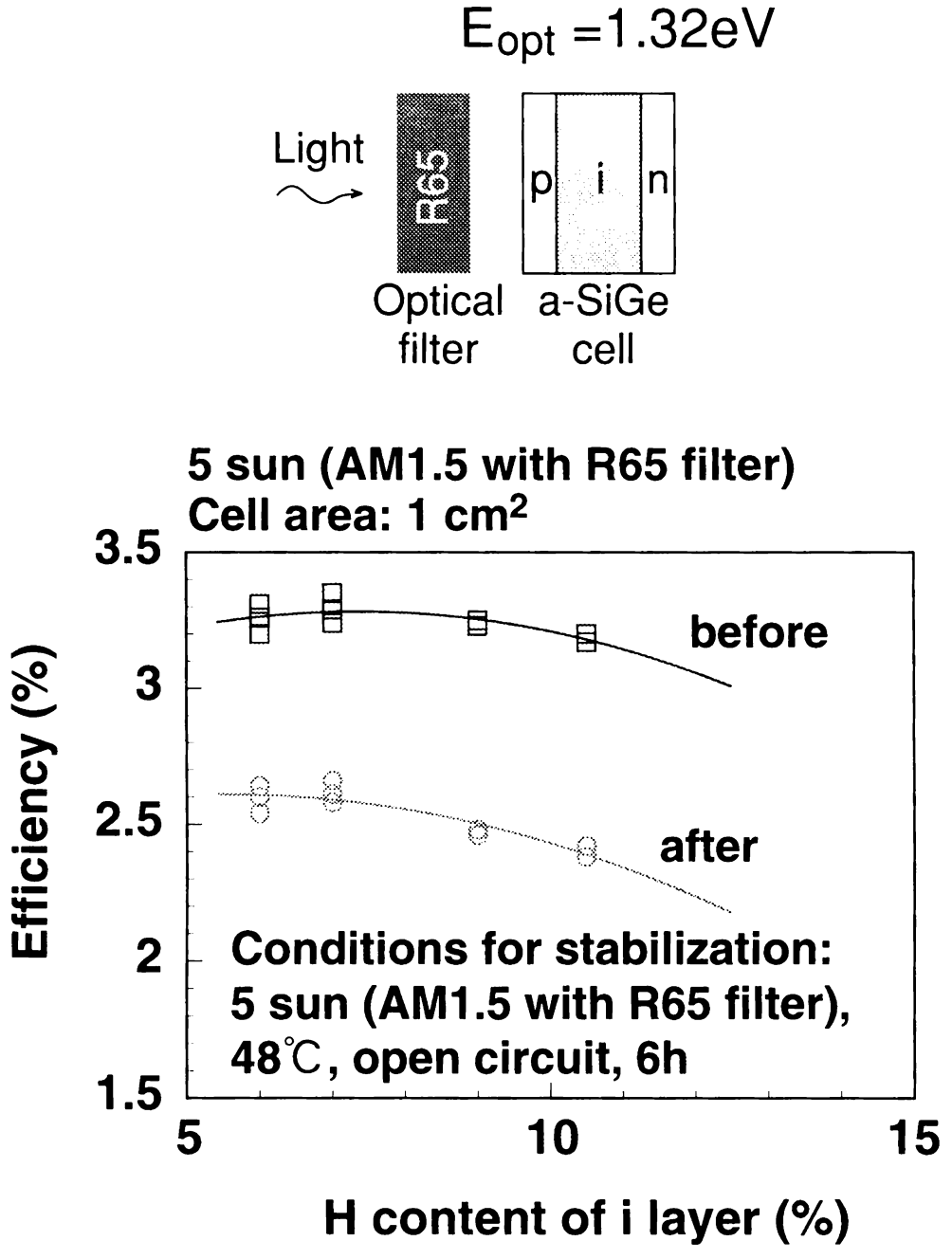

Fig. 5.4. The initial and stabilized conversion efficiencies of an a-SiGe single-junction solar cell under red light (5 sun AM-1.5 through R65 optical filter) plotted against C_H of a-SiGe:H layer.

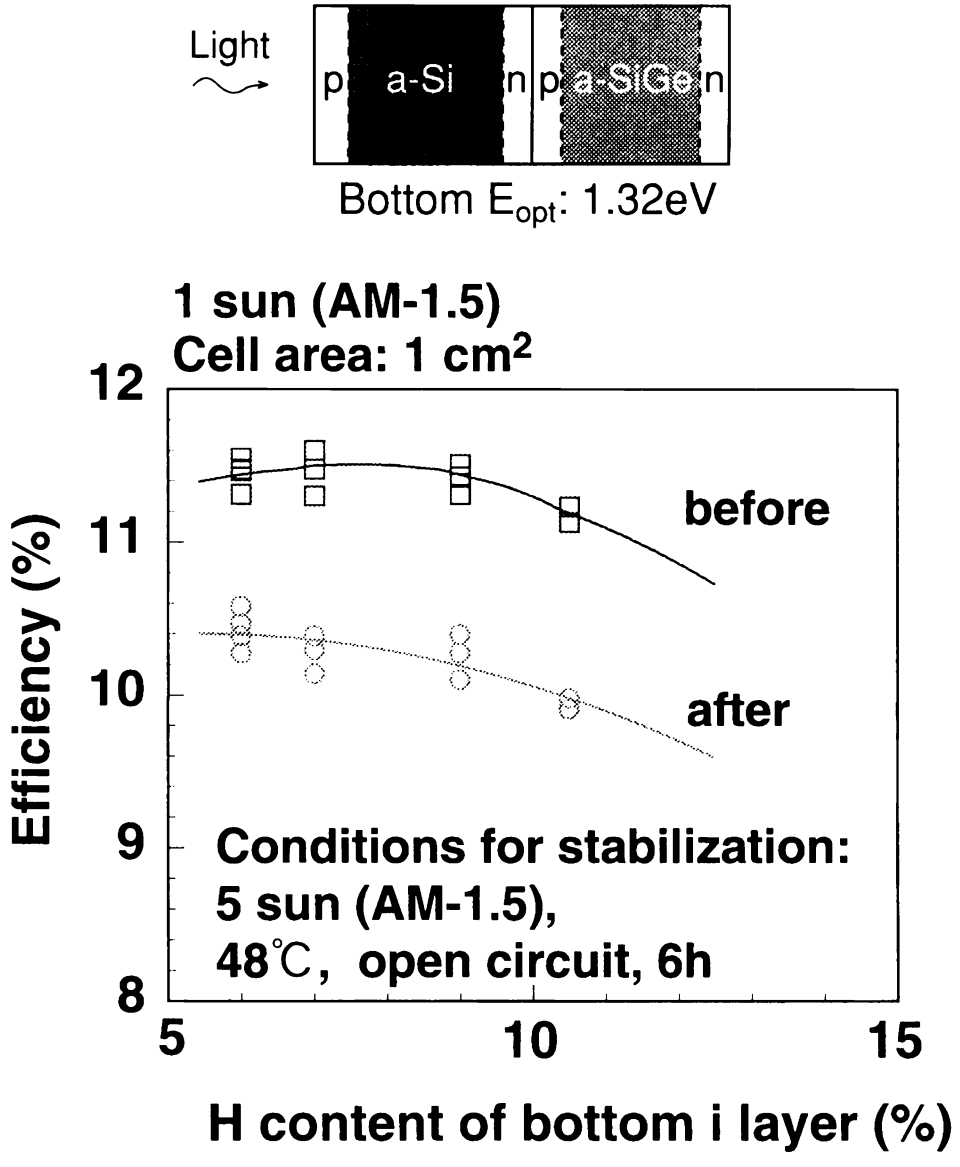

Fig. 5.5. The initial and stabilized conversion efficiencies of an a-Si/a-SiGe tandem solar cell under 1 sun AM-1.5 light plotted against C_H of a-SiGe:H layer.

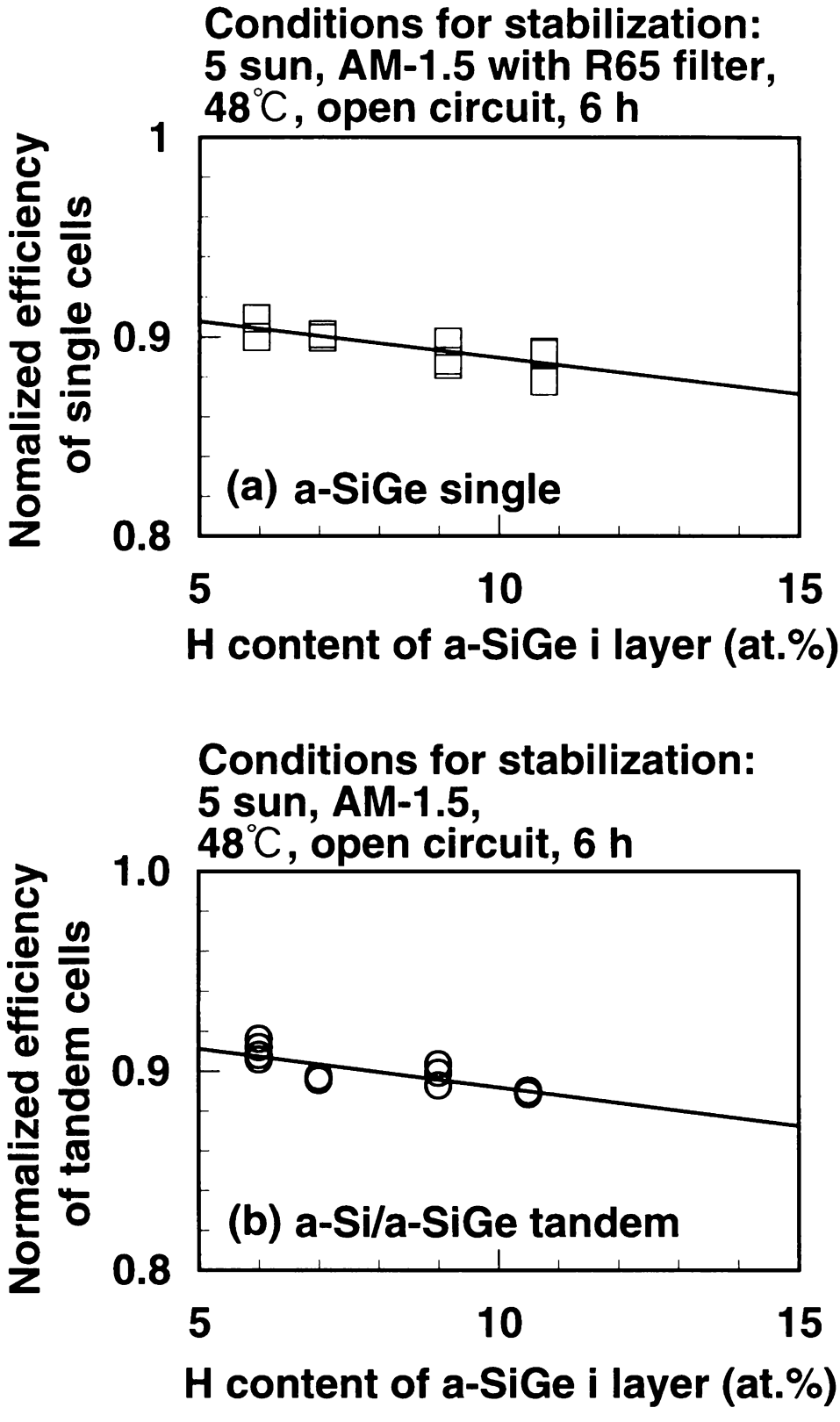

Fig. 5.6. The efficiencies after prolonged illumination normalized by the initial values of (a) an a-SiGe single, and (b) an a-Si/a-SiGe tandem solar cells plotted against C_H of a-SiGe:H layer.

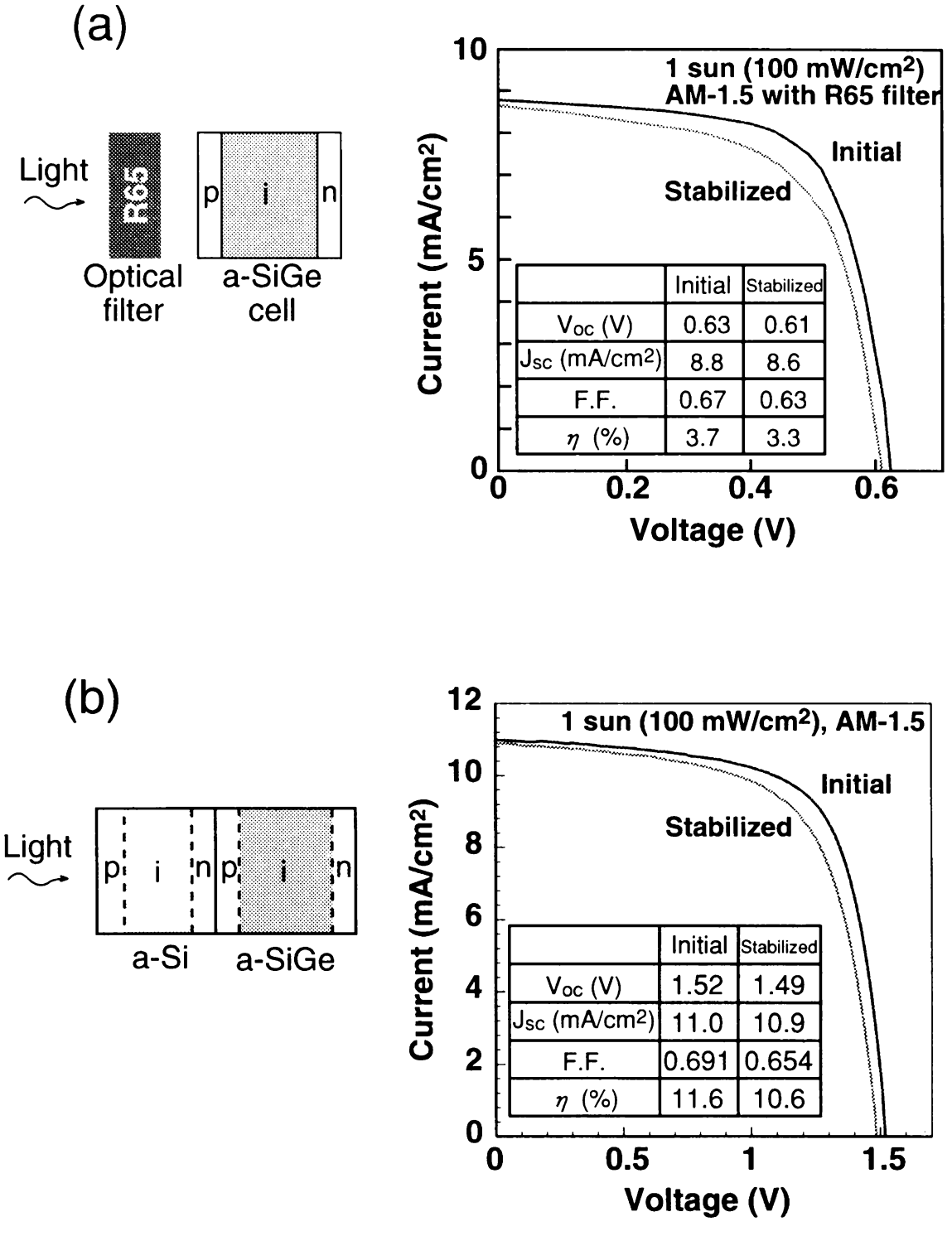

Fig. 5.7. The illuminated I-V characteristics of (a) an a-SiGe single-junction solar cell and (b) an a-Si/a-SiGe tandem solar cell before and after intense light soaking. The stabilized efficiencies for single- and tandem cells are the world's highest values ever reported for this size (1 cm^2) of an a-Si-based solar cell.

5.3.3 a-Si/a-SiGe tandem submodule

The cell design techniques shown above were extended to the fabrication of larger-scale superstrate submodules (Fig. 5.8) combining with other technologies, such as a uniform deposition of thin film layers, a high-resolution laser patterning and an optimized module structure. Especially, the bottom a-SiGe:H i-layers were deposited at a relatively low temperature, ~200°C, from very highly H_2 diluted source gases (SiH_4 + GeH_4) in order to relieve the thermal damage to under-lying layers.[11] Although the H_2 dilution method is effective to reduce Si-H_2 bonds instead of increasing process temperatures, higher-ratios of dilution are required for a-SiGe:H than that for a-Si:H, as mentioned in Chapter 4. Figure 5.9 shows the illuminated I-V characteristics of an a-Si/a-SiGe tandem submodule (area: 30×40 cm^2), before and after light soaking. The world's highest stabilized efficiency of 9.5% has been achieved.[11-13] The light-soaking test and measurements were performed and authorized by JQA (Japan Quality Assurance Organization).

5.4 Future prospects for industrialization

In this way, the performance of solar cells containing a-SiGe:H layers has been progressing. Although the stabilization test of JQA standard by intense light soaking was carried out at 48°C, the surface temperature of outside roof panels practically elevates to 70-80°C in summer. It was shown that the advantage in the stability of a-SiGe cells against a-Si cells are more conspicuous at higher temperatures as was discussed in Chapter 4. The feasibility of a-SiGe:H is, thus, more than the value of the authorized stabilized efficiency.

The "Fundamental Principles of Renewable Energy Introduction" was approved as drafted by the Diet in 1994, in which 4600 MW photovoltaic systems are planning to be totally installed by 2010. The target was revised upword to 5000 MW in 1998. In order to achieve the goal, it is necessary to introduce considerable amount of thin film solar cells in addition to the conventional c-Si or poly-Si, because Si wafers are running short. Now, the author's group in Sanyo is developing larger-scale a-Si/a-SiGe tandem submodules (60×90 cm^2) for superstrate monolithic solar panels, and is planning to ship them on trial for outdoor use in 1999. Other companies in Japan and the US, also announced to market solar cell products using a-SiGe:H alloys. The a-Si/a-

Fig. 5.8. The outlook photograph of an a-Si/a-SiGe tandem superstrate submodule.

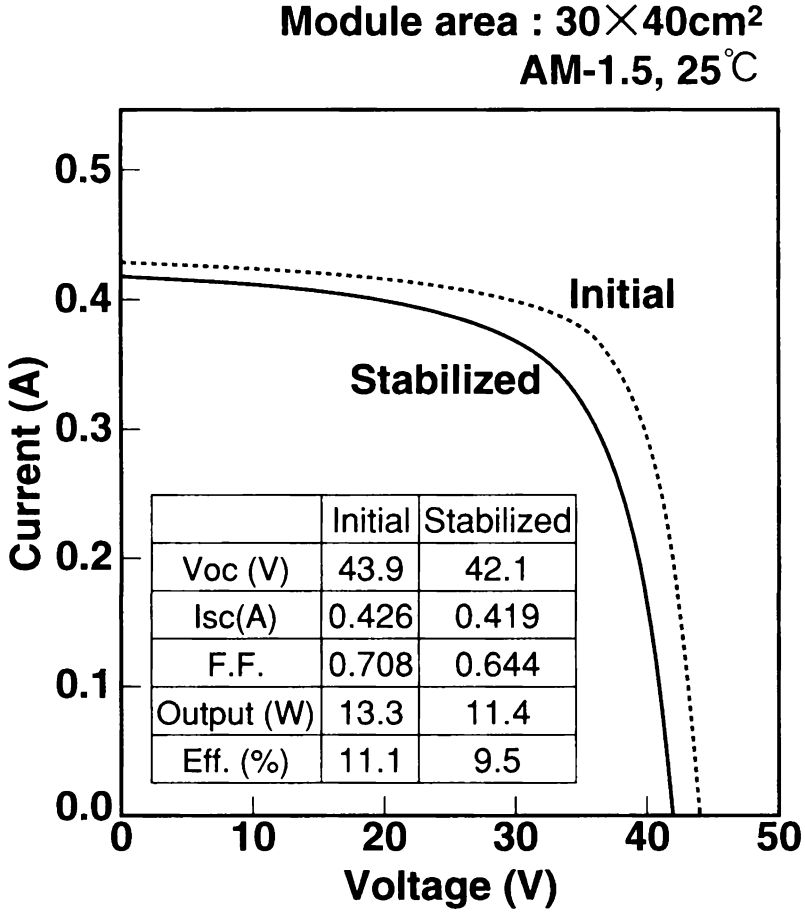

Fig. 5.9. The illuminated I-V characteristics of an a-Si/a-SiGe tandem superstrate submodule before and after intense light soaking. The stabilized efficiency of 9.5% is the world's highest value for this size (1200 cm^2) of an superstrate-type a-Si solar submodule.

SiGe tandem is the nearest thin film solar cells to take the place of the c-/poly-Si as commercial products.

5.5 Summary

The knowledge of the present study, described in Chapters 2-4, was applied to the a-SiGe:H material design for high-efficiency solar cells and modules. The world's highest stabilized efficiency of 3.3% for an a-SiGe single junction solar cell (1 cm^2) was achieved under R65 filtered light. Using this a-SiGe cell as the bottom, the world's highest stabilized efficiencies of 10.6% for an a-Si/a-SiGe tandem cell (1 cm^2) was also achieved. Furthermore, the world's highest stabilized efficiencies of 9.5% for an a-Si/a-SiGe superstrate submodule (30×40 cm^2) was achieved by combining the cell design technique with some other technologies.

References

1. S. Guha, J. Yang, A. Pawlikiewic, T. Glatfelter, R. Ross and S.R. Ovshinsky, Proc. 20th IEEE Photovoltaic Specialists Conf. 79 (1988).
2. A. Pawlikiewic and S. Guha, Proc. 20th IEEE Photovoltaic Specialists Conf. 251 (1988).
3. J. Yang, R. Ross, T. Glatfelter, R. Mohr and S. Guha, Tech. Digest 4th Photovoltaic Solar Energy Conf. 205 (Sydney, 1989).
4. R.R. Arya, M.S. Bennett, K. Rajan and A. Catalano, Proc. 9th E.C. Photovoltaic Solar Energy Conf. 251 (Barcelona, 1989).
5. C.M. Fortmann, Mater. Res. Soc. Symp. Proc. **192**, 27 (1990).
6. E. Maruyama, A. Terakawa, K. Sayama, K. Ninomiya, Y. Hishikawa, H. Tarui, S. Tsuda, S. Nakano and Y. Kuwano, Proc. 23rd IEEE Photovoltaic Specialists Conf. 827 (Louisville, 1993).
7. K.D. Mackenzie, J.H. Burnette, J.R. Eggert, Y.M. Li and W. Paul: Phys. Rev. B **38**, 6120 (1988).
8. G.H. Bauer, C.E. Nebel, M.B. Schubert and G. Schumm, Mater. Res. Soc. Symp. Proc. **149**, 485 (1989).
9. Our stabilization conditions have been confirmed to be equivalent to the JQA standard.
10. A higher stabilized efficiency for a smaller area cell ($0.25cm^2$) has been reported in the following reference; J. Yang and S. Guha, Appl. Phys. Lett. **61**, 2917 (1992).
11. T. Kinoshita, M. Shima, A. Terakawa, M. Isomura, H. Haku, K. Wakisaka, M. Tanaka, S. Kiyama and S. Tsuda, Proc. 14th European Photovoltaic Solar Energy Conf., 566 (Barcelona, 1997).
12. M. Shima, A. Terakawa, M. Isomura, M. Tanaka, S. Kiyama and S. Tsuda, Appl. Phys. Lett. **71**, 84 (1997).
13. A. Terakawa, M. Shima, M. Isomura, M. Tanaka, S. Kiyama, S. Tsuda and H. Matsunami, Proc. of 17th ICAMS, 1267 (Budapest, 1998).

Chapter 6
Conclusions

In the present work, the material properties of a-SiGe:H alloys with various compositions and E_{opt} were systematically investigated to unravel the difficulty as ternary alloys. The knowledge from the investigation was applied to the material design for efficient and stable solar cells. The conclusions obtained from the experimental results and considerations in the previous chapters can be drawn as follows.

6.1 Composition Dependence of Optical Gap and Other Properties of a-SiGe:H alloys

A detailed study of a-SiGe:H films deposited by a plasma-CVD method using SiH_4, GeH_4, and H_2 gas mixtures has been demonstrated with paying careful attention to its composition: both C_H and C_{Ge}. Furthermore, the properties have been compared among a-SiGe:H films and solar cells with a constant optical gap of 1.32 eV and different combinations of C_H and C_{Ge}.

(1) Concerning the correlation of film properties with deposition conditions, (a) C_{Ge} depends only slightly on T_s and decreases with a rise in rf power, (b) C_H increases with a decrease in T_s or an upturn of R_D, (c) the optimum R_D, which corresponds to the maximum photo-sensitivity, depends on T_s.

(2) E_{opt} is controllable by changing T_s and R_D, in addition to the $[GeH_4]/[SiH_4]$ source gas mixture ratio, and can be expressed by a linear function of C_H and C_{Ge}. As a result, films with different compositions can have the same E_{opt}.

(3) The optimum composition for initial properties, such as the Urbach tail characteristic energy, defect density, and conversion efficiency of solar cells, was determined for a certain E_{opt} (= 1.32 eV). These tendencies can be explained in terms of the hydrogen bonding configuration.

(4) The optimum composition for a certain E_{opt} shifts to the lower C_H region after light soaking due to the larger degradation for higher C_H samples. This suggests that hydrogen or Si-H_2 plays an important role in light-induced degradation.

6.2 Inhomogeneous Hydrogen Bonding Structures in a-SiGe:H

The composition dependence of H bonding configurations in a-SiGe:H alloy films with various compositions deposited by rf plasma CVD was systematically investigated by comparisons to a-Si:H and a-Ge:H.

(1) As C_H increases from 7 to 27 at.% by varying the substrate temperature from 80 to 350℃, the normalized H content per Si atom ($C_{H(Si)}$) in a-SiGe:H drastically increases with C_H, while the normalized H content per Ge atom ($C_{H(Ge)}$) is almost constant at 2-4 at.%. This suggests that the structural differences of a-SiGe:H with C_H are mainly caused in the regions around Si atoms.

(2) When focusing on H–Si bonds, [Si–H_2]/[Si–H]-$C_{H(Si)}$ correlations in a-SiGe:H deposited from both low- and high- diluted source gases are equivalent with those in a-Si:H. This suggests that the construction mechanism of H bonding structures around Si atoms in a-SiGe:H is similar to that in a-Si:H.

(3) As C_{Ge} increases from 0 to 60 at.% at a constant substrate temperature of 230℃, only $C_{H(Si)}$ increases form 10 to 14 at.%. The increase in $C_{H(Si)}$ with C_{Ge} is considered to be caused by the existence of Ge atoms which prevent H-elimination reactions around Si atoms. This increase in $C_{H(Si)}$ indirectly causes an increase in [Si–H_2]/[Si–H] and a material deterioration by alloying.

(4) The preferential attachment coefficient, $P = C_{H(Ge)}/C_{H(Si)}$, has positive correlations to both C_H and C_{Ge}. The P value is considered to be determined not simply by the statistical difference of the bonding probabilities of H to Si and to Ge, but by the kinetics of H elimination during film growth. The $C_{H(Ge)}$ value is supposed to be solubility limited, while the $C_{H(Si)}$ value is surface reaction limited.

(5) Two random models were proposed to describe the construction kinetics of H–Si bonding structures, and these models were compared to the experimental results. H-bonding configurations of high-diluted samples are almost random. On the other hand, H-bonding configurations of low-diluted samples are not random but selectively contains polyhydride bonds.

6.3 Effects of i-layer Optical Gap and Compositions on a-SiGe Solar Cell Stability

In order to reveal the effects of i-layer E_{opt} and the composition of a-SiGe solar cells on stability against light soaking, the light-induced degradation and thermally-induced recovery behaviors of a-SiGe cells with a constant E_{opt} and different compositions and those with various E_{opt} were systematically investigated.

(1) There are at least two aspects that should be considered for stability against light exposure. One is the saturated defect density, N_{sat}, and the other is the degradation time constant. It was shown that compositional factors such as C_H mainly affect N_{sat}, and E_{opt} affects the time constant.

(2) It was clearly shown that a-SiGe cells with lower C_H and/or Si-H_2 content were more stable in a constant E_{opt} system. This result confirms the contribution of incorporated hydrogen atoms on metastable defect creation. The investigation of the light-induced degradation behavior of a-SiGe:H alloys in a constant E_{opt} system is significant, not only for improving the performance of these alloys themselves, but also for verifying the kinetic models proposed for a-Si materials.

(3) a-SiGe solar cells with a narrower E_{opt} degrade more slowly than, but recover as fast as, cells with a wider E_{opt}. This is because light-induced processes, such as LIC and LIA, are suppressed in materials with a narrower E_{opt}, while thermally-induced processes, such as TIC and TIA, do not depend on E_{opt}.

(4) Both the time constant (τ_{TIA}) and the activation energy (ΔE_a) for thermal annealing of metastable defects do not depend strongly on E_{opt}. These results suggest that the variation of E_{opt} causes little energetic difference in the trap depth preventing hydrogen diffusion for removing metastable defects during network relaxation by annealing, and indirectly reconfirm the suppression of the light-induced defect creation process in narrower E_{opt} alloys due to the smaller recombination energy.

(5) The degree of degradation for narrower E_{opt} cells exhibits a greater temperature dependence after sufficient long time light soaking. This suggests that the saturated defect density, N_{sat}, which is determined by the balance of light-induced and thermally-induced processes, depends on the temperature more strongly for the narrower E_{opt} alloys. Because, when E_{opt} is decreased the contribution of the thermally activated factor to N_{sat} becomes relatively larger due to the E_{opt} dependence of the light-induced defect creation process and the E_{opt} independence of the thermally

induced annealing process. Operating conditions should thus be considered in the design of highly-efficient solar cell submodules.

6.4 Applications to Efficient and Stable Solar Cells

The knowledge of the present study, described in Chapters 2-4, was applied to the a-SiGe:H material design for high efficiency solar cells and modules. The world's highest stabilized efficiency of 3.3% for an a-SiGe single junction solar cell (1 cm^2) was achieved under R65 filtered light. Using this a-SiGe cell as the bottom, the world's highest stabilized efficiencies of 10.6% for an a-Si/a-SiGe tandem cell (1 cm^2) was also achieved. Furthermore, the world's highest stabilized efficiencies of 9.5% for an a-Si/a-SiGe superstrate submodule (30×40 cm^2) was achieved by combining the cell design technique with some other technologies.

6.5 Suggestions for Future Works

Very high stabilized efficiencies for a-Si/a-SiGe tandem cells and modules were achieved through the present work. These performances are already at a feasible level for outdoor commercial products such as PV roof panels.

The next step for industrialization is further reduction of the production cost. Improvements in the through-put of the i-layer deposition process and in the utilization of GeH_4 source gas (which is much more expensive than SiH_4) will be effective in reducing the depreciation of CVD equipment and the direct material cost, respectively. These targets conflict with the previous guiding principles for high-quality a-Si:H deposition, in which large amounts of source gas flow and low rf power density were recommended. Therefore, study of the high deposition-rate (R_D) process under source-gas depletion conditions becomes important. An alternative to rf plasma CVD, VHF plasma[1] or Hot-Wire CVD[2,3] which achieved high R_D of high-quality a-Si:H might be also useful for a-SiGe:H.

Another area that needs to be investigated is the nature of unstable a-Si related materials. In this

thesis, the effect of hydrogen on light-induced degradation were clearly abstracted by using a-SiGe:H alloys with a constant E_{opt} and different compositions. However, the kinetics of metastable defect creation has not yet been clarified. This is still an important issue in order to make drastic improvements in the photo-stability of the materials.

From the point of view of material properties, an increase in the deposition temperature (which result in low C_H) is an appropriate direction due to the following reasons; (a) R_D can be increased because the optimum R_D becomes higher for higher process temperature (as mentioned in *2.3.2*), (b) usage of Ge can be suppressed since E_{opt} is determined by the combination of C_H and C_{Ge} (as mentioned in 2.4), and (c) the stability against light soaking is improved (as mentioned in *2.5.2*). However, the high-temperature (> 250 ℃) process causes thermal damage to the underlying layer and deteriorates the p-i-n device performance.[4] Thus, it is of interest to reduce C_H without adding thermal energy, or to develop thermally-stable device structures.

The author sincerely hopes that the results described in this thesis will contribute to the material science and device technology of a-Si alloys, and to the further progress of the industrialization of solar cells in the near future.

References

1. H. Keppner, U. Kroll, P. Torres, J. Meier, D. Fischer, M. Goetz, R. Tschamer and A. Shah, *Proc. 25th IEEE Photovoltaic Specialists Conf.* (Washington D.C., 1996) p.669.
2. A.H. Mahan, J. Carapella, B.P. Nelson, R.S. Crandall and I. Balberg, J. Appl. Phys. **69**, 6728 (1991).
3. H. Matsumura, Jpn. J. Appl. Phys. **30**, 1522 (1991).
4. T. Kinoshita, M. Shima, A. Terakawa, M. Isomura, H. Haku, K. Wakisaka, M. Tanaka, S. Kiyama, S. Tsuda, *Proc. 14th EU Photovoltaic Solar Energy Conf.* (Barcelona, 1997), p.566.

List of Publications

I. Regular Papers and Letters

1. "Film Property Control of Hydrogenated Amorphous Silicon Germanium for Solar Cells"

   Akira Terakawa, Masaki Shima, Katsunobu Sayama, Hisaki Tarui, Shinya Tsuda, Hidenori Nishiwaki and Shoichi Nakano, Japanese Journal of Applied Physics Vol. **32** (1993) pp. 4894-4899.

2. "Optimization of a-SiGe:H Alloy Composition for Stable Solar Cells"

   Akira Terakawa, Masaki Shima, Katsunobu Sayama, Hisaki Tarui, Hidenori Nishiwaki and Shinya Tsuda, Japanese Journal of Applied Physics Vol. **34** (1995) pp. 1741-1747.

3. "Effect of Optical Gap on the Stability of a-SiGe Solar Cells"

   Akira Terakawa, Masao Isomura and Shinya Tsuda, Journal of Non-Crystalline Solids Vol. **198-200** (1996) pp. 1097-1100.

4. "Effect of the i-Layer Optical Gap on the Light-Induced Degradation of a-SiGe Solar Cells"

   Akira Terakawa, Masao Isomura and Shinya Tsuda; Japanese Journal of Applied Physics Vol. **35** (1996) pp. 5612-5617.

5. "Effect of the Optical Gap on the Temperature Dependence of a-SiGe:H Solar Cells Stability"

   Akira Terakawa, Masaki Shima, Masao Isomura, Makoto Tanaka, Seiichi Kiyama, Shinya Tsuda and Hiroyuki Matsunami, Journal of Non-Crystalline Solids Vol. **227-230** (1998) pp. 1267-1271.

6. "Origin of the Optical Gap Dependence of a-SiGe Solar Cell Stability"

   Akira Terakawa, Hiroyuki Matsunami, Seiichi Kiyama and Shinya Tsuda, Journal of Applied Physics Vol. **84** (1998) pp. 4611-4616.

7. "Composition Dependence of Local H Bonding Structures in a-SiGe:H Deposited by RF Plasma CVD"

   Akira Terakawa and Hiroyuki Matsunami, submitted to be published.

8. "Random Models Describing the Construction Mechanism of Hydrogen-Silicon bonds in Hydrogenated Amorphous Silicon"

Akira Terakawa and Hiroyuki Matsunami, in preparation.

9. "Control of a-SiGe:H Film Quality with Regard of Their Composition"

Katsunobu Sayama, Akira Terakawa, Masaki Shima, Eiji Maruyama, Kunimoto Ninomiya, Hisaki Tarui, Shinya Tsuda and Shoichi Nakano, Solar Energy Materials and Solar Cells Vol. **34** (1994) pp. 423-429.

10. "Approaches for Stable Multi-Junction a-Si Solar Cells"

Yoshihiro Hishikawa, Kunimoto Ninomiya, Eiji Maruyama, Shigeo Kuroda, Akira Terakawa, Katsunobu Sayama, Hisaki Tarui, Manabu Sasaki, Shinya Tsuda and Shoichi Nakano, Solar Energy Materials and Solar Cells Vol. **41/42** (1996) pp. 441-452.

11. "Effects of High Hydrogen Dilution at Low Temperature on the Thin Film Properties of Hydrogenated Amorphous Silicon Germanium"

Masaki Shima, Akira Terakawa, Masao Isomura, Makoto Tanaka, Seiichi Kiyama and Shinya Tsuda, Applied Physics Letters Vol. **71** (1997) pp. 84-86.

12. "Effects of Very High Hydrogen Dilution at Low Temperature on Hydrogenated Amorphous Silicon Germanium"

Masaki Shima, Akira Terakawa, Masao Isomura, Makoto Tanaka, Seiichi Kiyama and Shinya Tsuda, Journal of Non-Crystalline Solids Vol. **227-230** (1998) pp.442-446.

II. Proceedings of International Conferences

1. "Improvement in Performance of a-SiGe:H Solar Cells For Multi-Junction Cells" (Oral)

Eiji Maruyama, Yukihiro Yoshimine, Akira Terakawa, Katsunobu Sayama, Kunimoto Ninomiya, Yoshihiro Hishikawa, Hisaki Tarui, Shinya Tsuda, Shoichi Nakano and Yukinori Kuwano, Materials Research Society Symposium Proceedings Vol. **297** (1993, San Francisco) pp. 821-826.

2. "Improvement For High-Efficiency, Stable Multijunction Cells" (Oral)

Eiji Maruyama, Akira Terakawa, Katsunobu Sayama, Kunimoto Ninomiya, Yoshihiro Hishikawa, Hisaki Tarui, Shinya Tsuda, Shoichi Nakano and Yukinori Kuwano, the Proceedings of the 23rd IEEE Photovoltaic Specialists Conference (1993, Louisville) pp. 827-832.

3. "Control of a-SiGe:H Film Quality with Regard of Their Composition" (Oral)

Katsunobu Sayama, Akira Terakawa, Masaki Shima, Eiji Maruyama, Kunimoto Ninomiya, Hisaki Tarui, Shinya Tsuda and Shoichi Nakano, Technical Digest of the 7th International Photovoltaic Specialists Conference (1993, Nagoya) pp. 273-274.

4. "Hydrogenated Amorphous Silicon Germanium for Stable Solar Cells" (Oral)

Akira Terakawa, Masaki Shima, Katsunobu Sayama, Hisaki Tarui, Hidenori Nishiwaki and Shinya Tsuda, Materials Research Society Symposium Proceedings Vol. **336** (1994, San Francisco) pp. 487-492.

5. "Approaches for Stable Multi-Junction a-Si Solar Cells" (Plenary)

Yoshihiro Hishikawa, Kunimoto Ninomiya, Eiji Maruyama, Shigeo Kuroda, Akira Terakawa, Katsunobu Sayama, Hisaki Tarui, Manabu Sasaki, Shinya Tsuda and Shoichi Nakano, the Proceedings of the 1st IEEE World Conference on Photovoltaic Energy Conversion (1994, Waikoloa) pp. 386-393.

6. "Effect of Optical Gap on the Stability of a-SiGe Solar Cells" (Oral)

Akira Terakawa, Masao Isomura and Shinya Tsuda, the Proceedings of the 16th International Conference on Amorphous Semiconductors - Science and Technology (1995, Kobe) pp. 1097-1100.

7. "Effect of Hydrogen on Stability of a-SiGe:H and a-SiC:H" (Poster)

Masaki Shima, Akira Terakawa, Masao Isomura and Shinya Tsuda, the Proceedings of the 13th European Photovoltaic Solar Energy Conference (1995, Nice) pp. 269-272.

8. "The Effect of the Optical Gap and Compositions of a-SiGe:H Cells on the Time Decay of Light-Induced Degradation" (Oral)

Akira Terakawa, Masaki Shima, Toshihiro Kinoshita, Masao Isomura, Makoto Tanaka, Seiichi Kiyama, Shinya Tsuda and Hiroyuki Matsunami, the Proceedings of the 14th European Photovoltaic Solar Energy Conference (1997, Barcelona), pp. 2359-2362.

9. "Effects of Hydrogen Dilution on a-Si/a-SiGe Tandem Solar Cells" (Poster; the best poster awarded)

   Toshihiro Kinoshita, Masaki Shima, Akira Terakawa, Masao Isomura, Hisao Haku, Kenichiro Wakisaka, Makoto Tanaka, Seiichi Kiyama and Shinya Tsuda, the Proceedings of the 14th European Photovoltaic Solar Energy Conference (1997, Barcelona), pp.566-569.

10. "Effects of Very High Hydrogen Dilution at Low Temperature on Hydrogenated Amorphous Silicon Germanium" (Oral)

    Masaki Shima, Akira Terakawa, Masao Isomura, Makoto Tanaka, Seiichi Kiyama and Shinya Tsuda, the Proceedings of the 17th International Conference on Amorphous Semiconductors - Science and Technology (1997, Budapest) pp.442-446.

11. "Effect of the Optical Gap on the Temperature Dependence of a-SiGe:H Solar Cells Stability" (Poster)

    Akira Terakawa, Masaki Shima, Masao Isomura, Makoto Tanaka, Seiichi Kiyama, Shinya Tsuda and Hiroyuki Matsunami, the Proceedings of the 17th International Conference on Amorphous Semiconductors - Science and Technology (1997, Budapest) pp. 1267-1271.

III. Related Papers

1. "Low-Hydrogen-Content, Stable Amorphous Silicon Thin Films Prepared by Ion-Assisted Method"

   Subal Chandra De, Hisaki Tarui, Akira Terakawa, Eiji Maruyama, Katsunobu Sayama, Kunimoto Ninomiya, Shinya Tsuda and Shoichi Nakano, Japanese Journal of Applied Physics Vol. **33** (1994) pp. 5652-5656.

2. "Effect of Composition on the Properties of Amorphous Silicon Carbide at a Certain Optical Gap"

   Masaki Shima, Akira Terakawa, Masao Isomura and Shinya Tsuda, Japanese Journal of Applied Physics Vol. **36** (1997) pp. 2044-2048.

Biographical Note

The author was born to Makoto and Katsuko Terakawa on July 13th, 1967, in Nara City, Japan. After completing three years at Nara High School, a prefectural coeducational school in Nara City, he entered Kyoto University in 1986. There he began his studies in the field of engineering and graduated from the Department of Precise Engineering in 1990. He then joined the R&D Headquarters of Sanyo Electric Co., Ltd., with a great interest in the development of large-scale, low-cost solar cells as a clean energy source for the future.

At the New Materials Research Center (the Functional Materials Research Center until 1993) of Sanyo, he started working in the field of amorphous silicon-related materials and their applications to solar cells in 1990. He began to work with hydrogenated amorphous silicon germanium alloys in the fall of 1992. After several years of working in this field, he decided to study material science and the device physics of semiconductors at graduate school. In April 1997, he entered the Graduate School of Kyoto University to begin his Ph.D course in the Department of Electronic Science and Engineering under Professor Hiroyuki Matsunami, an authority in semiconductor physics, while continuing his research activities in Sanyo.

He is a member of the Japan Society of Applied Physics and of the Japan Society of Solar Energy.